

97 Jan 63

NATIONAL RESEARCH COUNCIL OF CANADA

AERONAUTICAL REPORT

LR - 352

TECHNISCHE HOOGESCHOOL DELFT
VLEGTUIGBOUWKUNDE
DE MONNIK

DEVELOPMENT OF A MODEL-CONTROLLED V/STOL
AIRBORNE SIMULATOR

BY

D. DAW AND D. M. MCGREGOR

NATIONAL AERONAUTICAL ESTABLISHMENT

OTTAWA

AUGUST 1962

THIS REPORT MAY NOT BE PUBLISHED IN WHOLE OR
IN PART WITHOUT THE WRITTEN CONSENT OF
THE NATIONAL RESEARCH COUNCIL

N. R. C. NO. 7041

H

terugbezorgen voor:

NATIONAL RESEARCH LABORATORIES

Ottawa, Canada

REPORT

National Aeronautical Establishment

Flight Research Section

Pages - Preface - 9
Text - 31
Figures - 57

Report: LR-352
Date: August 1962
Lab. Order: NAE-762
File: CM2-17-13T-6-4

For: Internal

Subject: DEVELOPMENT OF A MODEL-CONTROLLED V/STOL
AIRBORNE SIMULATOR

Prepared by: D. Daw and D. M. McGregor

Submitted by: A. D. Wood
Head
Flight Research Section

Approved by: F. R. Thurston
Director

SUMMARY

To establish valid handling quality requirements for VTOL and STOL aircraft a need exists for a simulator which adequately reproduces the dynamic responses and environment of the vehicle under consideration. To this end a variable stability helicopter has been constructed in such a way that it is possible to vary many of the stability and control parameters requiring investigation by making suitable adjustments to electrical analogue models inserted between the pilot's controls and an autopilot system.

This report describes the installation and tests of the autopilot, the analogue computer, and other equipment installed in an H-13G helicopter to achieve this variable stability feature.

Flight test data are reported and compared with the predicted response of the autopilot-helicopter combination. Good agreement was found between the two with the actual performance of the simulator somewhat greater than that predicted.

TABLE OF CONTENTS

	<u>Page</u>
SUMMARY	(i)
LIST OF ILLUSTRATIONS	(iv)
LIST OF SYMBOLS	(vii)
1.0 INTRODUCTION	1
2.0 GENERAL DESCRIPTION OF VTOL SIMULATOR	2
3.0 PRINCIPLES OF THE VTOL SIMULATOR	3
4.0 INSTALLATION OF COMPONENTS	4
4.1 Mounting of Autopilot Actuators	4
4.2 Pneumatic System	5
4.3 Mounting of Electrical and Electronic Components	5
4.4 Artificial Feel System	7
4.5 Instrument Flying Panel	8
4.6 Miscellaneous Components	9
5.0 AUTOPILOT FUNCTIONAL TESTS	9
5.1 Steady State Response Tests	9
5.1.1 Variation of the Modulator Output with Input Voltage	9
5.1.2 Variation of the Pneumatic Servo Motor Rate with Input Resistance	9
5.2 Transfer Function Tests	10
5.2.1 The Pneumatic Servo Motor Transfer Function, P(S)	10
5.2.2 Transfer Function of the Pneumatic Servo Motor and Compensation	11
5.3 Closed Loop Tests	11
5.3.1 Closed Loop Frequency Response Tests	11
5.3.2 Closed Loop Responses to Step Inputs	12
6.0 EXPERIMENTAL DETERMINATION OF THE BASIC HELICOPTER TRANSFER FUNCTIONS	12
6.1 Flight Test Instrumentation	13
6.2 Flight Test Techniques	13
6.3 Method of Analysis of Flight Test Data	13

TABLE OF CONTENTS (Cont'd)

	<u>Page</u>
6.4 Method of Assessing Constants Derived	17
6.5 Results and Discussion	19
7.0 PREDICTED CLOSED LOOP PERFORMANCE	20
7.1 Longitudinal Loop	22
7.1.1 Longitudinal Control Loop Transfer Function - One Stage of Compensation (60 Knots Forward Velocity)	22
7.1.2 Longitudinal Control Loop Transfer Function - Two Stages of Compensation (60 Knots Forward Velocity)	23
7.2 Lateral Loop	23
7.2.1 Lateral Control Loop Transfer Function - One Stage of Compensation (20 Knots Forward Velocity)	23
7.2.2 Lateral Control Loop Transfer Function - Two Stages of Compensation (20 Knots Forward Velocity)	24
7.3 Directional Loop	25
7.3.1 Directional Control Loop Transfer Function - One Stage of Compensation (60 Knots Forward Velocity)	25
7.3.2 Directional Control Loop Transfer Function - Two Stages of Compensation (60 Knots Forward Velocity)	26
7.4 The Realization of Additional Stages of Compensation	27
8.0 DETERMINATION OF THE CLOSED LOOP FREQUENCY RESPONSE FROM FLIGHT TESTS	27
8.1 Test Equipment	27
8.2 Test Procedure	28
8.2.1 Closed Loop Gain Setting	28
8.2.2 Frequency Response Determination	28
8.3 Discussion of Results	28
9.0 CONCLUSIONS	29
10.0 REFERENCES	30

LIST OF ILLUSTRATIONS

	<u>Figure</u>
View of VTOL Simulator	1
Block Diagram of Simulator System	2
Bottom View of Control Feel System	3
Top View of Control Feel System	4
View of Cockpit from Right Side	5
View of Cockpit from Left Side	6
Simplified Model-Controlled Autopilot	7
Linearization of "Bang-Bang" Servo Actuator	8
Servo Actuator - Longitudinal Cyclic Control	9
Servo Actuator - Lateral Cyclic Control	10
Servo Actuator - Tail Rotor Control	11
Block Diagram of Pneumatic System	12
Pneumatic Pump Assembly	13
View of Filter, Oil Separator, and Pressure Relief Valve	14
Mounting of Rate Gyros and Pressure Transducers	15
Calibration Box In Position	16
Mounting of Analogue Computer	17
Control Spring Feel Unit	18
Installation of Total Head Pressure Probes	19
Simplified Block Diagram of the Autopilot	20
Calibration of Modulator	21
Variation of Dither Frequency	22
Variation of Autopilot Gain With Input Resistance	23

LIST OF ILLUSTRATIONS (Cont'd)

	<u>Figure</u>
Sample of Autopilot Response to a Step Input	24
Circuit for Frequency Response Test	25
Pneumatic Servo Transfer Function	26
Transfer Function of Pneumatic Servo and Compensation	27
Closed Loop - Autopilot With Simulated Helicopter Response	28
Simulation of Helicopter Pitch Rate Response	29
Calculated Open Loop Response, $L(S) = (0.0345) K \cdot AP(S) \cdot H(S)$	30
Closed Loop Response (Loop Gain = 2.32)	31
Typical Pitch Rate Response to a Pulse	32
Installation of Tail Rotor Control Position Potentiometer	33
Basic Helicopter Flight Test and Calculated Responses	34
Handling Qualities Boundaries as a Function of Damping and Control Sensitivity - From Reference 11	35
Typical Control Loop	36
Bode Diagram for Compensation Circuit	37
Bode Diagram Longitudinal Open Loop Transfer Function (One Stage Compensation)	38
Longitudinal Control Loop Variation of K_{MAX} , K_{OPT} , and ω_n with $\frac{1}{T}$ (One Stage Compensation)	39
Longitudinal Closed Loop Transfer Functions (One Stage Compensation)	40
Bode Diagram Longitudinal Open Loop Transfer Function (Two Stages of Compensation)	41
Longitudinal Control Loop Variation of K_{MAX} , K_{OPT} , and ω_n with $\frac{1}{T}$ (Two Stages of Compensation)	42

LIST OF ILLUSTRATIONS (Cont'd)

	<u>Figure</u>
Longitudinal Closed Loop Transfer Functions (Two Stages of Compensation)	43
Lateral Control Loop Open Loop Transfer Functions (One Stage Compensation)	44
Lateral Control Loop Variation of K_{MAX} , K_{OPT} , and ω_n with $\frac{1}{T}$ (One Stage Compensation)	45
Lateral Control Loop Closed Loop Transfer Functions (One Stage Compensation)	46
Lateral Control Loop Open Loop Transfer Functions (Two Stages of Compensation)	47
Lateral Control Loop Variation of K_{MAX} , K_{OPT} , and ω_n with $\frac{1}{T}$ (Two Stages of Compensation)	48
Lateral Control Loop Closed Loop Transfer Functions (Two Stages of Compensation)	49
Directional Control Loop Open Loop Transfer Functions (One Stage Compensation)	50
Directional Control Loop Variation of K_{MAX} , K_{OPT} , and ω_n with $\frac{1}{T}$ (One Stage Compensation)	51
Directional Control Loop Closed Loop Transfer Functions (One Stage Compensation)	52
Directional Control Loop Open Loop Transfer Functions (Two Stages of Compensation)	53
Directional Control Loop Variation of K_{MAX} , K_{OPT} , and ω_n with $\frac{1}{T}$ (Two Stages of Compensation)	54
Directional Control Loop Closed Loop Transfer Functions (Two Stages of Compensation)	55
Circuit Diagram for Control Loop with Additional Compensation and an Analogue Model	56
Installation of Oscillator	57

LIST OF SYMBOLS

A, B, C	Numerator constants in helicopter transfer functions
C	Electrical capacitance
E	Voltage
e	Base of natural logarithms
S	Laplace operator
K	Constant
R	Resistance, ohms
T	Factor in compensation transfer function, seconds
T_1	"on" time in autopilot modulator cycle, seconds
T_2	"off" time in autopilot modulator cycle, seconds
f	Frequency, cycles per second
t	Time, seconds
α, β, γ	Denominator constants in helicopter transfer functions
α	Factor in compensation transfer function
σ	Calibration of longitudinal control potentiometer, volts per inch (Fig. 56)
η	Factor in illustrative first order model (Fig. 56)
δ	Control deflection, inches or degrees
ω	Frequency, radians per second
ω_n	Natural frequency, radians per second
λ	Time lag, seconds
ϵ	Autopilot error signal
ρ	Dummy of integration
τ	Dummy of integration

LIST OF SYMBOLS (Cont'd)

Angular Rates, radians per second

$\dot{\theta}$	About lateral axis of helicopter
$\dot{\phi}$	About longitudinal axis
$\dot{\psi}$	About normal axis

Transfer Functions

C(S)	Compensation circuit
G(S)	Feedback components
AP(S)	Autopilot including feedback and compensation components
H(S)	Helicopter
M(S)	Analogue model
P(S)	Autopilot servo
L(S)	Open loop

Subscripts

Controls:

e	Longitudinal stick
a	Lateral stick
r	Rudder pedals

Transfer Function Constants:

1	Longitudinal
2	Lateral
3	Directional

LIST OF SYMBOLS (Cont'd)

s	Autopilot servo actuator
IN	Input
OUT	Output
OPT	Optimum
MAX	Maximum
i	Flight test data reading identifier
c	Calculated
m	Model
h	Helicopter



DEVELOPMENT OF A MODEL-CONTROLLED V/STOL AIRBORNE SIMULATOR

1.0 INTRODUCTION

The need for the specification of definite handling qualities requirements for use by VTOL aircraft designers is becoming increasingly more evident as various types of VTOL vehicles appear. Because of the different methods of attaining vertical flight, vast differences exist in the inherent stability and control characteristics of these aircraft and the designer needs to know at what level the important parameters have to be set to make the aircraft flyable.

Both fixed-base and motion-producing simulators have proved to be valuable tools in this work. However, many investigations (Ref. 1, 2 and 3) have shown significant differences between results obtained from the two types of simulators and since, in general, the addition of motion cues to the pilot produces a more realistic simulation, it is felt that this is the direction of greatest promise. Placing the pilot in an actual airborne situation further enhances the simulation by reproducing many elements of the true psychological environment. For example, he has to be conscious that a manoeuvre producing a force at the "seat of his pants" also stresses the structure holding him aloft.

For these reasons it is felt that the flight simulator herein described will be extremely useful in helping to establish many desirable and minimal V/STOL aircraft handling quality requirements. Such a facility is also useful in assessing the adequacy of stability augmentation, autopilot, landing aid, and instrument presentation systems while varying the aircraft dynamics.

The variable stability feature of this helicopter is obtained through a model-controlled autopilot*. The case for this method is well stated in the introduction of Reference 4 which says, in part: "Although the variable stability aircraft can be used as a simulator to give a more realistic psychological environment, one of its distinct disadvantages compared with ground simulators has been the relative difficulty of providing versatility to simulate complex aircraft equations of motion. In the case of ground based simulators, this versatility is achieved by making use of standard computing components to construct electrical analogues of the equations of motion. Light-weight transistor computing elements and techniques employed in adaptive control processes developed in recent years make it possible to provide the variable stability aircraft with similar versatility, with regard to aircraft dynamics, to that of ground simulators".

* The autopilot is referred to here as "model controlled" rather than "adaptive", although the latter term is sometimes applied to the system described.

The simulator discussed in this report controls the three angular rates of the helicopter which for the planned investigations of handling qualities (under instrument flying conditions) are considered to be the most significant parameters (Ref. 4).

A detailed description of the autopilot installation in an H-13G helicopter is given along with the results of tests to determine the characteristics of the helicopter and autopilot components.

The three angular rate control loops were analysed and the optimum values of the loop variables were determined.

Finally, flight test data are presented and compared with predicted closed loop responses.

2.0 GENERAL DESCRIPTION OF VTOL SIMULATOR

The NAE flight simulator consists basically of an H-13G helicopter, on loan from the U.S. Army, (civilian designation, Bell 47G) together with portions of a Minneapolis-Honeywell H-14 autopilot. Passive networks may be used for simple models and Pace TR5 computing elements are available to allow simulation of more complex transfer functions. An over-all view of the helicopter is shown in Figure 1.

The right-hand cockpit has been fitted with "fly-by-wire" systems on the longitudinal and lateral stick and rudder. These controls supply command signals to the model. Figure 2 shows a block diagram of the system. The collective pitch and throttle controls are operated by the evaluation pilot, but are unmodified from the basic helicopter systems. A safety pilot who occupies the left cockpit can take control of the helicopter at any time by either overriding the autopilot or by disengaging it. His controls are the normal helicopter controls.

The analogue model outputs are signals representing the desired angular rates about the three mutually perpendicular helicopter axes and are used as the inputs to three high gain loops with angular rate feedback. The difference between the commanded and the actual angular rates causes the autopilot to move its pneumatic servo controls, which are connected to the helicopter controls, to decrease the difference. Hence, if the difference is small the helicopter motion closely resembles that represented by the model and a handling qualities investigation may be conducted on the model characteristics.

The evaluation pilot has been provided with a simple spring feel system with small breakout forces and constant gradients for all three controls. Figures 3 and 4 give two views of this system.

A full instrument panel containing the six basic flight instruments, an ILS indicator, and two engine instruments is installed as shown in Figures 5 and 6.

A fourteen-channel galvanometer flight recorder is used to record the various parameters of interest.

Because of the limited lifting capacity of this helicopter various modifications have been incorporated to reduce the weight. These include replacement of all radio equipment with a 3½-pound VHF set and complete removal of the battery. Warm weather operation necessitates limiting the fuel load.

3.0 PRINCIPLES OF THE VTOL SIMULATOR

The VTOL simulator utilizes a model-controlled autopilot (Ref. 5) to modify the angular rate responses of the helicopter so that they correspond to the responses of a desired analogue model. This is accomplished by adjusting the angular rate control loops to have high natural frequencies and high loop gains, and by comparing the helicopter angular rate responses with the desired rate responses produced by passing the pilot's command signals through suitable analogue models.

These models may be constructed of passive elements such as resistances, condensers, and inductances, or they may contain active analogue computing components such as operational amplifiers.

Figure 7 shows in block diagram form a model-controlled autopilot for a single-degree-of-freedom system. If it is assumed that the components are linear and possess the transfer functions as shown, then the over-all transfer function will be:

$$\frac{\ddot{\theta}(S)}{\delta_e(S)} = \frac{M(S)}{G(S) + \frac{1}{C(S) \cdot P(S) \cdot H(S)}}$$

The output will follow the model response to an input signal providing:

(1) The feedback transfer function, $G(S)$, has a modulus equal to unity and an argument of zero degrees. (This condition is met in the rate feedback systems considered in this report by using a rate gyro with a natural frequency that is very high compared with the upper frequency of the bandwidth of interest and with a very low damping ratio.)

(2) The product $C(S) \cdot P(S) \cdot H(S)$ has a large enough modulus to ensure an output of the required accuracy and an argument that is less than 180 degrees over the bandwidth of interest. One attempts to meet this condition by properly matching the compensation network to the other frequency sensitive components of the system and by choosing a sufficiently large value of loop gain.

A compensation circuit of the type used in this simulator provides phase lead over a band of frequencies and this tends to cancel the phase lags of the other control loop components. Unfortunately, the compensation circuits also provide amplification of the high frequencies which imposes an upper limit on the loop gains, and hence the closed loop bandwidths attainable.

Generally, the compensation circuit is the only element in the loop that the designer may control and in order that its parameters may be correctly chosen the transfer functions of all the other elements in the control loop must be known. Given the complete open loop transfer function the compensation circuit may be adjusted for either:

- (1) an increase in the bandwidth of the system enabling the aircraft to respond to higher frequencies, or
- (2) an increase of the gain of the closed loop resulting in a reduction of the steady state error.

Another feature of this autopilot is that it is a "bang-bang" servo system which is made to approximate a linear system by the methods described in References 6 and 7. In this system the error signal is used to pulse-width modulate a square wave oscillation having a frequency (called the dither frequency) much greater than the bandwidth of the closed control loop. The modulated square wave is applied to a pneumatic servo actuator to produce a control surface displacement as shown in Figure 8. As the linear approximation of this displacement is the integral of the error signal, the transfer function of the autopilot servo may be approximated by $P(S) = \frac{K_2}{S}$ at low frequencies.

4.0 INSTALLATION OF COMPONENTS

4.1 Mounting of Autopilot Actuators

The autopilot servo actuators (Minneapolis-Honeywell Part MC113A1) are capable of producing a torque of 100 inch-pounds while travelling through a maximum output shaft rotation of ± 30 degrees. These units are secured to the helicopter frame close to linkages controlling the existing lateral cyclic, longitudinal cyclic, and the tail rotor controls. To keep the loads on the actuators as low as possible they are connected into the system before the lateral and longitudinal cyclic hydraulic servo valves. Pulleys mounted on the actuator output shafts and on appropriate helicopter control points are connected by steel cables to transmit the actuator motions to the helicopter. Views of the three actuators so installed appear in Figures 9, 10 and 11.

A limited authority system was initially conceived since the danger of a "hard-over failure" of the autopilot system during flight was anticipated as a problem. The servo rate was found to be such that this eventuality was unlikely to cause an

unmanageable situation for the safety pilot. As a result a 100 percent authority system was finally accepted in order to permit a more rapid control response. Full rotation of the autopilot actuators moves the helicopter controls from stop to stop.

4.2 Pneumatic System

A schematic of the entire pneumatic system is presented in Figure 12. The three autopilot servo actuators require air at a pressure of 10 p.s.i. at a flow rate of approximately 0.8 cubic foot per minute per actuator. This supply is obtained by mounting an ARO 505 pneumatic pump on an unused drive pad of the engine right-hand magneto unit modified to be the same as that of the left-hand magneto used for the standard helicopter hydraulic pump. Figure 13 shows the pneumatic pump mounted as described. Since the pump located in this position turns at 1.5 times its recommended r.p.m., an over-heating problem was anticipated. However, pump temperature measurements during extended ground running, and observations immediately following the early flights, indicated that the pump performed admirably and at a reasonable temperature.

The intake side of the pump is used to supply the artificial horizon with suction regulated by a valve set to give approximately $4\frac{1}{2}$ in. Hg suction at the instrument.

From the pump the high pressure air is led through a bleed-off valve where a portion of the excess air is dumped overboard. This valve was set during ground trials and locked in a position to ensure an adequate volume of air to the actuators.

An oil separator is next employed to remove the major portion of the pump lubricating oil that makes its way into the air supply, and a filter (Minneapolis-Honeywell Part No. CSX-12937) follows to complete this task as well as to remove any other undesired particles. A pressure relief valve (ARO model 2138) set at 11 to 12 p.s.i. is situated between the oil separator and the filter. The relief pressure is set slightly higher than the required 10 p.s.i. to prevent starvation of the actuators during rapid application of control. A three-way distributor divides the air supply for final introduction to the servo valves. Figure 14 shows the arrangement of the filter, separator and pressure relief valve. High grade rubber hose is used from the pump to the filter, but to prevent the possibility of any rubber particles fouling the servo valves, steel tubing conducts the supply from the filter to the actuators.

4.3 Mounting of Electrical and Electronic Components

The model shown in the block diagram of Figure 2 receives command signals from three 5000-ohm Model G Helipot wire wound potentiometers suitably geared to the electric flight controls to provide approximately 350 degrees rotation at the potentiometer for full control movement. The outputs of the model are

compared with the actual helicopter angular rates provided in electrical form by Minneapolis-Honeywell JG7005 A-28 rate gyros mounted to sense motion about the longitudinal, lateral and normal helicopter axes. These gyros, with 45 degree per second maximum rate springs installed, have an undamped natural frequency of 9 cycles per second and a damping ratio of 0.02. Hence the transfer function of these components may be taken as a constant in the closed loop transfer analysis conducted in Section 7. The gyro mounting arrangement is shown in Figure 15.

The autopilot computer, which is a standard unit from the Minneapolis-Honeywell H-14 autopilot, receives the error signal and converts it to a form suitable for use by the "bang-bang" servo actuator valves as described in Section 3. An "engage" switch located on the autopilot-analogue control panel (Fig. 5) is used to activate the autopilot. Control of the helicopter may be returned to the safety pilot's unmodified system by disengaging the autopilot through finger tip push buttons on either of the two control column grips, by switching the "engage" switch to the off position, or by pulling the autopilot circuit breaker. Normally the first method is used.

Three trim potentiometers are provided in the cockpit with "screw-driver" adjustments to compensate for any drift of the error signals (Fig. 5 and 6).

Either the control command signals or the angular rate error signals may be monitored through sensitive meters (International Model 163) located on the autopilot-analogue control panel by suitably selecting the toggle switches shown in Figure 5 adjacent to the meters. The central position of the three switches removes the meters from the circuits. These meters are used mainly to zero the command input signals by centering the electric controls before engaging the autopilot, thereby preventing the possibility of large initial responses being inadvertently commanded.

A fourteen-channel oscillograph recorder is being used to obtain records of the helicopter angular rate responses, electric control input signals, error signals, airspeed, altitude, ILS localizer and glide path deviations, and potentiometer supply voltage. Film is fed through the camera at approximately one inch per second with a faint timer flashing every 1/100 second and a darker timer every 1/10 second. The left stretcher carrier accommodates this complete unit as shown in Figure 1. The lower thumb button on the control column grip of either cockpit controls the recorder, while the upper thumb buttons provide the film coding for run identification.

A calibration of all the recording galvanometers is conducted before and after each flight by breaking the circuits and connecting a calibration box as shown in Figure 16. It is anticipated that this system will be replaced by a semi-automatic in-flight calibrator.

The models initially flown were simple resistive-capacitive networks giving first order responses. They were contained on cards which were inserted in the autopilot computer and had to be replaced to change the simulator's characteristics. This necessitated landing the helicopter after evaluation of each model. This

difficulty is overcome with the use of the analogue computer as explained below. Using either system, the evaluation pilot is not informed of the model characteristics prior to flight.

The analogue computer (Pace TR5) is transistorized throughout making it possible to carry up to fifty computing units (operational amplifiers, integrating networks, etc.) in the mounting racks shown in Figure 17. This figure shows one front panel in its open position allowing access to the computer components which are secured in plug-in receptacles of the rack. Thirteen gain-setting potentiometers, with shaft locks, are mounted at the computer and are set and locked before flight. Five direct reading potentiometers are situated on the autopilot-analogue control panel (Fig. 5 and 6) to be used by the safety pilot to vary the model characteristics during flight. It is seen that the great advantage in this model-controlled approach to variable stability aircraft is that very complicated models may be readily "patched" into the computer and changes made easily during flight.

To provide a realistic instrument flight task the ILS system was installed complete with antenna, localizer and glide slope receivers. The antenna is mounted well forward under the left cockpit and the receivers are contained in the box just forward of the normal battery position as shown in Figure 1.

4.4 Artificial Feel System

The electric controls are fitted with constant spring feel with various gradients available by changing the springs in the cartridge shown in Figure 18. The gradients currently in use are:

Longitudinal stick	1 1/4 pounds per inch
Lateral stick	0.6 pound per inch
Rudder	10 pounds per inch

The longitudinal travel of the stick is $12\frac{1}{2}$ inches from stop to stop, the lateral travel is 11 inches, and that of the rudder pedals 9 inches from one limit to the other. All gradients and distances quoted are measured at the points of application of the control forces.

The longitudinal control has been fitted with a "beep" type trimmer and provision has been made for the addition of similar devices for the other two electric controls. Since displacement of any one of the three controls commands an angular rate about the appropriate axis, their positions remain unchanged for steady un-accelerated flight regardless of airspeed. Hence, little use is expected to be made of the trimmers except during sustained manoeuvres.

4.5 Instrument Flying Panel

A complete instrument flying panel has been installed containing the following instruments:

Standard Flight Instruments :

- (i) Altimeter
- (ii) Airspeed Indicator
- (iii) Vertical Speed Indicator - 0 to 6000 feet per minute range
- (iv) Artificial Horizon - pneumatically driven by suction side of auto-pilot supply pump
- (v) Turn and Bank Indicator - turn gyro driven from d. c. supply
- (vi) Compass - magnesyn system with sensing unit mounted in the nose of the cockpit bubble

Engine Instruments :

- (i) Manifold Pressure Gauge
- (ii) Dual Tachometer - containing needles and scales for engine and rotor r. p. m.

Navigation Instruments :

- (i) ILS Indicator

A view of the panel is shown in Figure 5.

The pressure sensing instruments have their static lines connected to the helicopter static system while pitot pressure is sensed by a separate source mounted beside the standard helicopter pitot head as shown in Figure 19.

The normal instrument pedestal has been left virtually unmodified for use by the safety pilot.

During the execution of tasks requiring instrument flying simulation, the evaluation pilot wears an instrument flying hood attached to his protective helmet. This prevents him from seeing the outside world, the safety pilot, and the movement of the safety pilot's controls while allowing an unrestricted view from the left seat.

4.6 Miscellaneous Components

Altimeter and Airspeed Capsules: Two Giannini pressure sensing capsules are used to supply electrical signals proportional to the static and dynamic pressures for recording in the flight oscillograph. The cabin is used as the static source while the total head pressure is obtained from the pitot system added as described in Section 4.5. The altimeter capsule is used at present to indicate changes in altitude of approximately ± 200 feet from a reference altitude.

5.0 AUTOPILOT FUNCTIONAL TESTS

Certain tests were made of the autopilot, both in the laboratory and after installation in the helicopter, to determine the steady state responses, the transfer functions of the various components, and the performance of the autopilot in a closed loop. These tests provided a means of becoming familiar with the equipment, enabling the closed loop performances to be predicted, and of checking the complete system before the flight test programme was commenced.

As shown in the block diagram of a typical autopilot channel (Fig. 20), a single summing resistor (R_1) was used as a model and a potentiometer was coupled to the shaft of the pneumatic servo motor for recording the responses. The transfer functions and wave form that were anticipated are also shown in this figure.

5.1 Steady State Response Tests

5.1.1 Variation of the Modulator Output with Input Voltage

The modulator output was measured for various amplifier input voltages to determine the modulator linearity and to determine the variation of the dither frequency with input voltage. The output of the modulator, a square wave, was viewed on an oscilloscope and measurements were made of T_1 and T_2 , the "on" and "off" times of the square wave. The variation of the ratio $\frac{T_1}{T_1 + T_2}$ for steady state values of E_{IN} and for two values of R_1 is shown in Figure 21.

Variations of the dither frequency $f = \frac{1}{2\pi(T_1 + T_2)}$ for variations of E_{IN} were measured and are shown in Figure 22.

These tests were conducted with no air pressure on the pneumatic servo motor.

5.1.2 Variation of the Pneumatic Servo Motor Rate with Input Resistance

The response of the pneumatic servo motor to a step input to the summing amplifier is approximately a ramp, the slope of which may be controlled by varying

the input resistor R_1 . The variation of this slope with R_1 is shown in Figure 23 and a copy of a sample recording is shown in Figure 24. This test was conducted using a step of 1.0 volt and with no load on the servo motor. The air pressure on the servo motor was 10 p.s.i. The 0.13-second lag between the application of the step input voltage and the servo response was interpreted as an indication of a transport lag in the servo response.

The variation of the servo motor rate with input resistance can be predicted knowing the characteristics of the servo amplifier. This amplifier is assumed to be of the form shown in Figure 20 and tests to determine the amplifier input resistance R and the amplifier gain A gave the expression:

$$\frac{E}{E_{IN}} = \frac{-1.815 \times 10^7}{R_1 \left[9 \times 10^3 + \frac{8.41 \times 10^7 (R_1 + R_2)}{R_1 R_2} \right]} = \frac{K_1}{21.1}$$

Assuming further that the gain of the modulator and servo motor is

$$\frac{\dot{\delta s}}{E} = -9.48 \frac{\text{degrees}}{\text{second volt}} = K_2$$

the complete autopilot gain becomes

$$\frac{\dot{\delta s}}{E_{IN}} = \frac{K}{21.1} = \frac{1.72 \times 10^8}{R_1 \left[9 \times 10^3 + \frac{8.41 \times 10^7 (R_1 + R_2)}{R_1 R_2} \right]} \frac{\text{degrees}}{\text{second volt}}$$

This calculated gain is shown in Figure 23.

5.2 Transfer Function Tests

5.2.1 The Pneumatic Servo Motor Transfer Function, P(S)

The transfer function of the pneumatic servo motor was found experimentally using the circuit shown in Figure 25. The autopilot was excited sinusoidally and the experimental points shown in Figure 26 were obtained. For comparison the transfer

functions $\frac{0.305 e^{-0.1S}}{S}$ and $\frac{0.91}{S(S+3)}$ are shown, the former being the transfer function suggested by the manufacturer and the latter being the transfer function which best fits the observed amplitude ratio points.

The experimental points were obtained under the following conditions:

- (a) The pneumatic servo motor was installed in the helicopter and coupled to the yaw control system with 60 percent authority.
- (b) The air pressure was set at 11 p. s. i.
- (c) The compensation circuit was removed.
- (d) The input signal was 6 volts peak-to-peak.

Although this data would indicate that no transport lag exists in the autopilot, the transfer function of the autopilot was taken as $P(S) = \frac{0.91 e^{-0.1S}}{S(S+3)}$ for subsequent analysis work, the transport time lag of -0.1 second being retained because of the data of Section 5.1.2. This transfer function is a good approximation to the amplitude ratio but overestimates the observed phase lag for frequencies up to 10 radians per second.

5.2.2 Transfer Function of the Pneumatic Servo Motor and Compensation

The circuit of Figure 25 was also used to determine the transfer function of the pneumatic servo motor and compensation. Figure 27 compares the experimental points with the transfer function $C(S) \cdot P(S) = \frac{2.25 e^{-0.1S} (S+0.91)}{S(S+3)(S+19.2)}$ suggested from the results of the previous tests and the expression for the compensation circuit transfer function supplied by the manufacturer. Once again this transfer function is a good approximation to the amplitude ratio but over-estimates the phase lag.

This test was conducted with the servo installed in the helicopter and coupled to the yaw control system with 60 percent authority. The air pressure was 11 p. s. i. The input signal was 3.1 volts peak-to-peak.

5.3 Closed Loop Tests

5.3.1 Closed Loop Frequency Response Tests

The frequency response of the closed pitch rate loop shown in Figure 28 was experimentally determined utilizing an analogue computer simulation of the

helicopter pitch rate response to fore and aft control stick movement. This helicopter simulation (shown in Fig. 29) was based on early estimates of the helicopter response and resulted in the open loop transfer function,

$$L(S) = \frac{63.6 e^{-0.1S} (S + 0.91) (S^2 + 0.0401S + 0.115)}{(S + 3) (S + 19.2) (S^2 + 1.06S + 0.317) (S^2 + 0.157)}$$

shown in Figure 30.

Figure 31 compares the experimental closed loop data with the calculated closed loop response curve for this transfer function.

The experimental data were obtained with no load applied to the servo motor.

5.3.2 Closed Loop Responses to Step Inputs

Closed loop tests were conducted with the autopilot installed in the helicopter and the servo motor coupled to the longitudinal control system with 80 percent authority. The circuit for this test was the same as Figure 28 with the following modifications:

- (1) The low frequency generator and 470K ohm input resistor were replaced by the electrical control stick and a 100K ohm input resistor.
- (2) The aircraft air supply was 11 p. s. i.

Pulses were fed into the autopilot through the electrical control stick for various values of loop gain. Figure 32 shows typical pitch rate responses and illustrates how the autopilot modifies the response of the helicopter.

When the loop gain was set at 8.0 the loop began to oscillate at a frequency of 5.4 radians per second. The gain predicted from Figure 30 for oscillation to occur was 15.8 and the frequency was 4.3 radians per second.

6.0 EXPERIMENTAL DETERMINATION OF THE BASIC HELICOPTER TRANSFER FUNCTIONS

To predict the angular rate responses of the VTOL simulator to electric control inputs, it was necessary to know the transfer function of each component in the system represented by Figure 2. This information was also necessary in the design of compensation circuits used to improve the performance of the closed loop.

For these purposes the basic helicopter relations between angular responses and normal control inputs were obtained at two different flight speeds

through a flight test programme conducted on a similar helicopter and described in the following sections.

6.1 Flight Test Instrumentation

A helicopter of the same type as that used for the flight simulator was equipped with the following instrumentation:

- (i) Three rate gyros suitably mounted to measure the angular rates about the helicopter's longitudinal, lateral, and normal axes.
- (ii) Three mechanically driven potentiometers, identical with those used with the simulator's electric controls, geared to the longitudinal cyclic, lateral cyclic, and the tail rotor controls. The tail rotor position pick-off was as shown in Figure 33.
- (iii) A nine-channel galvanometer recorder.

Circuits were also supplied to allow calibration of the complete system before and after each flight.

6.2 Flight Test Techniques

The helicopter was stabilized at either 20 knots or 60 knots in straight and level flight and, for lateral and longitudinal tests, a chain stop was stretched taut between the control column and an anchor point on the aircraft. The flight recorder was then switched on for approximately 10 seconds while the controls were held fixed to obtain a qualitative record of the turbulence in the flight region immediately before the test run. The control was moved sharply through approximately one-third of its full travel and then returned to its trim or chain held position. The resulting stick movement was a pulse of approximately one-second duration followed by a small step in the opposite direction. The oscillograph was left on for several minutes following the completion of the pulse or until movement of the controls was necessary to recover from the sometimes violent manoeuvres. Since it was possible for the pilot to hold a constant rudder position following a pulse input, no chain restraint was needed on this control.

To minimize the effect of atmospheric turbulence on the results, all flights were conducted on days with very light wind and no appreciable convective heating.

6.3 Method of Analysis of Flight Test Data

Many methods are available for determining the dynamic characteristics of an aircraft from flight data. One of these is the Matrix Method outlined in Reference 8 and used here with some modification. Solution for the transfer function coefficients using this type of analysis requires that the form of the transfer function

be known or assumed. If the wrong form is assumed it will be evident in the testing procedure subsequently described. These expressions may be approximated by considering the equations of motion of the vehicle, separating them into their symmetric and asymmetric modes, and solving the resulting two sets of simultaneous, linear, differential equations for the parameters of interest.

This procedure was followed for the H-13G helicopter, making extensive use of Reference 9 and the following forms of the transfer functions were estimated.

Longitudinal

$$\frac{\dot{\theta}(s)}{\delta_e} = \frac{A_1 S^2 + B_1 S + C_1}{S^3 + \alpha_1 S^2 + \beta_1 S + \gamma_1} e^{\lambda_1 S} \quad (1)$$

Lateral

$$\frac{\dot{\phi}(s)}{\delta_a} = \frac{A_2 S + B_2}{S^2 + \alpha_2 S + \beta_2} e^{\lambda_2 S} \quad (2)$$

Directional

$$\frac{\dot{\psi}(s)}{\delta_r} = \frac{A_3 S + B_3}{S^2 + \alpha_3 S + \beta_3} e^{\lambda_3 S} \quad (3)$$

The $e^{\lambda S}$ terms above are assumed transport time lags between control application and initiation of angular acceleration to account for the rotor blade dynamics and the slight control linkage free movement over the frequency bandwidth of interest.

The steps in the solution for the longitudinal coefficients using the matrix method will be described. The analysis of the other two modes was exactly parallel to that of the longitudinal mode with some simplification due to the less complicated form of their transfer functions.

Application of this method, as used, requires that the transfer function expression be written in integral form. Since all tests were started from quiescent

trimmed conditions, equation (1) may be written as:

$$\begin{aligned} \dot{\theta}(t) = & A_1 \int_0^t \delta_e dt + B_1 \int_0^t \int_0^t \delta_e d\tau dt + C_1 \int_0^t \int_0^t \int_0^t \delta_e d\rho d\tau dt \\ & - \alpha_1 \int_0^t \dot{\theta} dt - \beta_1 \int_0^t \int_0^t \dot{\theta} d\tau dt - \gamma_1 \int_0^t \int_0^t \int_0^t \dot{\theta} d\rho d\tau dt \end{aligned} \quad (4)$$

Analytic expressions are not available for $\dot{\theta}(t)$ and $\delta_e(t)$; hence, numerical integrations had to be performed. These variables were recorded during the flight tests and were subsequently read directly from the recorder film on to punched digital tape. Readings were taken for the longitudinal case every 1/20 second for three seconds and then every 1/2 second for 20 more seconds. This change in time interval was necessary for the longitudinal mode since a significant long period, lightly damped oscillation continued for an extremely long time. A reading interval of 1/20 second only was used for the other two modes of motion and the total length of test data reduced was just under 5 seconds. Using the integrating matrix suggested in Reference 10, integrals of the input and output variables were obtained.

Equation (4) is valid for the entire test time provided the flight conditions such as speed, altitude, power setting, etc., do not vary enough to cause large changes in the coefficients. Consequently, this equation may be written for each interval of time and a matrix equation of "n" rows, where n - 1 = number of time intervals read, may be constructed as follows:

$$\begin{array}{c}
 \int_0^{t_1} \delta_e dt \quad \int_0^{t_1} \int_0^{t_1} \delta_e d\tau dt \quad \int_0^{t_1} \int_0^{t_1} \int_0^{t_1} \delta_e d\rho d\tau dt - \int_0^{t_1} \dot{\theta} dt - \int_0^{t_1} \int_0^{t_1} \dot{\theta} d\tau dt - \int_0^{t_1} \int_0^{t_1} \int_0^{t_1} \dot{\theta} d\rho d\tau dt \\
 - \\
 - \\
 - \\
 \text{n Rows, 6 Columns} \\
 - \\
 - \\
 - \\
 - \\
 - \\
 - \\
 - \\
 - \\
 \int_0^{t_n} \delta_e dt \quad \cdot \quad \cdot \quad \cdot \quad \cdot \quad \cdot \quad \int_0^{t_n} \int_0^{t_n} \int_0^{t_n} \dot{\theta} d\rho d\tau dt
 \end{array}
 \left\{ \begin{array}{c} A_1 \\ B_1 \\ C_1 \\ \alpha_1 \\ \beta_1 \\ \gamma_1 \end{array} \right\} = \left\{ \begin{array}{c} \dot{\theta}_1 \\ \dot{\theta}_2 \\ - \\ - \\ - \\ - \\ - \\ - \\ - \\ - \\ - \\ \dot{\theta}_n \end{array} \right\} \quad (5)$$

Using the simplified notation of Reference 8 this may be written

$$\left\| A \right\| \left\{ \begin{array}{c} A_1 \\ B_1 \\ C_1 \\ \alpha_1 \\ \beta_1 \\ \gamma_1 \end{array} \right\} = \{ \dot{\theta}_i \} \quad (6)$$

where $i = 1$ to n .

This matrix equation represents a set of "n" simultaneous equations in the six unknown coefficients where "n" is greater than the number of coefficients. A least squares approach was used to effect a solution which in matrix manipulation involved the following steps. Each side of equation (6) was pre-multiplied by the transpose of $\|A\|$ giving

$$[A^1A] \begin{Bmatrix} A_1 \\ B_1 \\ C_1 \\ \alpha_1 \\ \beta_1 \\ \gamma_1 \end{Bmatrix} = \{A^1 \dot{\theta}_i\} \quad (7)$$

Matrix $[A^1A]$ is a square matrix with the number of rows and columns equal to the number of unknown coefficients. The coefficients were obtained simultaneously after one more operation which involved the multiplying of each side of equation (7) by the inverse of $[A^1A]$.

Then

$$\begin{Bmatrix} A_1 \\ B_1 \\ C_1 \\ \alpha_1 \\ \beta_1 \\ \gamma_1 \end{Bmatrix} = [A^1A]^{-1} \{A^1 \dot{\theta}_i\} \quad (8)$$

This entire procedure was carried out, of course, using a digital computer.

6.4 Method of Assessing Constants Derived

After the transfer function coefficients were obtained, as described above, it remained to demonstrate how well the calculated transfer function suited the physical

system. This was done by calculating the response of the derived system to the control input used during the flight test. The measured flight test response did not enter into this calculation except for comparison after the calculated response was determined.

The process involved an iteration procedure at each point in time until succeeding approximations were within a very small region of one another. The steps in the calculation are as follows: The first value of $\dot{\theta}_c$ - the calculated response - at time $t = 0$ was assumed zero since all tests were begun from trimmed conditions. The first approximation to its value at the end of the first time interval (t_1) was assumed the same and the following expression was computed for this time

$$\begin{aligned}
 & A_1 \int_0^{t_1} \delta_e dt + B_1 \int_0^{t_1} \int_0^{t_1} \delta_e d\tau dt + C_1 \int_0^{t_1} \int_0^{t_1} \int_0^{t_1} \delta_e d\rho d\tau dt \\
 & - \alpha_1 \int_0^{t_1} \dot{\theta}_c dt - \beta_1 \int_0^{t_1} \int_0^{t_1} \dot{\theta}_c d\tau dt - \gamma_1 \int_0^{t_1} \int_0^{t_1} \int_0^{t_1} \dot{\theta}_c d\rho d\tau dt \quad (9)
 \end{aligned}$$

where i assumes values from 1 to n for succeeding times.

It will be noted that (9) is the right-hand side of equation (4) with $\dot{\theta}$ replaced by $\dot{\theta}_c$. The integrals of $\dot{\theta}_c$, calculated during each iteration using a trapezoidal approximation, were, of course, zero for this first approximation. Nevertheless, the input integrals and their corresponding coefficients yielded the second approximation to $\dot{\theta}_c(t_1)$ which was compared with the first. If the two values were not within 0.1 percent of each other or 4×10^{-6} radians per second (an absolute value test became necessary at times when $\dot{\theta}_c$ became very small to prevent oscillation in the approximating method) the numerical average of the two was taken as the next approximation and the procedure was repeated. If either one of the two criteria was satisfied, the last approximation given by expression (9) was accepted as the response at the time considered and as the first approximation to the response at the end of the next time interval. The final approximation at this new time was derived by the same iterating method. Hence, the response was extended in time from point to point until the entire test interval was covered.

The difference between the actual and calculated responses was determined at each reading point along with its value squared. Finally, the sum of the squares of the errors - the quantity minimized by the method of Section 6.3 - and the RMS error were calculated for the entire test.

Because the RMS error seemed to be an unreliable indicator, a direct comparison of the graphs of the two responses was accepted as the final criterion of how well the calculated transfer function satisfied the physical system. An

illustrative longitudinal pitch rate response and the corresponding calculated output are shown in Figure 34 for a high speed flight test.

6.5 Results and Discussion

The transfer functions derived are presented in the following table:

BASIC HELICOPTER TRANSFER FUNCTIONS

	Low Speed (20 Knots)	High Speed (60 Knots)
Longitudinal, $\frac{\dot{\theta}}{\delta_e} \frac{\text{rad./sec.}}{\text{inch}}$	$\frac{0.130S+0.418}{S^2+2.74S+4.61} e^{-0.1S}$	$\frac{0.202S^2+.0252S-.0011}{S^3+2.04S^2+.290S+.412} e^{-0.1S}$
Lateral, $\frac{\dot{\phi}}{\delta_a} \frac{\text{rad./sec.}}{\text{inch}}$	$\frac{0.418S+0.394}{S^2+3.37S+3.59} e^{-0.1S}$	$\frac{0.412S+0.355}{S^2+3.51S+2.49} e^{-0.1S}$
Directional, $\frac{\dot{\psi}}{\delta_r} \frac{\text{rad./sec.}}{\text{inch}}$	NOT DONE	$\frac{0.773S+0.208}{S^2+1.25S+4.99} e^{-0.1S}$

It is noted that the longitudinal transfer function for the lower speed is one order less than that of the higher speed. The same form was initially assumed in both cases, but the calculations for several runs yielded almost identical (within 10 percent) positive real roots in both the numerator and denominator polynomials. These roots were cancelled before the testing procedure described in the previous section was applied and good agreement resulted between the calculated and observed responses.

It can be shown that the control sensitivity, defined as the initial angular acceleration per unit step control deflection $\left(\frac{\text{rad./sec.}^2}{\text{inch}} \right)$, is given by the constant "A" of each of the numerators. Similarly, the denominator term "a" gives the angular rate damping/aircraft inertia $\left(\frac{\text{ft. lb./sec.}}{\text{slug ft.}^2} \text{ or } \frac{1}{\text{sec.}} \right)$. Both of these are important handling qualities parameters in that their values have a distinct

effect on the pilot's opinion as shown by the work of Reference 11. Figure 35 shows where this helicopter falls on the graphs of Reference 11 and indicates that the directional characteristics therein specified seem much too drastic, since this helicopter is in general pleasant to fly.

The previous table represents the average of several runs for each transfer function presented. Since the separate runs did not always agree well with one another and since no reason was obvious for their differences, work is being conducted utilizing combinations of derivatives and integrals of the flight test data in the least squares method to attempt to derive a better method of analysis.

7.0 PREDICTED CLOSED LOOP PERFORMANCE

On examining the dynamic responses of the three closed control loops of the autopilot-helicopter combination, it is found that variations to the responses may be obtained by adjusting the compensation circuits within the autopilot.

Two parameters which may be controlled are:

- (1) The undamped natural frequencies of the control loops.
- (2) The optimum gains of the control loops.

The control loop undamped natural frequency (ω_n) may be defined as the frequency where the feedback signal (E_{OUT} of Figure 36) is 180 degrees out of phase with the input signal (E_{IN}). The value of the gain when oscillation occurs is called the maximum gain (K_{MAX}).

The control loop optimum gain, for the purposes of this report, is defined as the gain required for E_{OUT} to be equal in magnitude to E_{IN} but lagging by 150 degrees. This value of phase lag (equivalent to 30 degrees of phase margin) is somewhat arbitrary, but has been chosen as the maximum phase lag that will give a good dynamic response when the control loop is closed (Ref. 12).

By maximizing the control loop undamped natural frequency the greatest possible band width for the closed loop transfer function is ensured. By maximizing the optimum gain of the closed loop the steady state error between the output signal and input signal will be minimized. Because it is anticipated that the use of this autopilot helicopter combination as a VTOL simulator may at times require a maximum band width and at other times a minimum steady state error, data for both cases are presented.

The control loop transfer function is the product of the transfer functions of the compensation circuit, the modulator, the pneumatic servo motor, the helicopter,

and the rate gyroscope such that:

$$L(S) = K \cdot AP(S) \cdot H(S) = C(S) \cdot P(S) \cdot H(S) \cdot G(S).$$

The transfer functions P(S) and H(S) are discussed in Sections 5.2 and 6.0, respectively, and are considered to be beyond the control of the designer.

The rate gyroscope transfer function is considered to be a constant (K_4) over the range of frequencies of interest. This assumption is valid because the rate gyroscope has a high natural frequency (approximately 57 radians per second) and a very low damping ratio (approximately 0.02).

The compensation circuit is an RC lead-lag network whose transfer function is:

$$C(S) = K_1 \frac{(S + 0.91)}{(S + 19.2)}$$

which is a specific form of the more general expression:

$$C(S) = K_1 \left[\frac{(S + \frac{1}{T})}{(S + \frac{\alpha}{T})} \right]^n$$

where n is the number of stages of compensation used.

α determines the maximum phase lead available per section of compensation and should be made as large as possible. A value of 21.1 as supplied by the autopilot manufacturer has been used for all calculations.

T determines the frequency at which the maximum phase lead is applied to the open loop transfer function. It is this number which may be varied by changing R or C to control the undamped natural frequency and optimum loop gain of the control loop.

The pitch, roll, and yaw rate control loops were analysed to determine how the undamped natural frequencies and optimum loop gains vary with T. This analysis has been carried out for a single stage ($n = 1$) and two stages ($n = 2$) of compensation to indicate the improvement that may be obtained. The Bode diagram

for $C(S) = \left[\frac{21.1 (S + 1.0)}{(S + 21.1)} \right]^n$ is shown in Figure 37.

7.1 Longitudinal Loop

7.1.1 Longitudinal Control Loop Transfer Function - One Stage of Compensation (60 Knots Forward Velocity)

The transfer function describing the pitch rate response to fore and aft control stick motion has been found by experiment (Section 6.5) to be:

$$H(S) = \frac{\dot{\theta}(S)}{\delta_e(S)} = \frac{0.202 e^{-0.1S} (S + 0.1593) (S - 0.0342)}{(S + 2) (S^2 + 0.0418S + 0.206)}$$

Combining this expression with the transfer function for the autopilot the pitch rate open loop transfer function is:

$$K \cdot AP(S) \cdot \frac{\dot{\theta}(S)}{\delta_e(S)} = \frac{0.202K e^{-0.2S} (S + \frac{1}{T}) (S + 0.1593) (S - 0.0342)}{S(S + \frac{21.1}{T}) (S + 2) (S^2 + 0.04185S + 0.206) (S + 3)}$$

The Bode diagram of this expression for $K = 911$ and for various values of $\frac{1}{T}$ is shown in Figure 38.

The variations of K_{OPT} , K_{MAX} , and ω_n with $\frac{1}{T}$ are shown in Figure 39.

The values of these three parameters and the values of $\frac{1}{T}$ for the two conditions

- (a) maximum optimum gain, and
- (b) maximum undamped natural frequency are tabulated below:

CONDITION	$\frac{1}{T}$ sec. ⁻¹	20 log K_{OPT}	20 log K_{MAX}	ω_n sec. ⁻¹	0.202 K_{OPT}
Maximum Optimum Gain	1.85	62.9	69.2	3.23	282.0
Maximum Undamped Natural Frequency	0.72	59.2	63.4	3.72	184.0

The Bode diagrams of these closed loop transfer functions are shown in Figure 40.

7.1.2 Longitudinal Control Loop Transfer Function - Two Stages of Compensation (60 Knots Forward Velocity)

An analysis of the longitudinal control loop assuming two stages of compensation was also made. The open loop transfer function for this case is:

$$K \cdot AP(S) \cdot \frac{\dot{\theta}(S)}{\delta_e(S)} = \frac{0.202K e^{-0.2S} (S + 0.1593) (S - 0.0342)}{S (S + 2) (S + 3) (S^2 + 0.0418S + 0.206)} \left[\frac{(S + \frac{1}{T})}{(S + \frac{21.1}{T})} \right]^2$$

The Bode diagram for this transfer function for various values of $\frac{1}{T}$ and for $K = 26,900$ is shown in Figure 41. The variations of K_{MAX} , K_{OPT} , and ω_n with $\frac{1}{T}$ are shown in Figure 42 and the values of these parameters for the conditions of maximum optimum gain and maximum undamped natural frequency are tabulated below:

CONDITION	$\frac{1}{T}$ sec. ⁻¹	20 log K_{OPT}	20 log K_{MAX}	ω_n sec. ⁻¹	0.202 K_{OPT}
Maximum Optimum Gain	2.60	95.7	99.9	6.45	12,300
Maximum Undamped Natural Frequency	1.40	88.6	90.8	6.87	5,430

The Bode diagrams of these closed loop transfer functions are shown in Figure 43.

7.2 Lateral Loop

7.2.1 Lateral Control Loop Transfer Function - One Stage of Compensation (20 Knots Forward Velocity)

The transfer function describing the roll rate response to lateral stick motion has been found by experiment (Section 6.5) to be:

$$\frac{\dot{\phi}(S)}{\delta_a(S)} = \frac{0.418 e^{-0.1S} (S + 0.94)}{(S^2 + 3.37S + 3.59)}$$

Combining this expression with the transfer function for the autopilot the roll rate open loop transfer function is:

$$K \cdot AP(S) \cdot \frac{\dot{\phi}(S)}{\delta_a(S)} = \frac{0.418K e^{-0.2S} (S + \frac{1}{T}) (S + 0.94)}{S(S + 3)(S^2 + 3.37S + 3.59)(S + \frac{21.1}{T})}$$

The Bode diagram of this expression for $K = 1183$ and for various values of $\frac{1}{T}$ is shown in Figure 44.

The variations of maximum gain (K_{MAX}), the optimum gain (K_{OPT}), and the undamped natural frequency (ω_n) with the compensation circuit time constant are shown in Figure 45.

The values of these three parameters for the condition of maximum optimum gain and the condition of maximum undamped natural frequency are tabulated below:

CONDITION	$\frac{1}{T}$ sec. ⁻¹	20 log K_{OPT}	20 log K_{MAX}	ω_n sec. ⁻¹	0.418 K_{OPT}
Maximum Optimum Gain	2.5	61.5	67.1	3.83	495
Maximum Undamped Natural Frequency	0.9	57.3	61.2	4.18	305

Bode diagrams for the closed loop transfer functions describing these conditions are shown in Figure 46.

7.2.2 Lateral Control Loop Transfer Function - Two Stages of Compensation (20 Knots Forward Velocity)

The effect of an additional stage of compensation in the lateral control loop was investigated. For this case the transfer function becomes:

$$K \cdot AP(S) \cdot \frac{\dot{\phi}(S)}{\delta_a(S)} = \frac{0.418K e^{-0.2S} (S + 0.94)}{S(S + 3)(S^2 + 3.37S + 3.59)} \left[\frac{(S + \frac{1}{T})}{(S + \frac{21.1}{T})} \right]^2$$

and the Bode diagram of this expression for $K = 36,200$ and for various values of $\frac{1}{T}$ is shown in Figure 47.

The optimum gain, maximum gain and undamped natural frequency as functions of the compensation circuit time constant ($\frac{1}{T}$) are shown in Figure 48.

The values of these parameters and the values of $\frac{1}{T}$ for conditions of

- (a) maximum optimum gain, and
- (b) maximum undamped natural frequency

from Figure 48 are tabulated below.

CONDITION	$\frac{1}{T}$ sec. ⁻¹	20 log K _{OPT}	20 log K _{MAX}	ω_n sec. ⁻¹	0.418 K _{OPT}
Maximum Optimum Gain	3.3	91.2	95.9	6.4	15,150
Maximum Undamped Natural Frequency	1.55	83.8	86.8	7.10	6,460

Bode diagrams for the closed loop transfer functions describing these two conditions are shown in Figure 49.

7.3 Directional Loop

7.3.1 Directional Control Loop Transfer Function - One Stage of Compensation (60 Knots Forward Velocity)

The transfer function describing the yaw rate response to rudder pedal motion has been found experimentally (Section 6.5) to be:

$$\frac{\dot{\psi}(S)}{\delta_r(S)} = \frac{0.773 (S + 0.269) e^{-0.1S}}{(S^2 + 1.25S + 4.99)}$$

Combining this expression with the transfer function for the autopilot the yaw rate open loop transfer function is:

$$K \cdot AP(S) \cdot \frac{\dot{\psi}(S)}{\delta_r(S)} = \frac{0.773K e^{-0.2S} (S + 0.269) (S + \frac{1}{T})}{S(S + 3) (S^2 + 1.25S + 4.99) (S + \frac{21.1}{T})}$$

The Bode diagram for this expression for $K = 383$ and various values of $\frac{1}{T}$ is shown in Figure 50.

The variation of the maximum gain (K_{MAX}), the optimum gain (K_{OPT}), and the undamped natural frequency (ω_n) with the compensation circuit time constant is shown in Figure 51.

Tabulated below are the values of these three parameters for the conditions of maximum gain and for maximum undamped natural frequency.

CONDITION	$\frac{1}{T}$ sec. ⁻¹	$20 \log K_{OPT}$	$20 \log K_{MAX}$	ω_n sec. ⁻¹	$0.773 K_{OPT}$
Maximum Optimum Gain	3.5	49.4	54.6	3.06	229.0
Maximum Undamped Natural Frequency	0.85	44.5	49.9	3.82	130.3

Bode diagrams for the closed loop transfer functions describing these two conditions are shown in Figure 52.

7.3.2 Directional Control Loop Transfer Function - Two Stages of Compensation (60 Knots Forward Velocity)

The effect of an additional stage of compensation in the directional control loop was investigated. For this case the transfer function becomes:

$$K \cdot AP(S) \cdot \frac{\dot{\psi}(S)}{\delta_r(S)} = \frac{0.773K e^{-0.2S} (S + 0.269)}{S(S + 3)(S^2 + 1.25S + 4.99)} \left[\frac{(S + \frac{1}{T})}{(S + \frac{21.1}{T})} \right]^2$$

and the Bode diagram of this expression for $K = 9700$ and for various values of $\frac{1}{T}$ are shown in Figure 53.

The optimum gain, maximum gain, and undamped natural frequency as functions of $\frac{1}{T}$ are shown in Figure 54.

For (a) maximum optimum gain, and

(b) maximum undamped natural frequency

the value of these parameters are tabulated in the following table.

CONDITION	$\frac{1}{T}$ sec. ⁻¹	20 log K _{OPT}	20 log K _{MAX}	ω_n sec. ⁻¹	0.773 K _{OPT}
Maximum Optimum Gain	2.9	79.7	86.2	5.65	7,500
Maximum Undamped Natural Frequency	1.35	73.2	76.0	6.50	3,530

Bode diagrams for the closed loop transfer functions describing these two conditions are shown in Figure 55.

7.4 The Realization of Additional Stages of Compensation

In the autopilot circuitry there is provision for only one stage of compensation; consequently, an additional stage of compensation requires amplifiers and filters external to the autopilot. Some of the amplifiers of the analogue computer, recently installed in the helicopter, were used for this additional compensation.

Figure 56 illustrates how the extra stage of compensation was added to the control loops using analogue components. The control loop is shown with a simple analogue model between the control stick and the autopilot input.

8.0 DETERMINATION OF THE CLOSED LOOP FREQUENCY RESPONSE FROM FLIGHT TESTS

The closed loop performance of the flight simulator was determined experimentally at flight speeds of 20 and 50 miles per hour.

8.1 Test Equipment

A sine wave generator capable of producing electrical signals of continuously variable frequency and amplitude, and a variable resistance decade box were the only two pieces of equipment added to the flight simulator for this investigation. The oscillator was mounted between the cockpits as shown in Figure 57 and the decade box was held on the floor of the right cockpit. These tests were carried out before the installation of the analogue computer.

The output of the oscillator was applied to the autopilot in place of the model pitch rate signal of Figure 7 with frequencies ranging from 0.2 radian per second to 10 radians per second available.

The decade box was used to set the gain of the closed loop to the desired value, as will be described in the following section.

It was found advisable early in the investigation to de-energize completely two of the autopilot channels while the third was being excited. This was accomplished by removing the electrical connections to the autopilot pneumatic actuators and installing an equivalent electrical load to keep the autopilot characteristics unchanged. This procedure greatly simplified the piloting task which was otherwise most difficult while trying to overpower two channels of the autopilot and simultaneously allowing the third to oscillate freely.

The oscillograph recorder yielded traces of the input and output variables along with altitude, airspeed, and autopilot error signals.

8.2 Test Procedure

8.2.1 Closed Loop Gain Setting

To obtain the desired closed loop response it was necessary to set the loop gain as described in Section 7. This was done in flight as follows: The helicopter was stabilized at the desired speed and the autopilot engaged. The oscillator was switched into the channel being investigated with the amplitude control zeroed and the decade box wired into the appropriate angular rate feed-back path with a very high resistance setting. The loop gain was gradually increased by decreasing the feed-back resistance as the helicopter was disturbed by pulse inputs from the "safety pilot's" controls. The resistance setting at which sustained oscillation occurred was noted and used to calculate the desired setting, as outlined in Section 7, giving maximum natural frequency. The feed-back resistances necessary were found to be: longitudinal, 100 K; lateral, 200 K; and directional, 95 K. With the system set up in this manner, the damping ratio on each of the three channels is approximately 0.2.

8.2.2 Frequency Response Determination

The helicopter was once again stabilized at the appropriate flight speed. The autopilot was engaged with the oscillator connected to the channel being investigated and the proper feed-back resistor was installed. The oscillator was set at the desired frequency with the amplitude first zeroed and then slowly increased until a reasonable response was obtained. Many cycles of the oscillation were filmed by the flight recorder after which the frequency was changed and the entire procedure repeated.

8.3 Discussion of Results

The amplitude ratios and phase angles relating the closed loop response and the input were readily determined from the flight film. The measured values, with one stage of compensation, are compared with the predicted values in Figures 40, 46, and 52, showing that the predicted values are pessimistic, particularly for the

longitudinal and directional control loops where the value of ω_n was from 2.0 to 1.5 radians per second greater than the predicted values. These differences are most likely due to over-estimation of the phase lag of the servo actuators discussed previously in Section 5.2.1.

While closed loop amplitude and phase angle measurements have not been obtained with two stages of compensation, values of ω_n obtained from flight experiments were 8.3, 8.8, and 8.8 radians per second for the longitudinal, lateral, and directional loops respectively, compared with predicted values of 6.87, 7.10, and 6.50 radians per second. These results also show that the predicted results were pessimistic and probably for the same reason as mentioned in the previous paragraph.

9.0 CONCLUSIONS

An airborne V/STOL simulator has been developed by providing a small helicopter with variable stability characteristics using a technique in which electrical analogue models determine the response of the aircraft. The capabilities and limitations of the simulator have been determined by flight test and a comparison has been made between measured and predicted responses.

It has been found that by employing two stages of compensation the undamped natural frequencies of the closed loops for the three axes fall between 8 and 9 radians per second. These measured values are slightly higher than those predicted from a synthesis of estimated and experimentally determined component characteristics. With the present pneumatic servos the closed loop performance is below that suggested in Reference 4 as necessary to provide an adequate representation of the desired response, the undamped natural frequencies being about 70 percent of the proposed value of 12 radians per second. The lower frequencies actually obtained result in an initial lag in response which is particularly noticeable in the pitching behaviour of the aircraft when high values of control sensitivity are employed. This effect is less evident to the pilot in the case of motion about the roll and yaw axes.

From preliminary experiments with models covering a wide range of values of control sensitivity and damping/inertia ratio it appears that the performance of the system will be adequate for the conduct of certain V/STOL flying qualities investigations provided that these are confined to relatively low values of control sensitivity, i.e. towards the left-hand side of diagrams such as those shown in Figure 35. This, however, is the region of most immediate practical interest to the aircraft designer. With this limitation the airborne simulator may be used to explore the effects on flying qualities of attitude, directional stability and coupling between the degrees of freedom as well as angular rate damping and control sensitivity.

To further improve the performance of the system it will be necessary to increase the closed loop undamped natural frequencies. For example, with the present pneumatic system a reduction of the air volume of the servo components or

an increase of system pressure would have a beneficial effect in making possible a more rapid loop response. Alternatively the present servos could be replaced by high frequency electro-hydraulic units. Both alternatives require investigation.

10.0 REFERENCES

1. McRuer, D. T.
Seskel, E.
Hall, I. A. M.
et al. Human Pilot Dynamic Response in Flight and Simulator.
U.S. Air Force, WADC Tech. Report 57-520,
August 1958.
2. McRuer, D. T.
Ashkenas, I. L.
Guerre, C. L. A Systems Analysis View of Longitudinal Flying Qualities.
U.S. Air Force, WADD Tech. Report 60-43,
January 1960.
3. McWeeney, R. J.
Davison, F. E. Flight Controls Human Dynamic Response Study.
U.S. Air Force, Bureau of Aeronautics, Report
AE-61-6.
4. Gould, D. G. The Model Controlled Method for Development of Variable Stability Aircraft.
NRC Aero. Report LR-345, June 1962.
5. Daw, D. F.
Ursel, L. V. A Model-Controlled Autopilot for an Airborne VTOL Simulator.
NRC Aero. Report LR-302, February 1961.
6. Honeywell Simplified Adaptive Autopilot.
Minneapolis-Honeywell Regulator Company,
Aeronautical Division, Minneapolis.
7. Amsler, B. E.
Gorozdos, R. E. On the Analysis of Bi-Stable Control Systems.
Paper Presented at the National Automatic Control Conference, Dallas, Texas, November 5, 1959.
8. Donegan, J. J.
Pearson, H. A. Matrix Method of Determining the Longitudinal-Stability Coefficients and Frequency Response of an Aircraft from Transient Flight Test Data.
NACA Report 1070, 1952.
9. Shapiro, J. S. Principles of Helicopter Engineering.
McGraw-Hill Book Co., New York, 1955.
10. Diederich, F. W. Calculation of the Aerodynamic Loading of Swept and Unswept Flexible Wings of Arbitrary Stiffness.
NACA Report 1000, 1950.

11. Salmirs, S.
Tapscott, R. J. The Effects of Various Combinations of Damping and
Control Power on Helicopter Handling Qualities During
Both Instrument and Visual Flight.
NASA Tech. Note D-58, October 1959.

12. Thaler, G. J.
Brown, R. G. Servomechanism Analysis.
McGraw-Hill Book Co., New York, 1953.

/LES

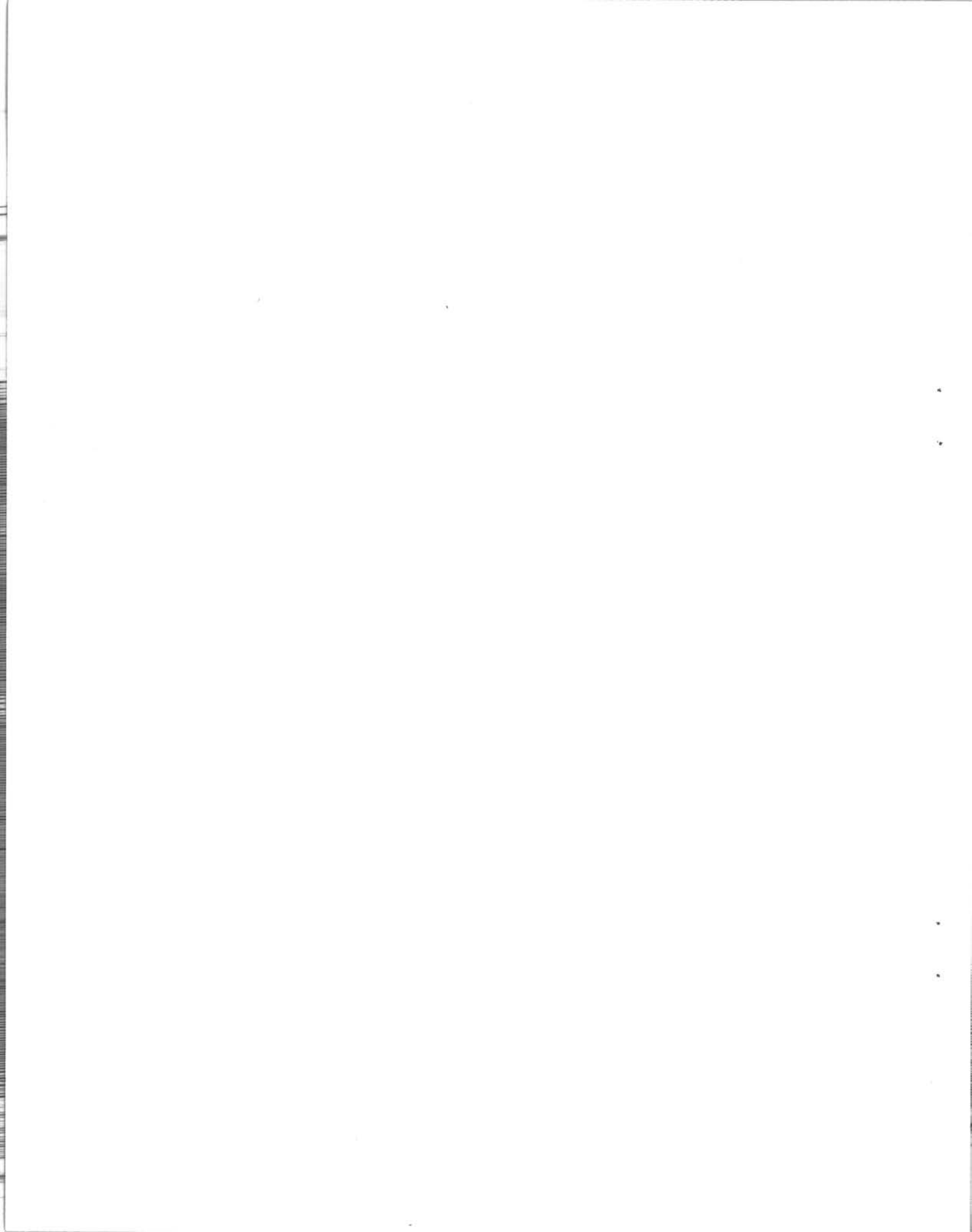
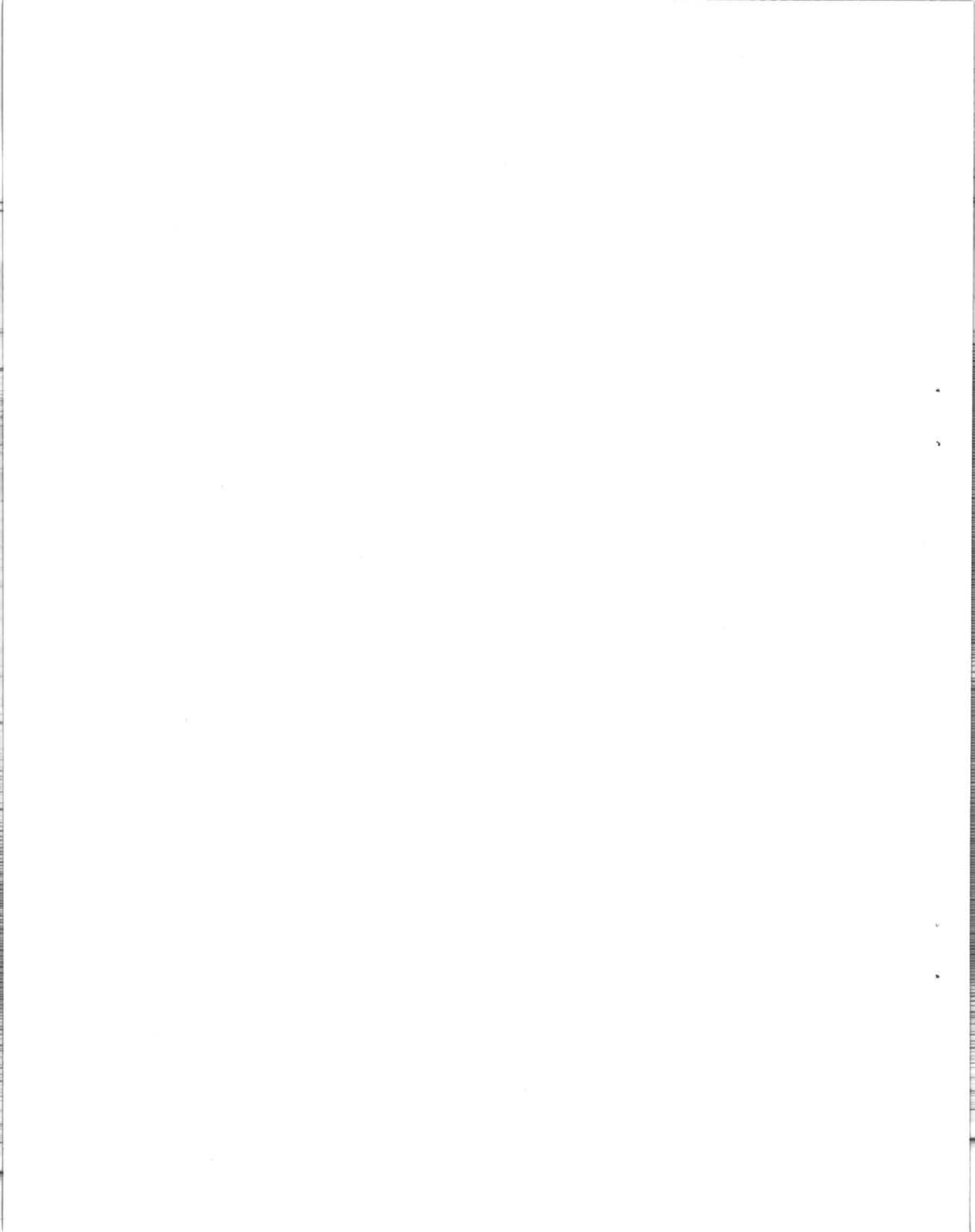
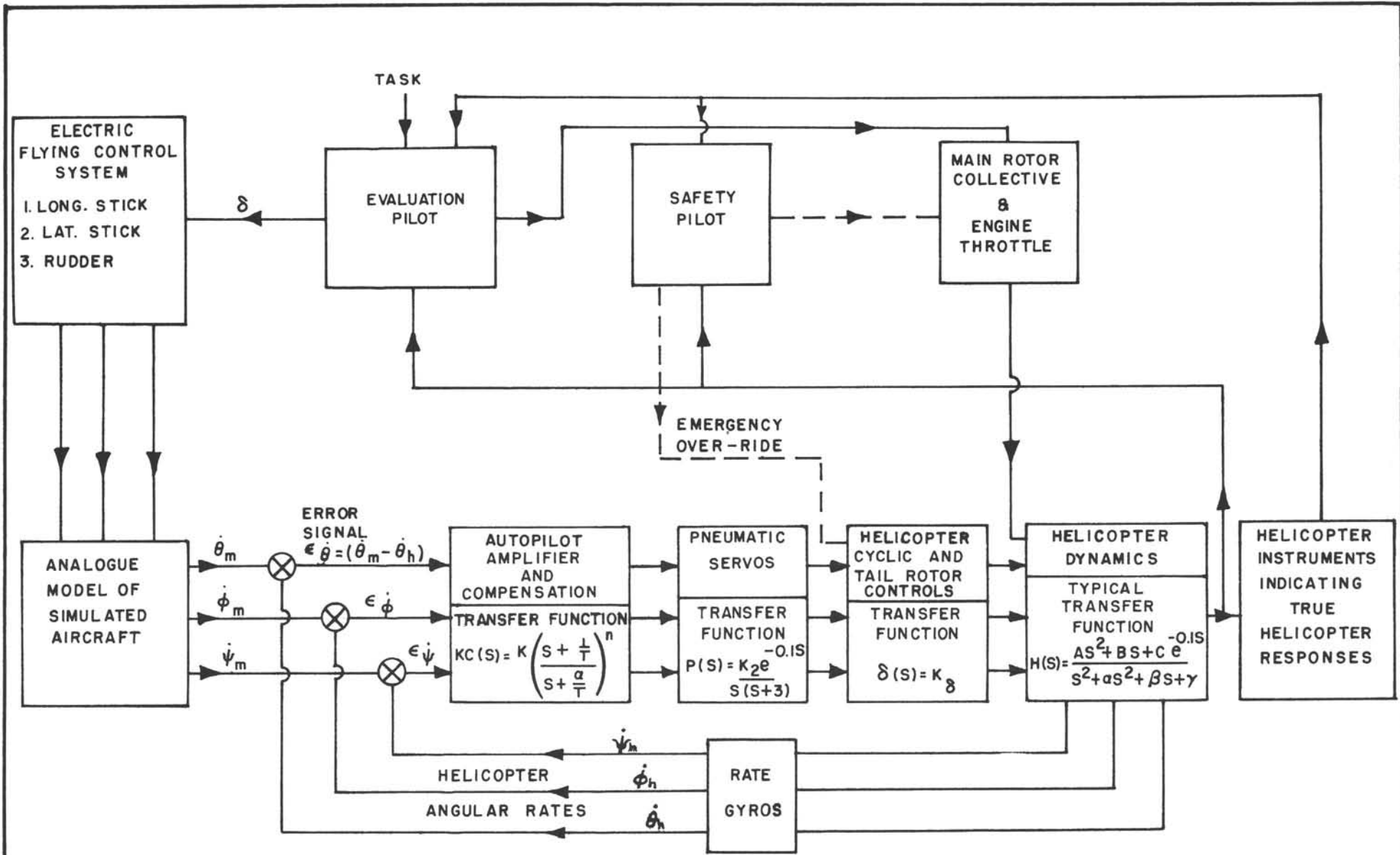


FIG. 1
LR-352



VIEW OF VTOL SIMULATOR

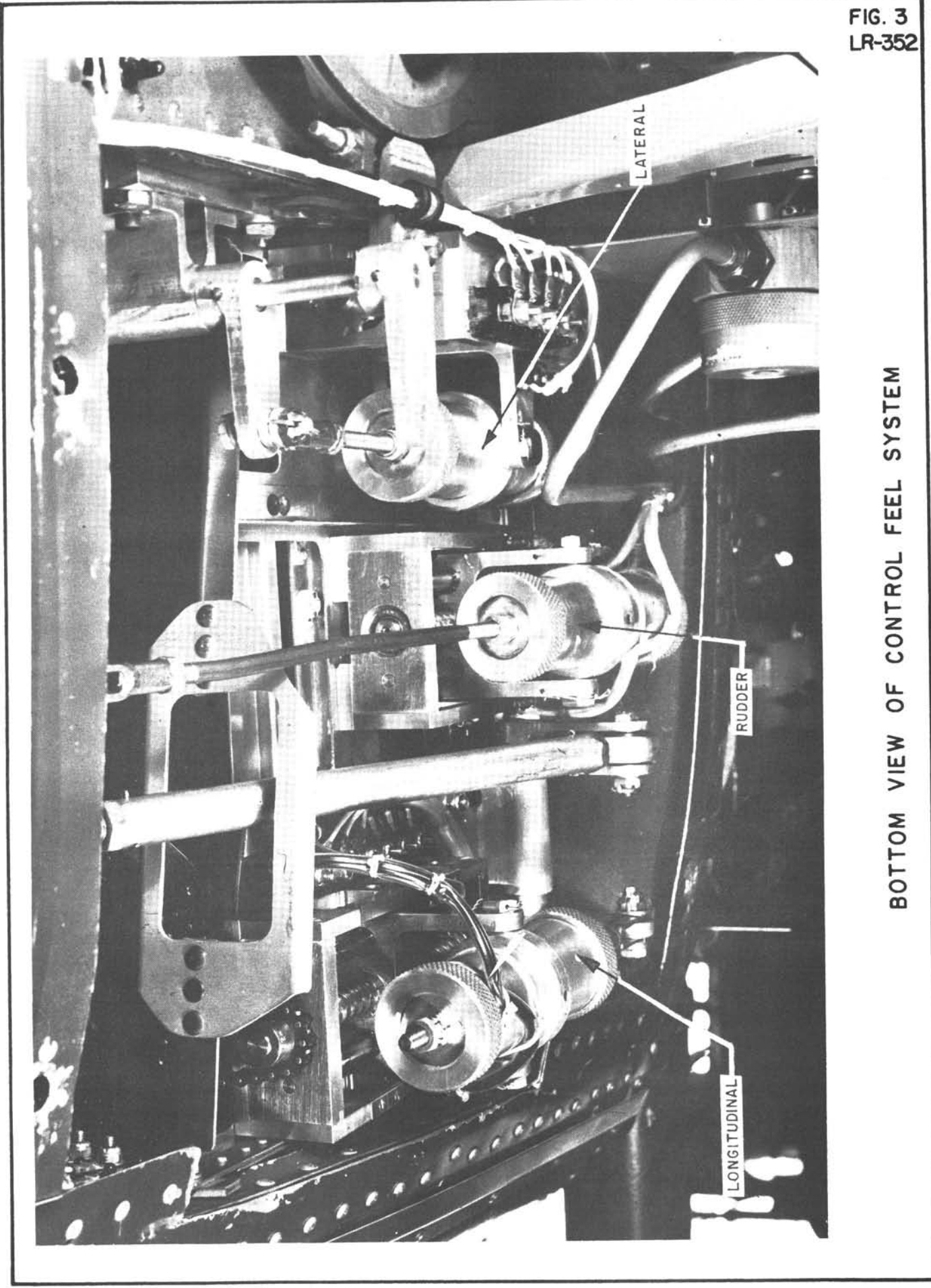




BLOCK DIAGRAM OF SIMULATOR SYSTEM



FIG. 3
LR-352



BOTTOM VIEW OF CONTROL FEEL SYSTEM

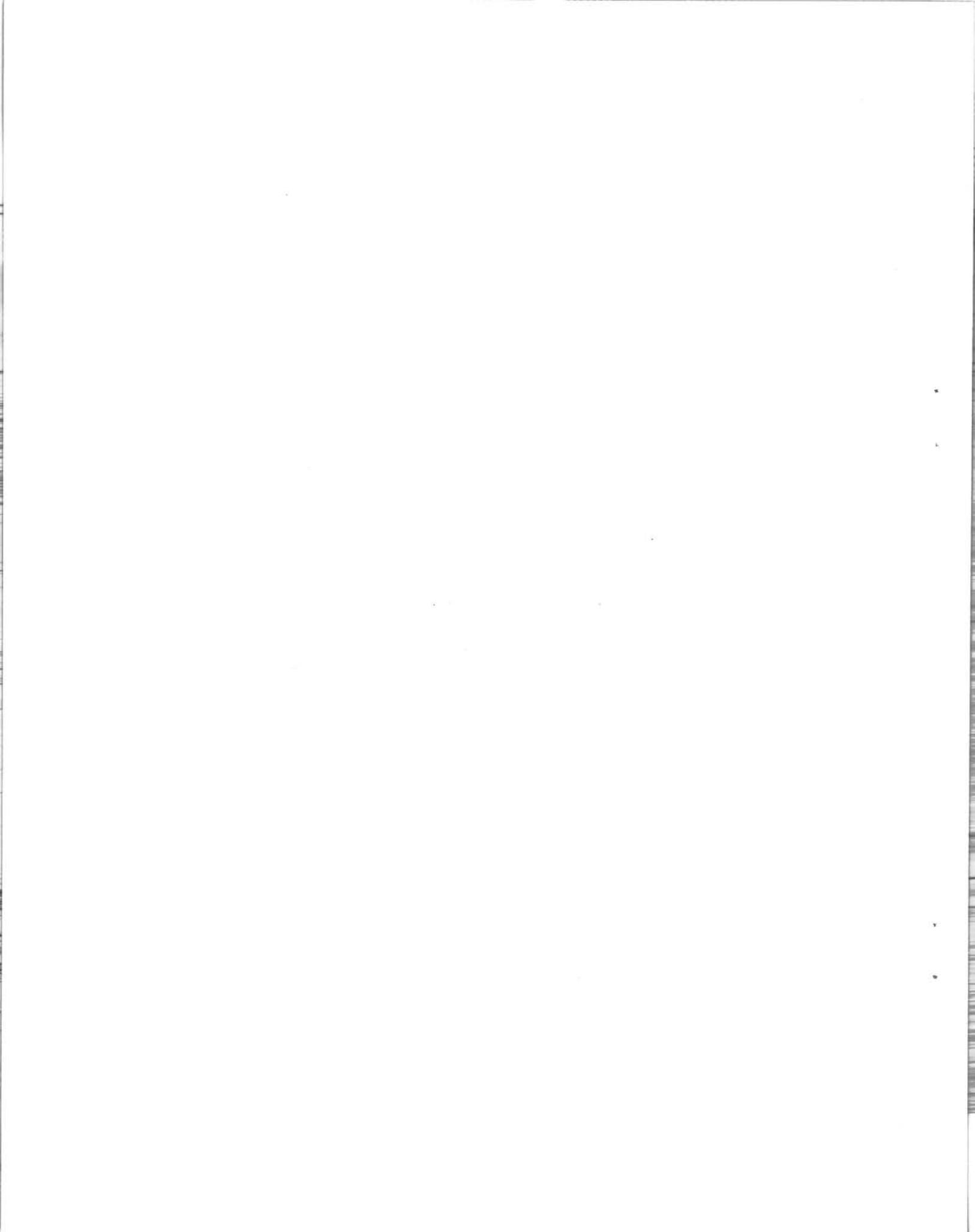
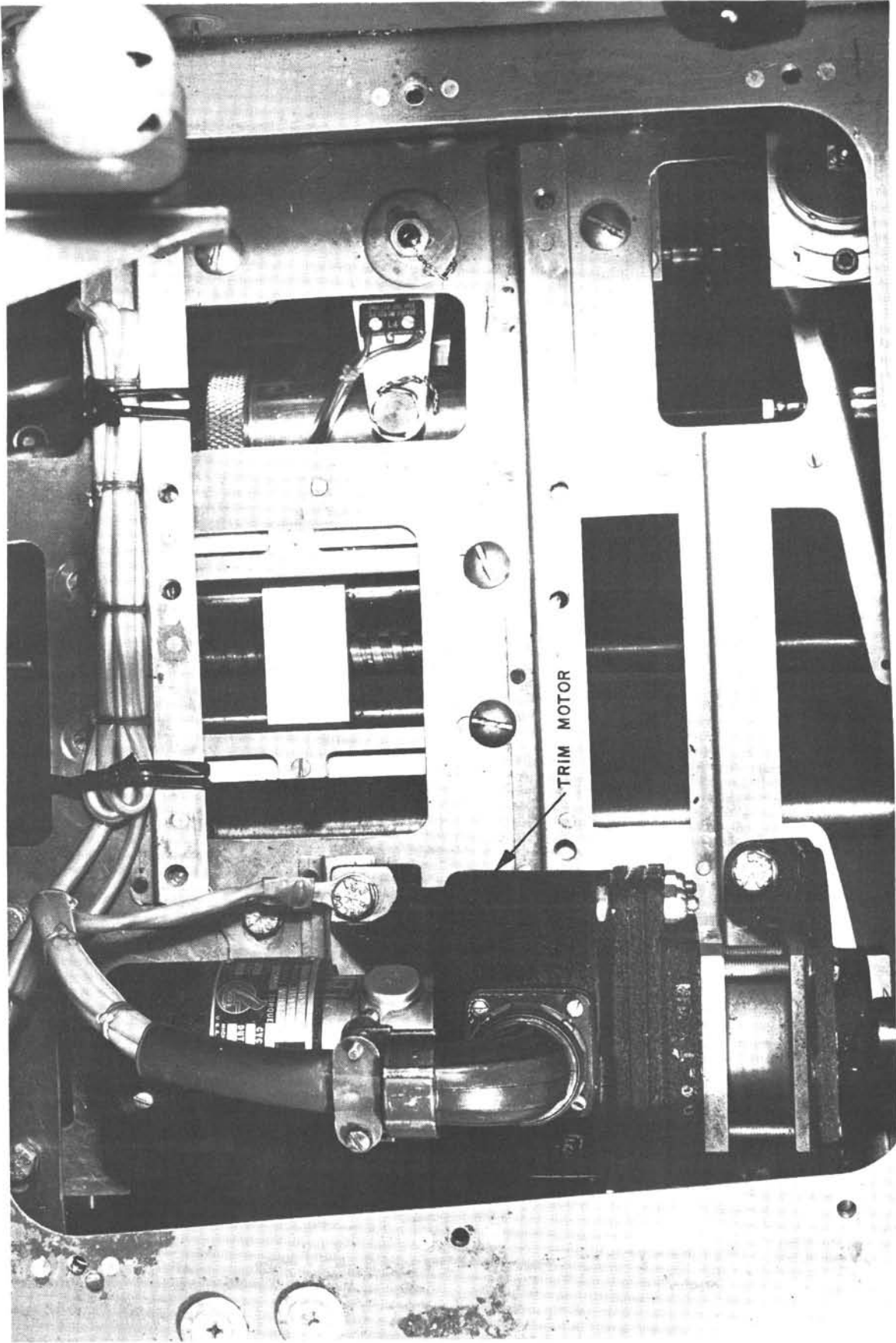


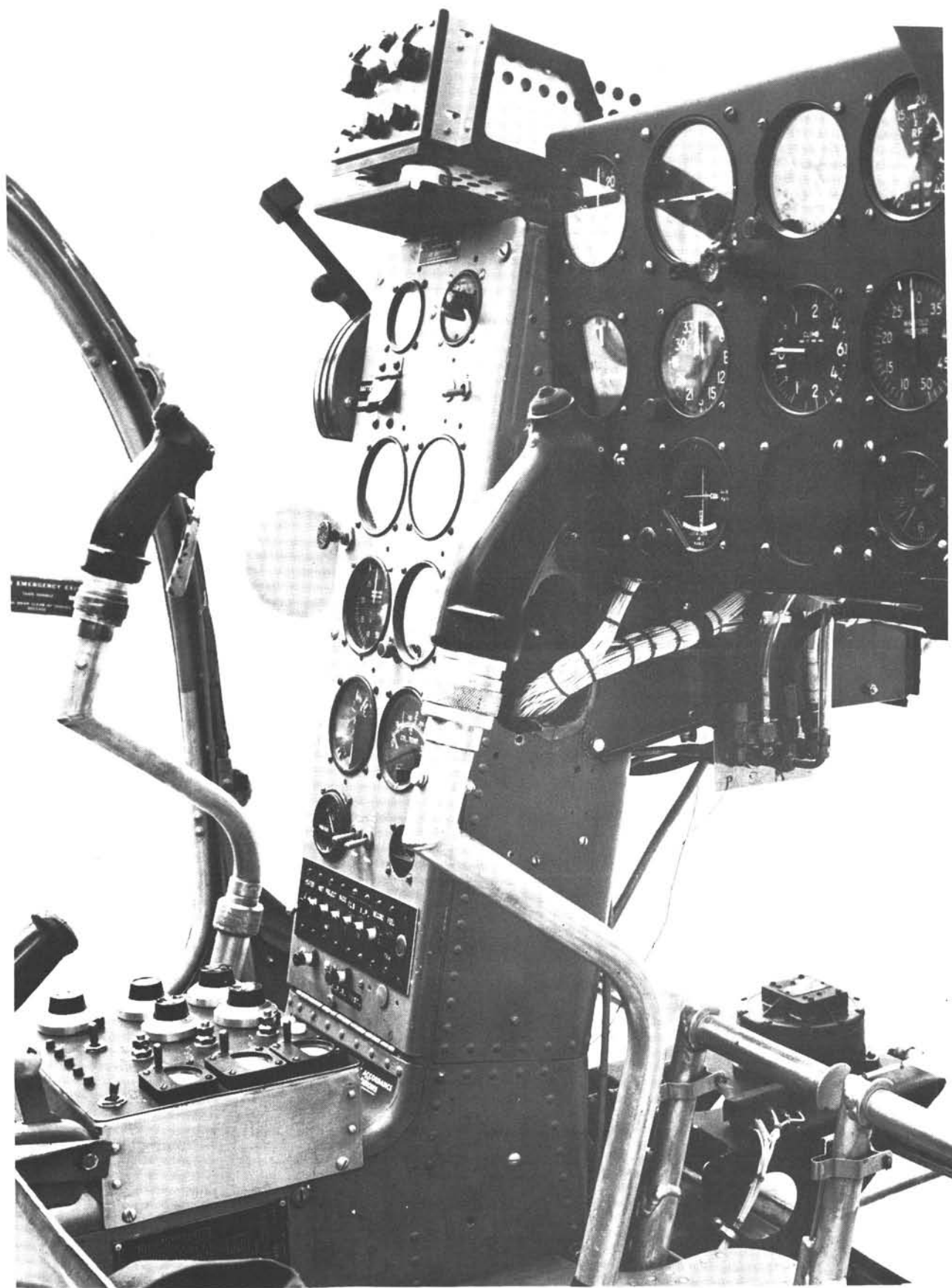
FIG. 4
LR-352



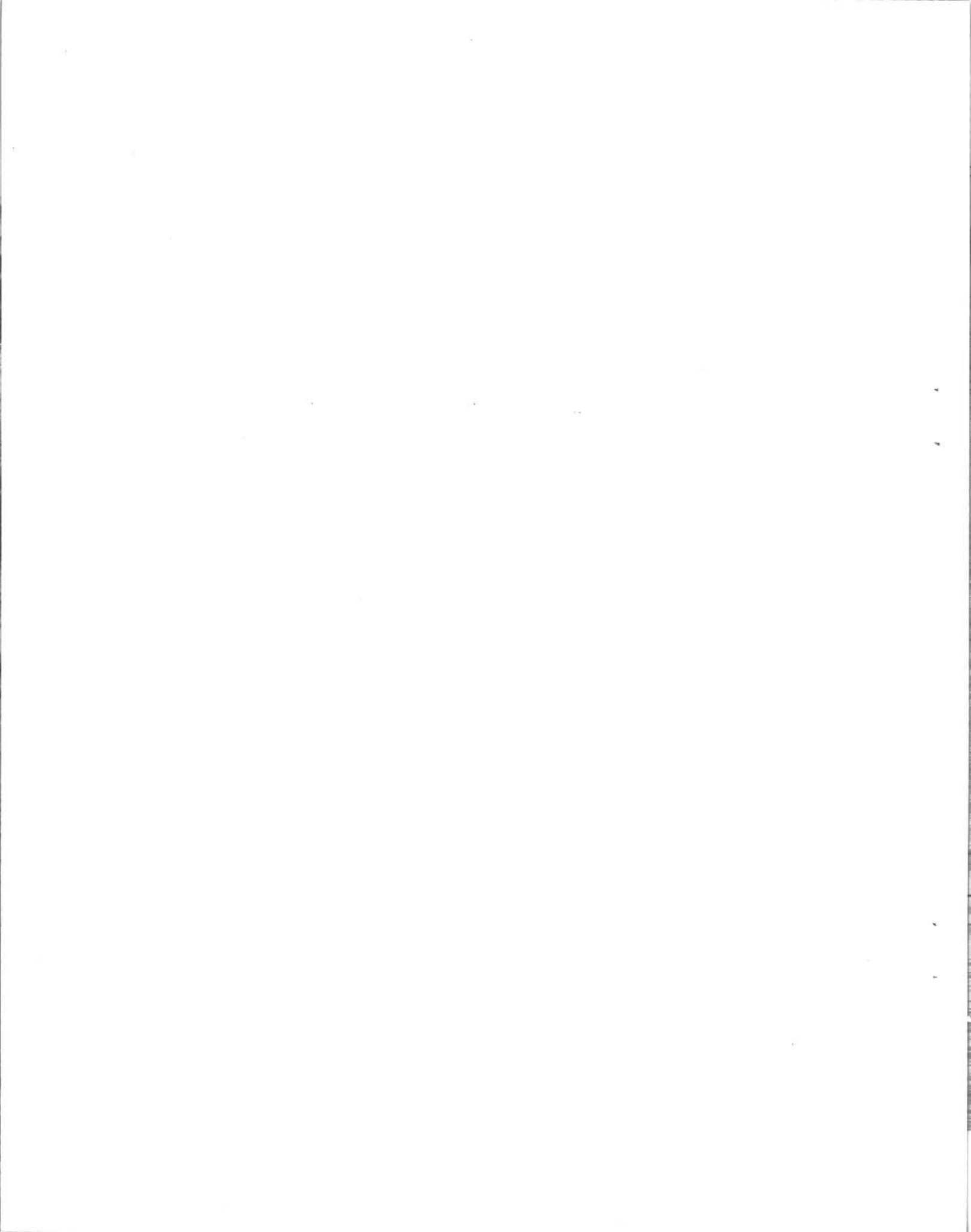
TOP VIEW OF CONTROL FEEL SYSTEM

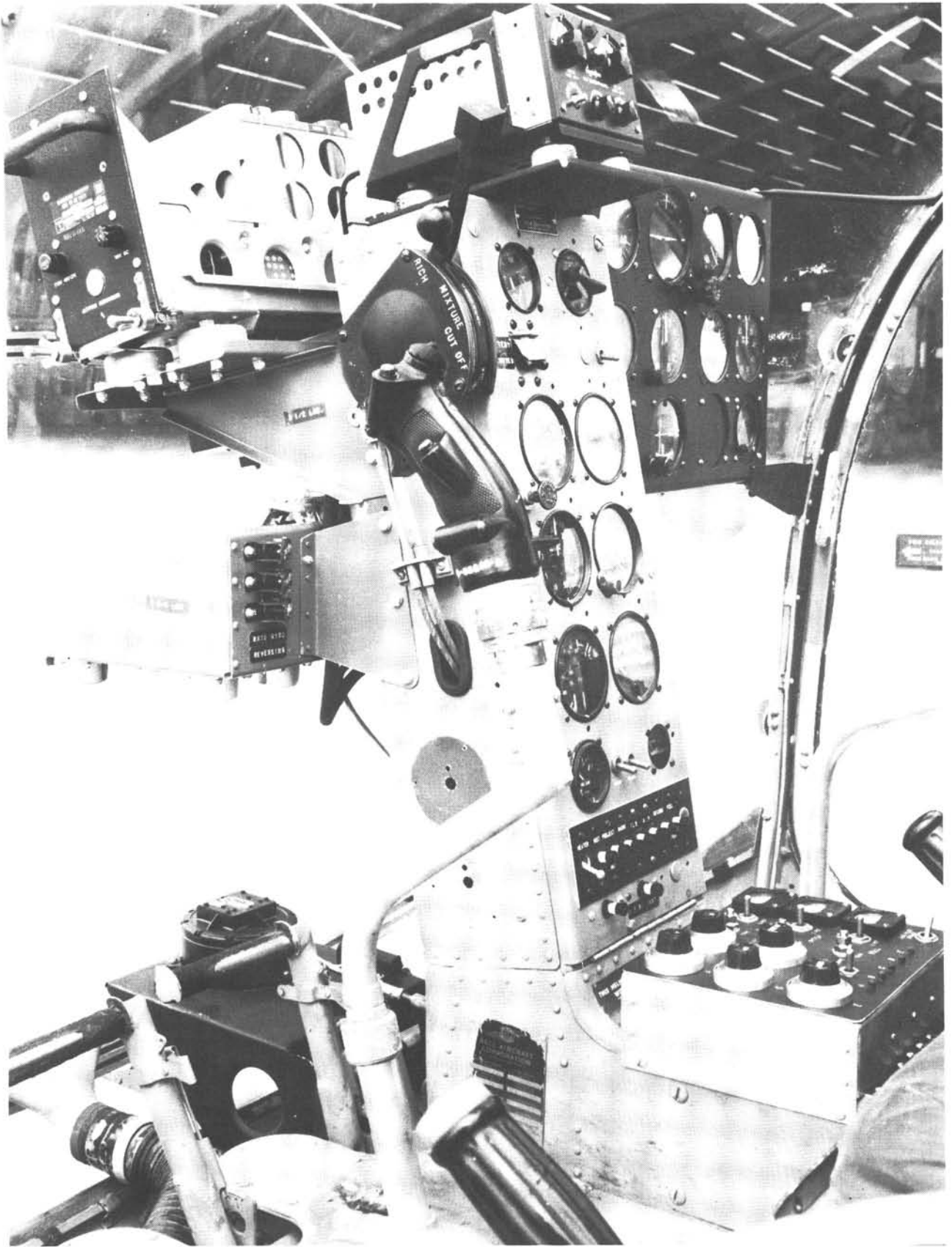


FIG. 5
LR-352

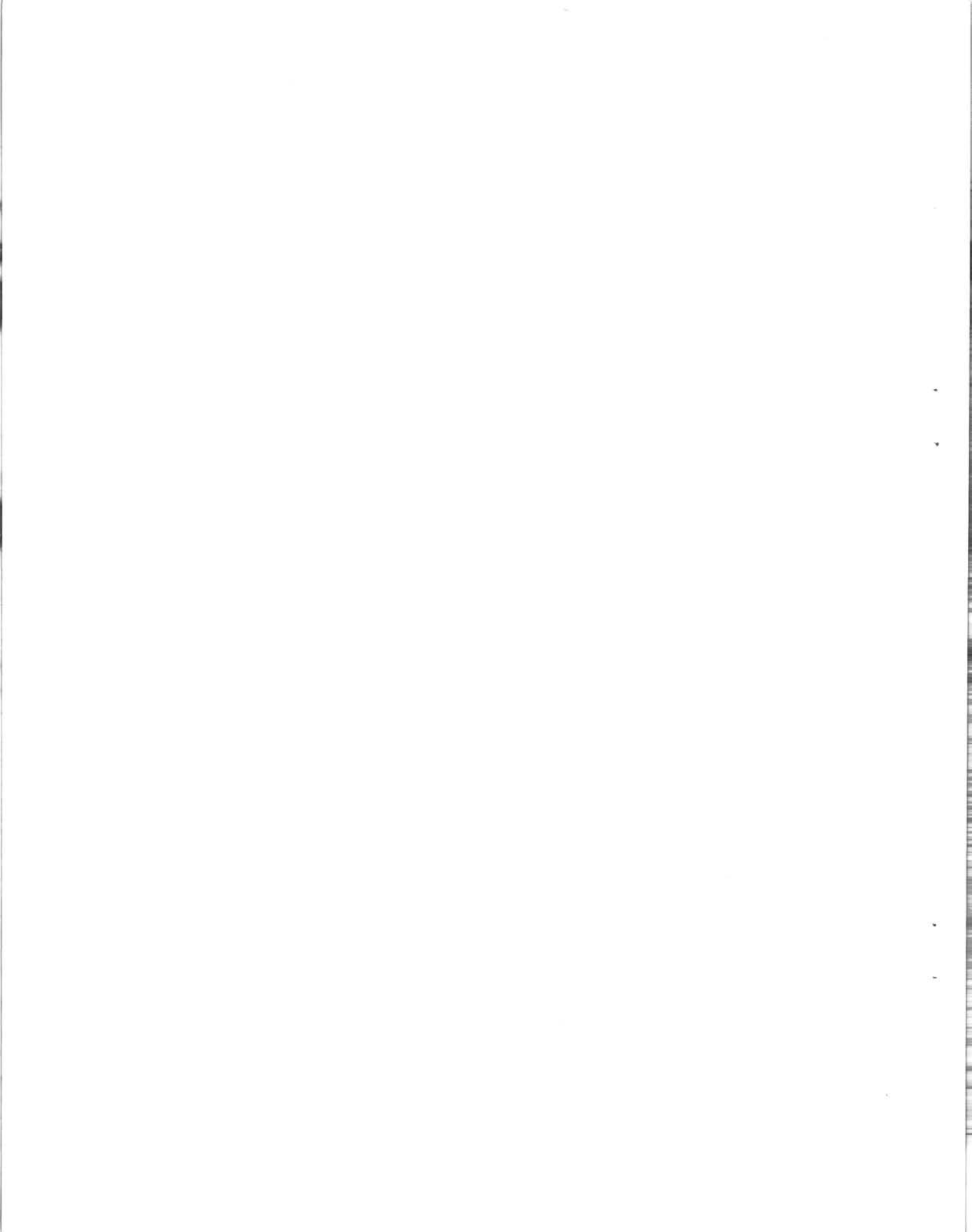


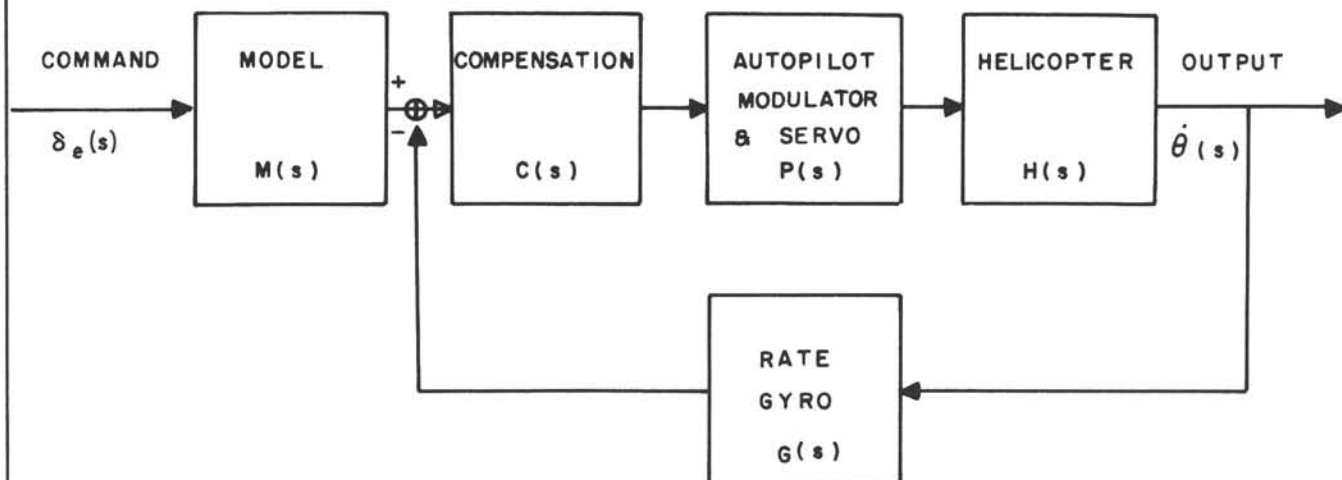
VIEW OF COCKPIT FROM RIGHT SIDE





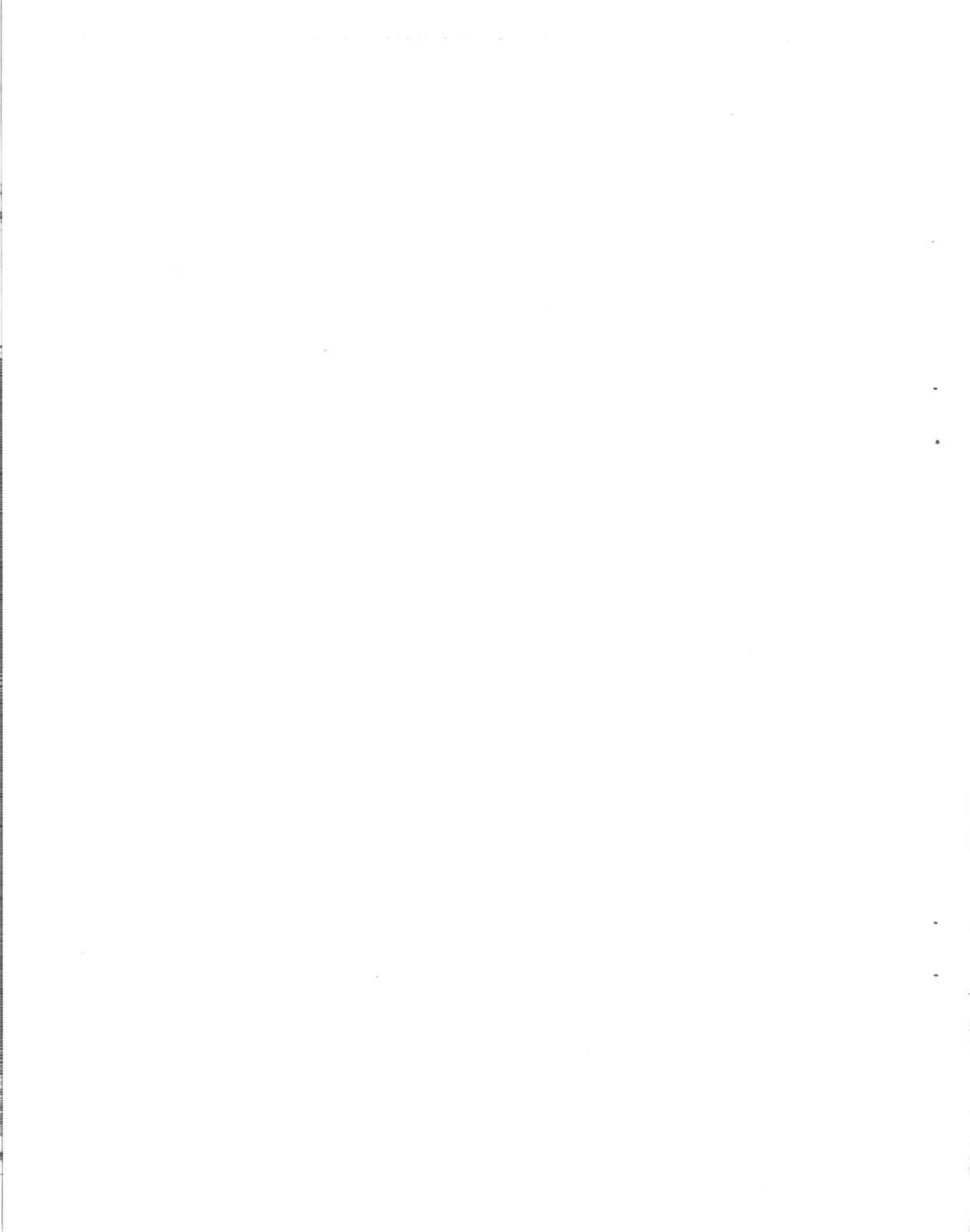
VIEW OF COCKPIT FROM LEFT SIDE

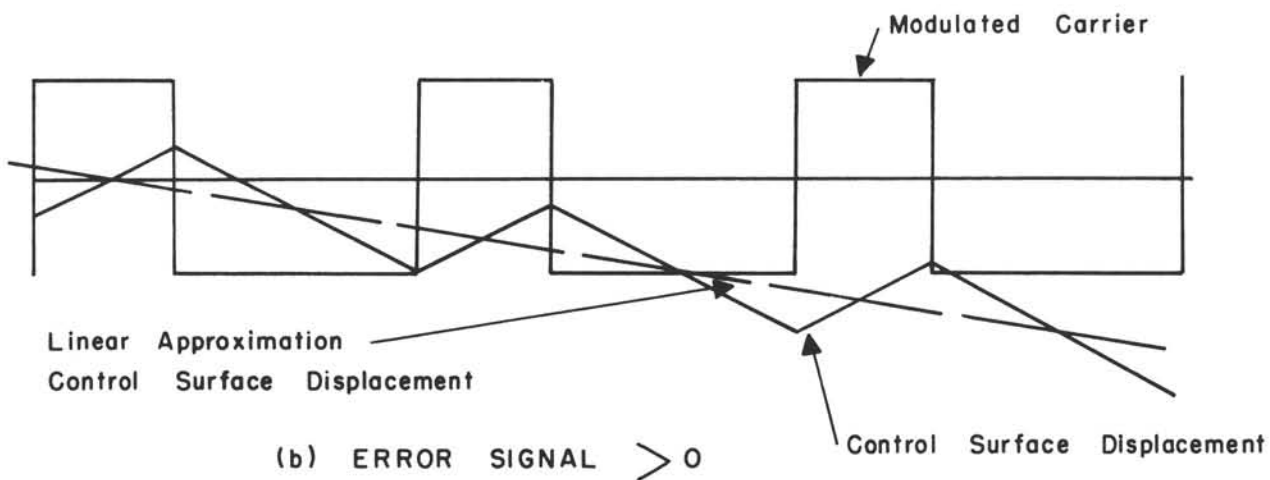
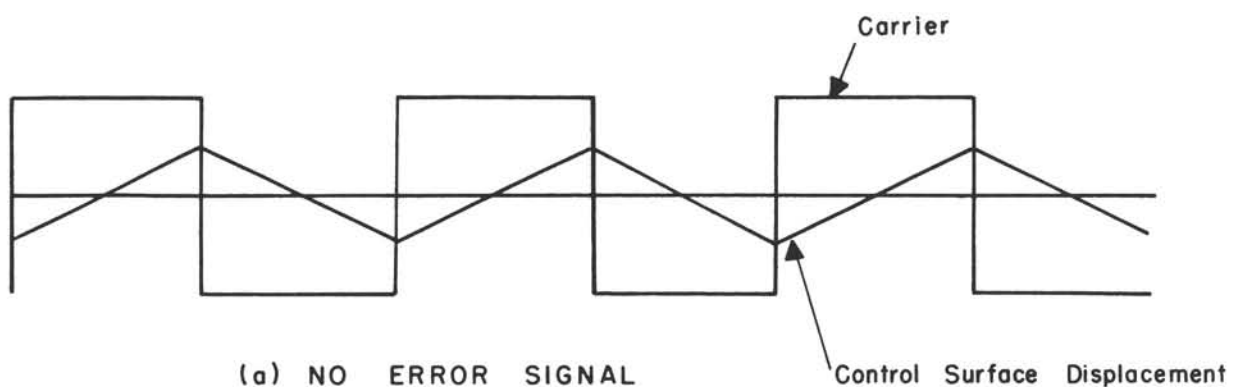
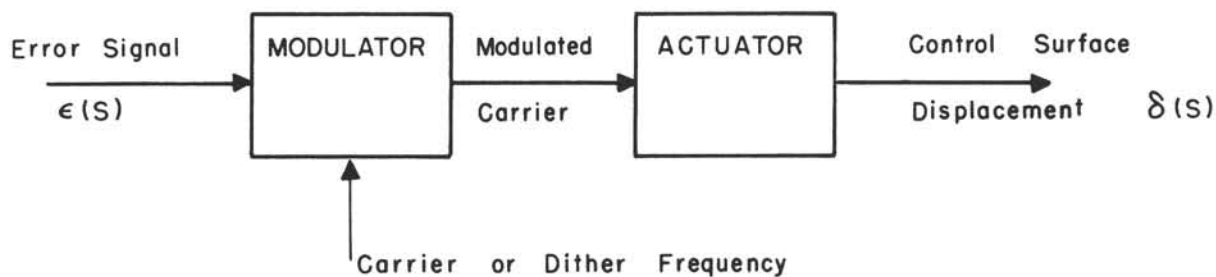




$$\frac{\dot{\theta}(s)}{\delta_e(s)} = \frac{M(s)}{G(s) + \frac{1}{C(s) \cdot P(s) \cdot H(s)}}$$

SIMPLIFIED MODEL-CONTROLLED AUTOPILOT

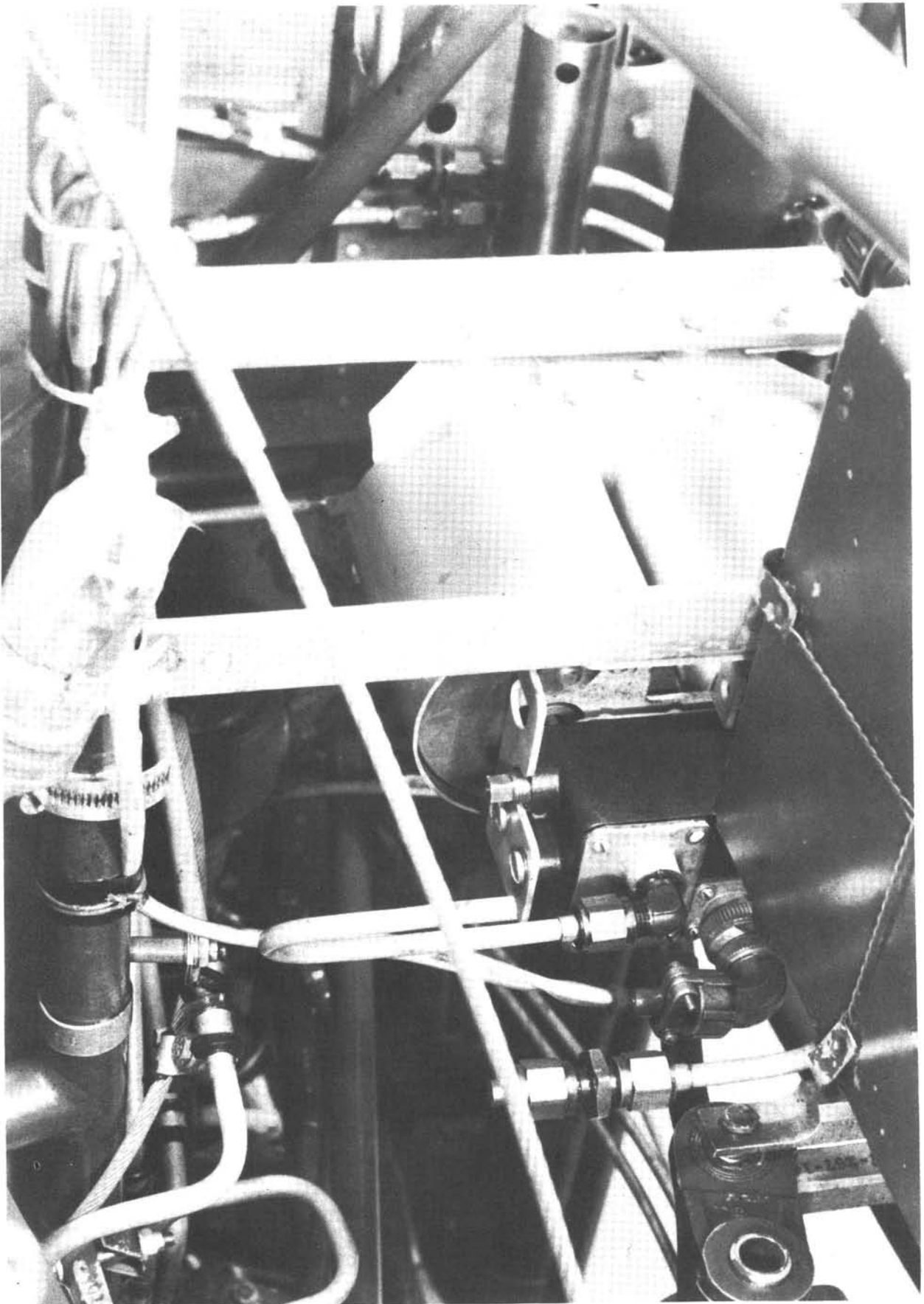




$$\frac{\delta(s)}{\epsilon(s)} = \frac{K_2}{s}$$

LINEARIZATION OF "BANG-BANG" SERVO ACTUATOR





SERVO ACTUATOR - LONGITUDINAL CYCLIC CONTROL

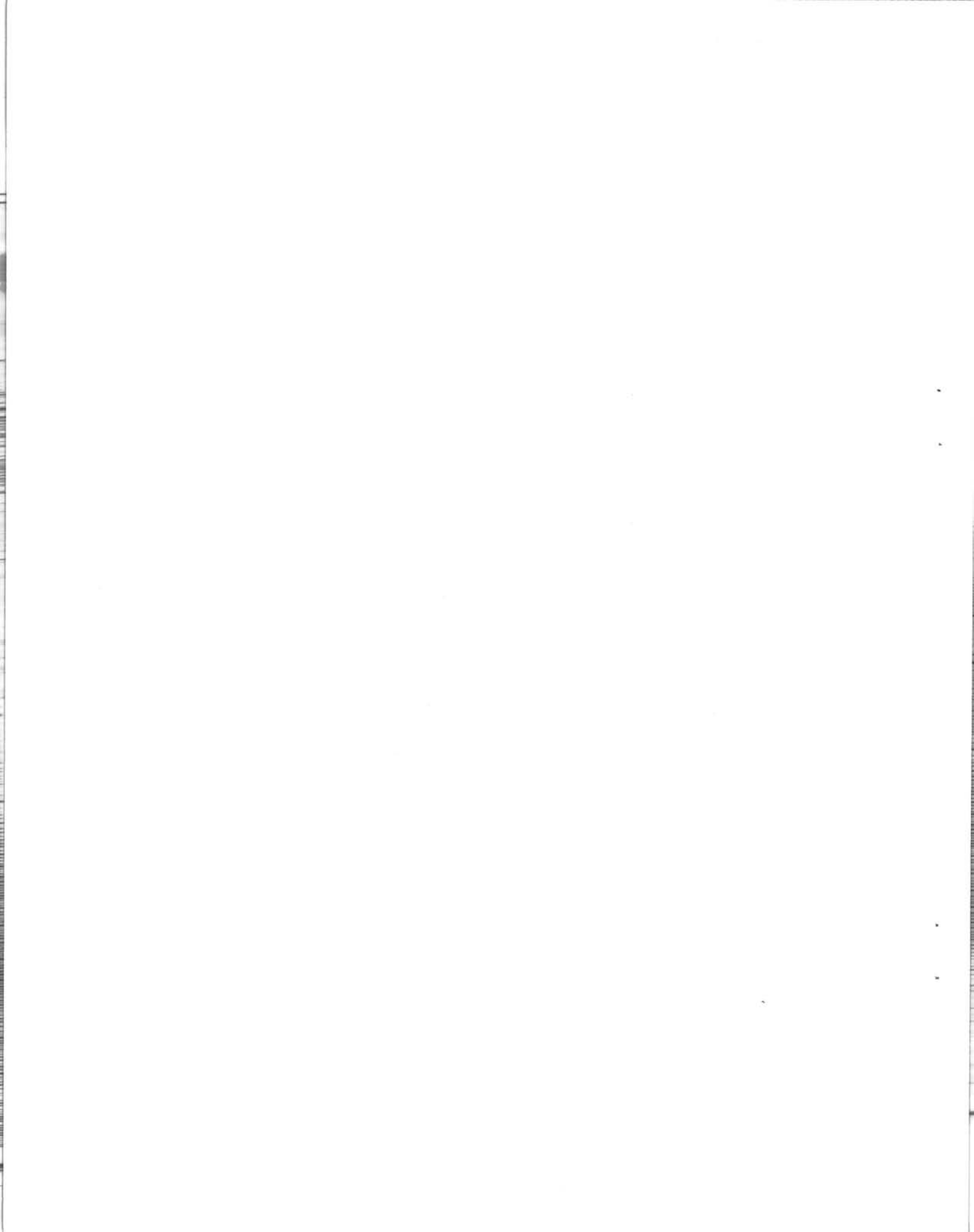
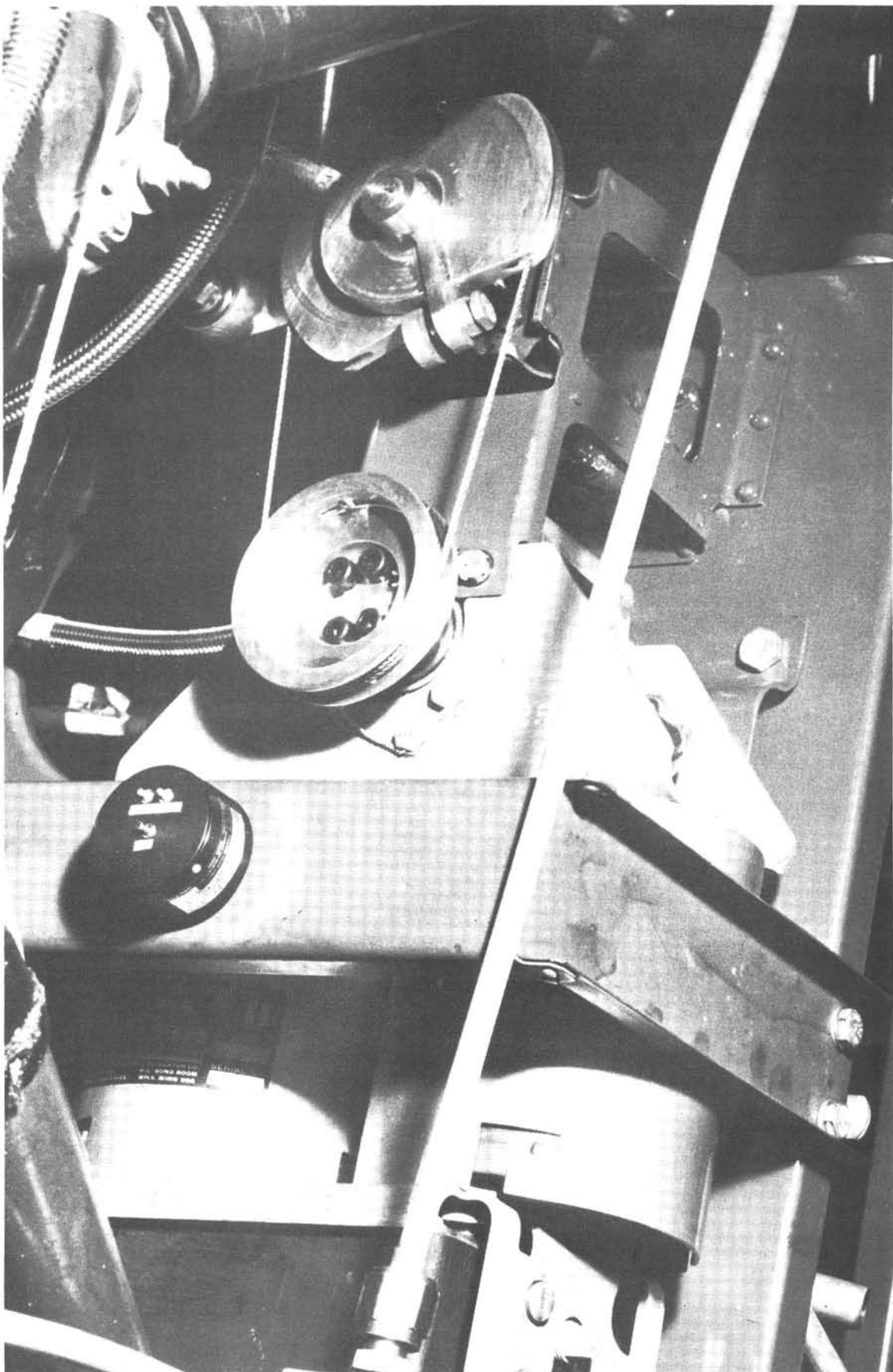


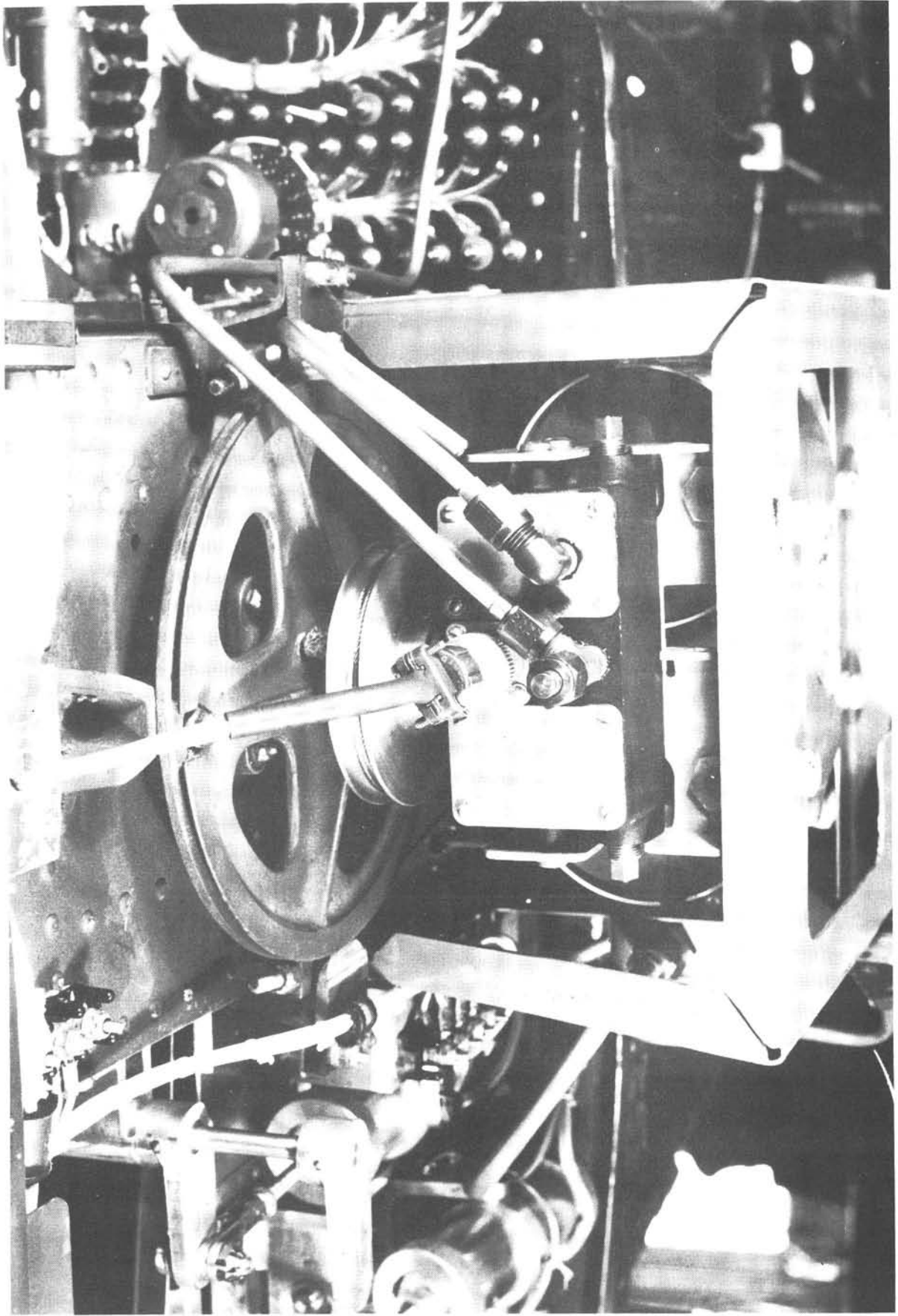
FIG. 10
LR-352



SERVO ACTUATOR - LATERAL CYCLIC CONTROL

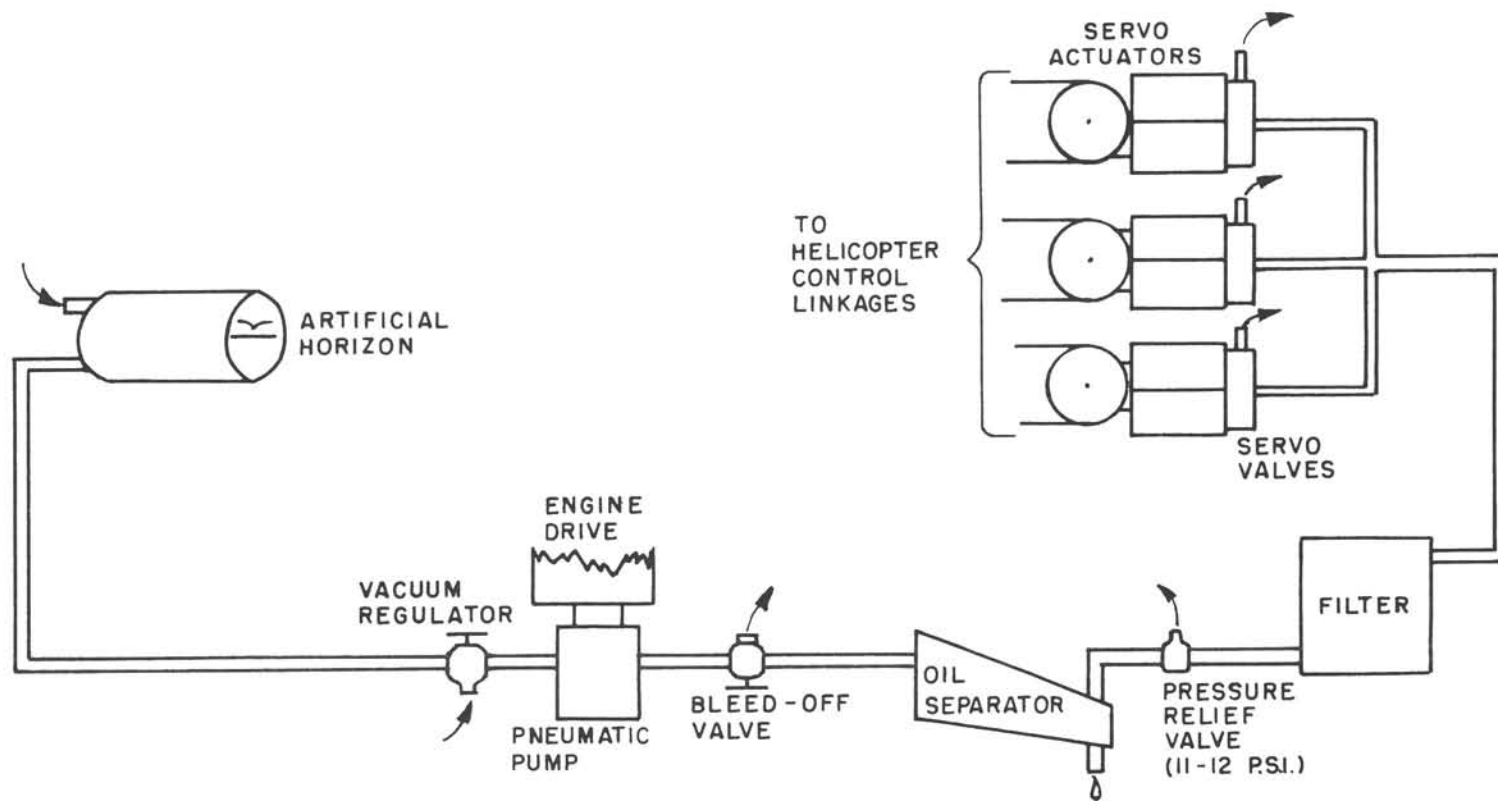


FIG. II
LR-352



SERVO ACTUATOR - TAIL ROTOR CONTROL





BLOCK DIAGRAM OF PNEUMATIC SYSTEM

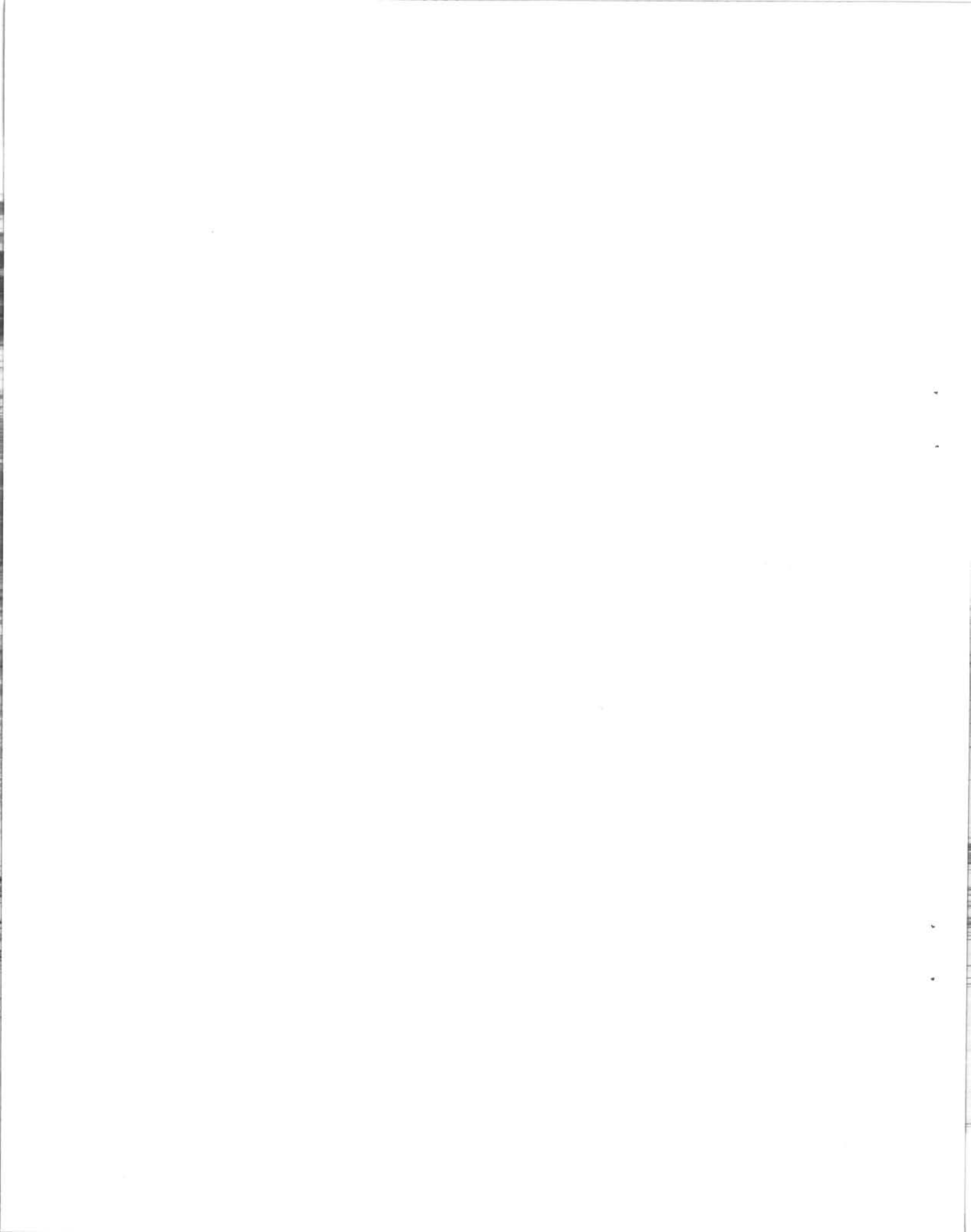
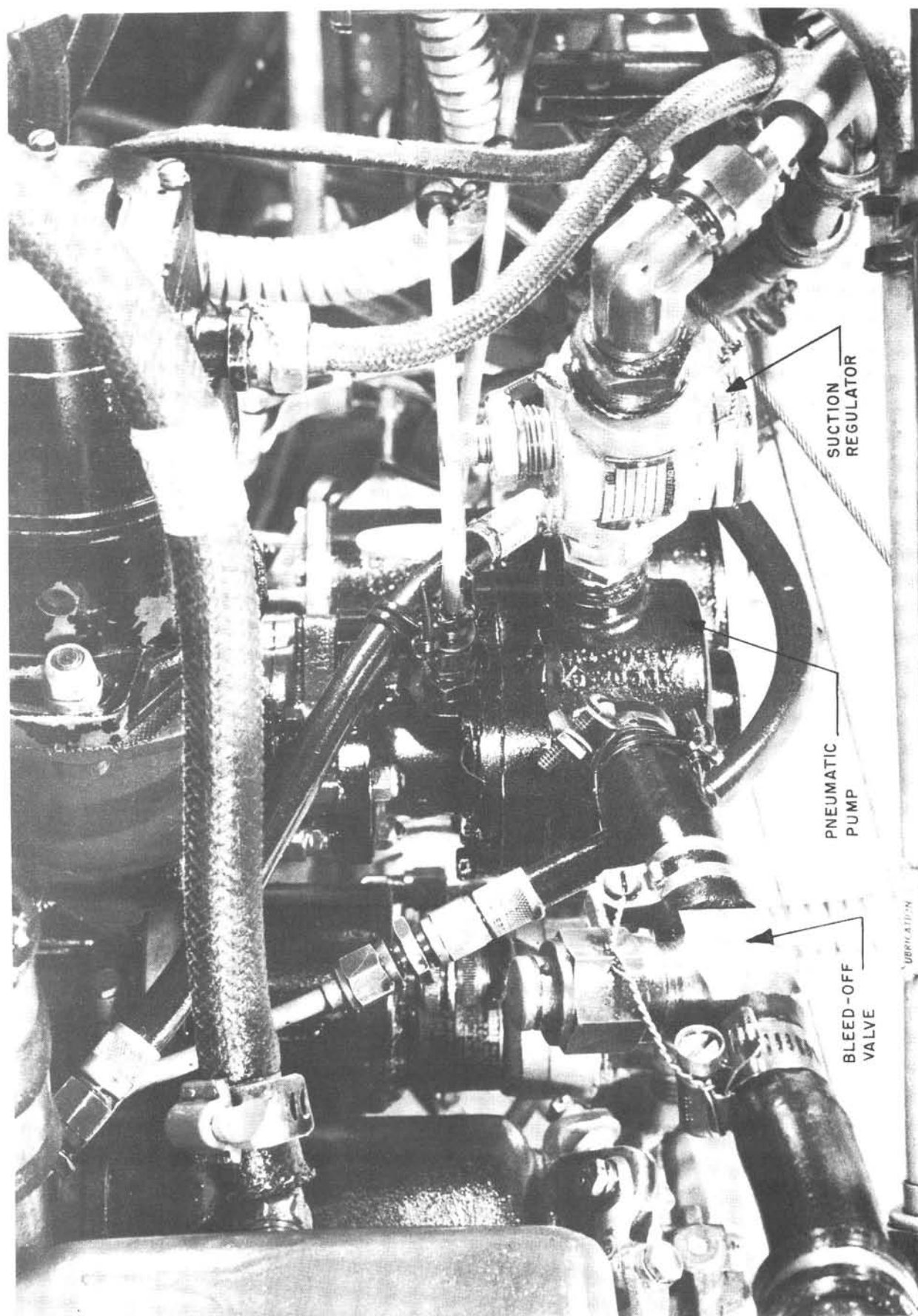


FIG. 13
LR-352



PNEUMATIC PUMP ASSEMBLY

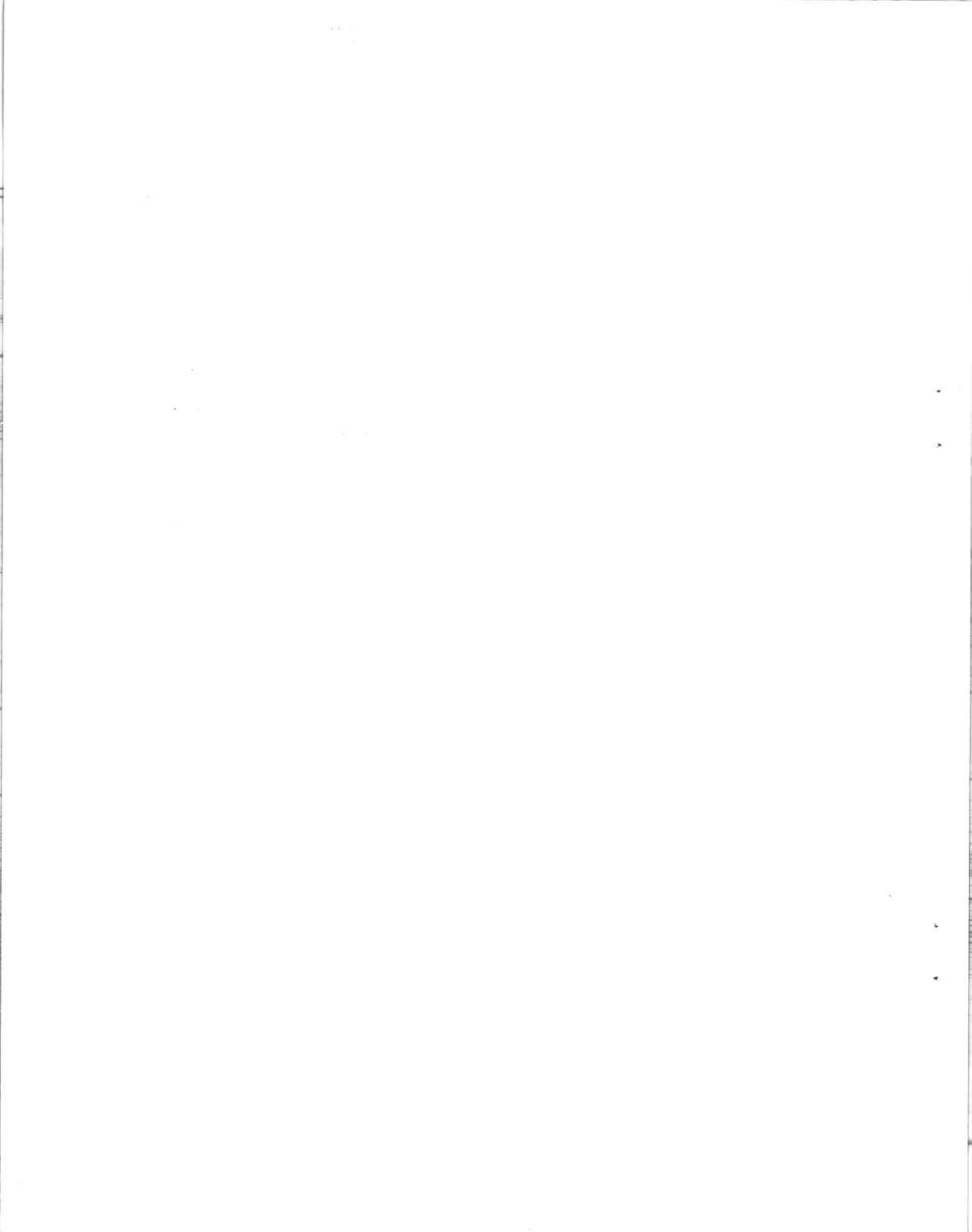
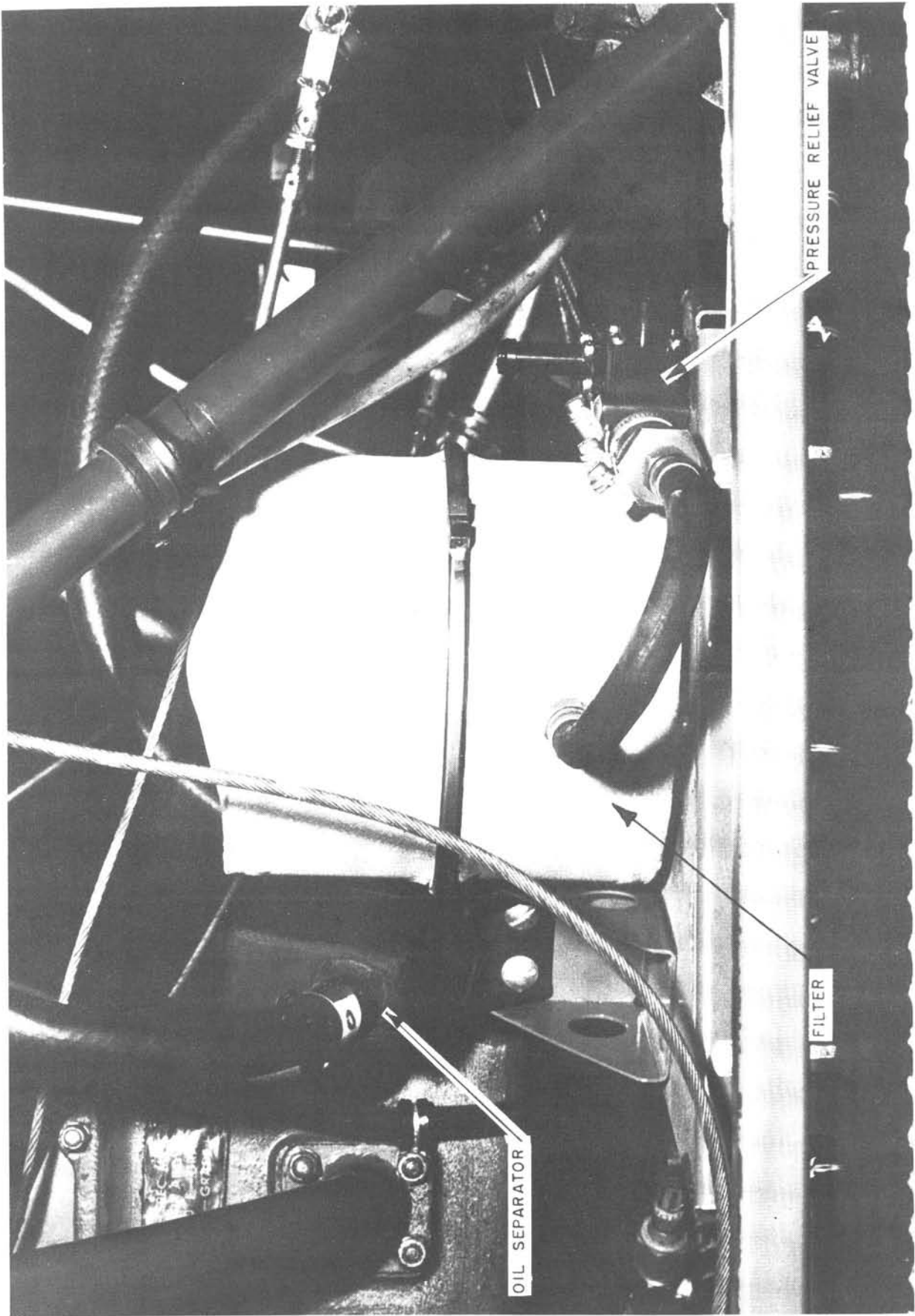
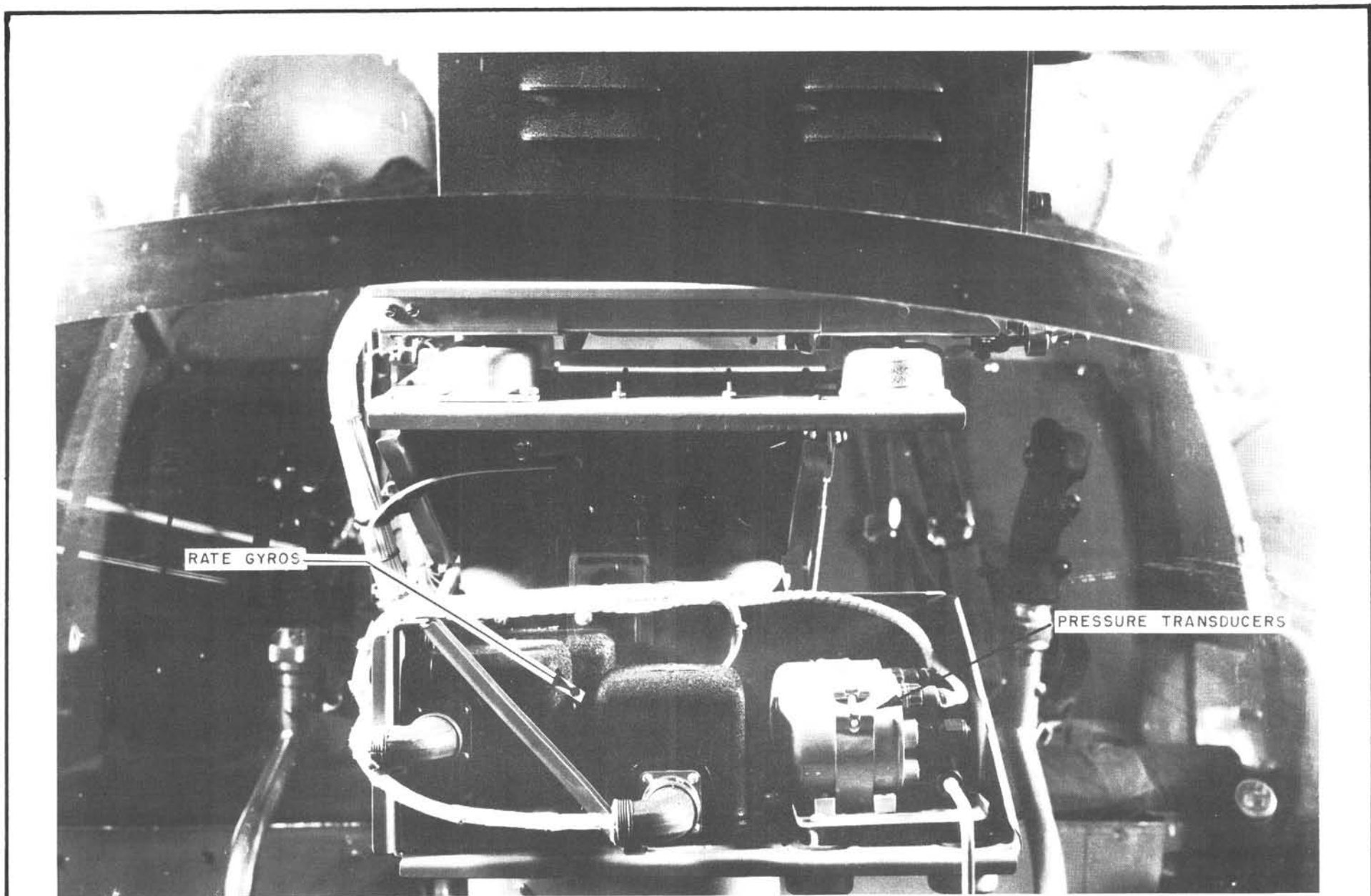


FIG. 14
LR-352



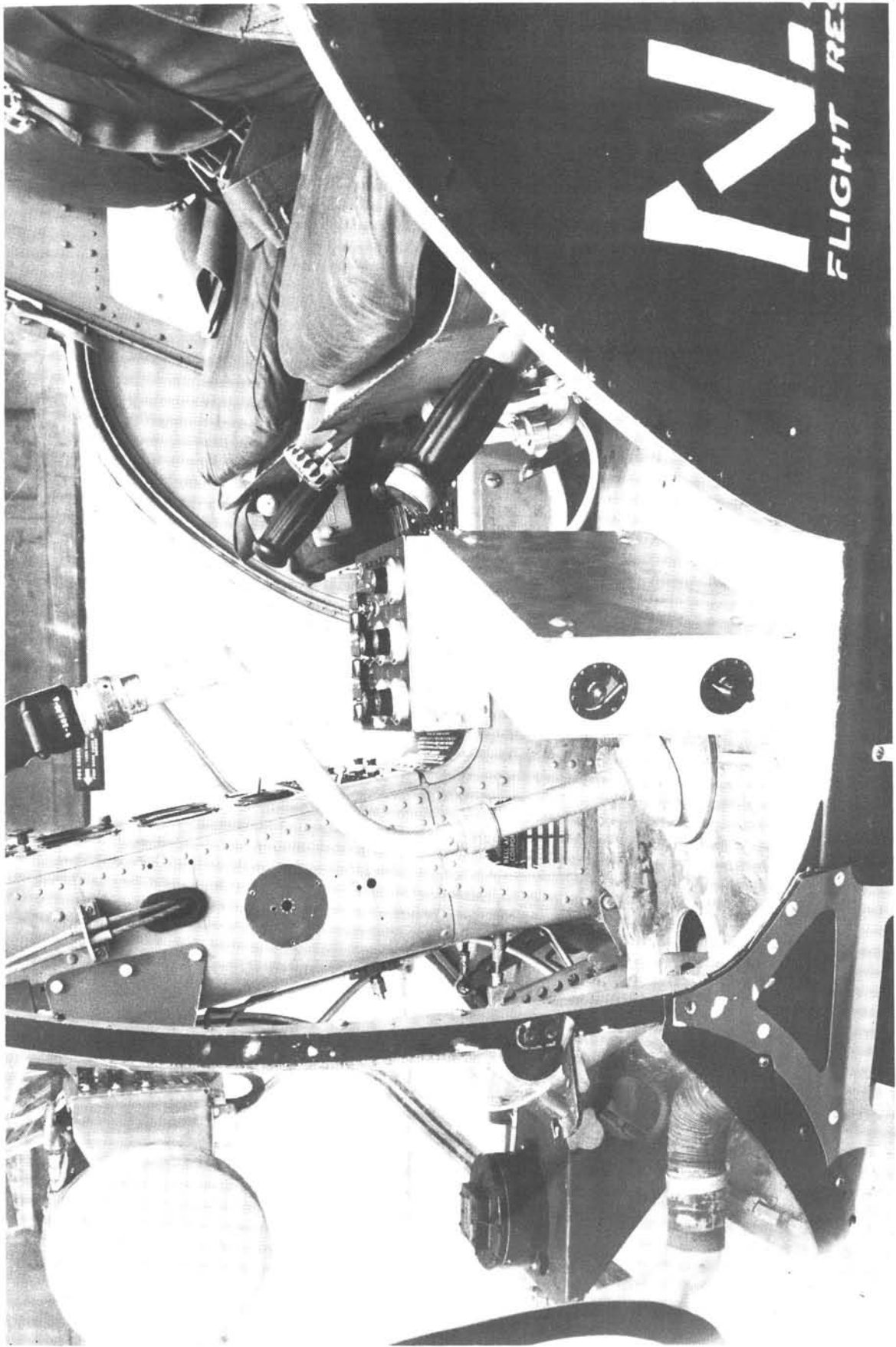
VIEW OF FILTER, OIL SEPARATOR, AND PRESSURE RELIEF VALVE



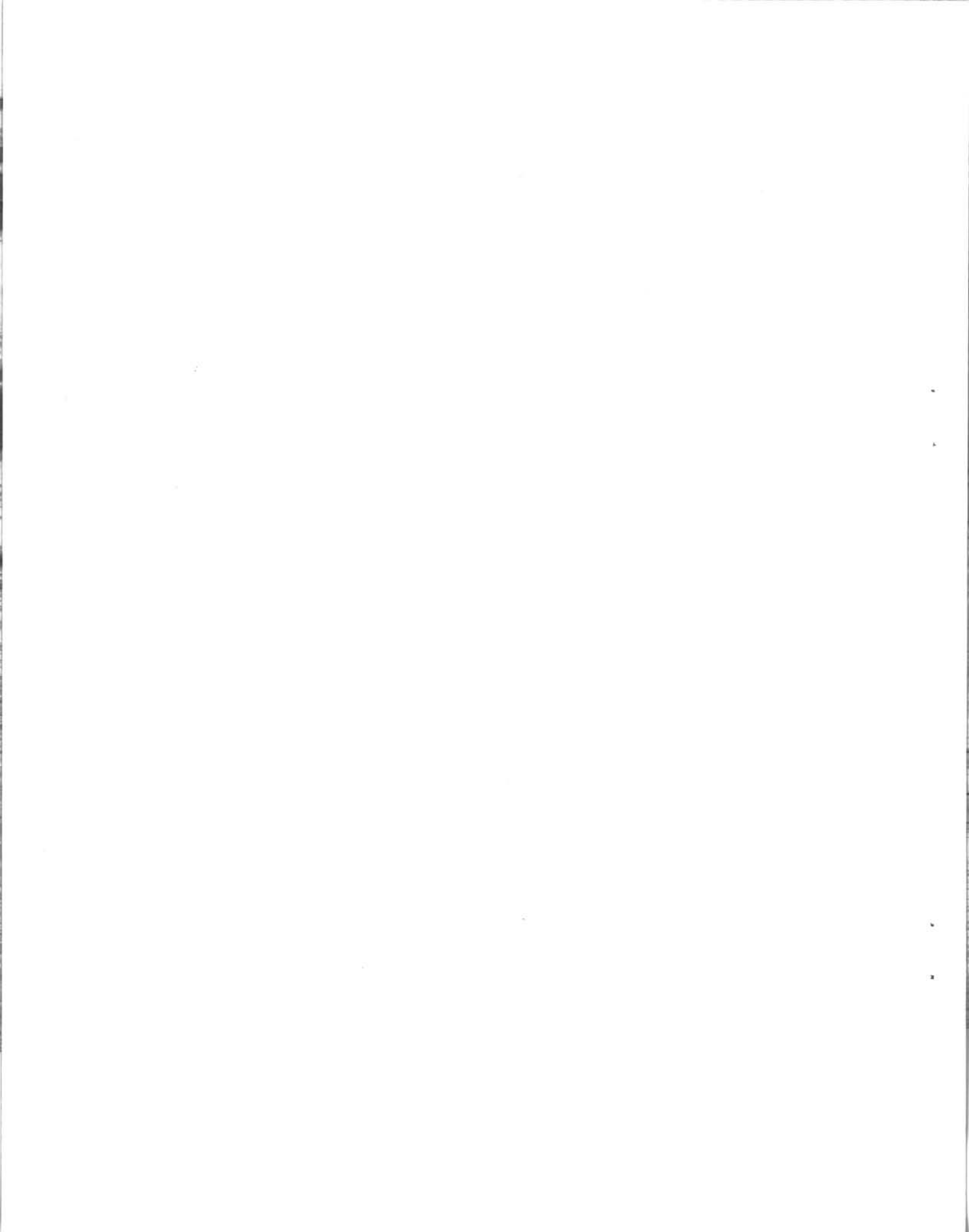


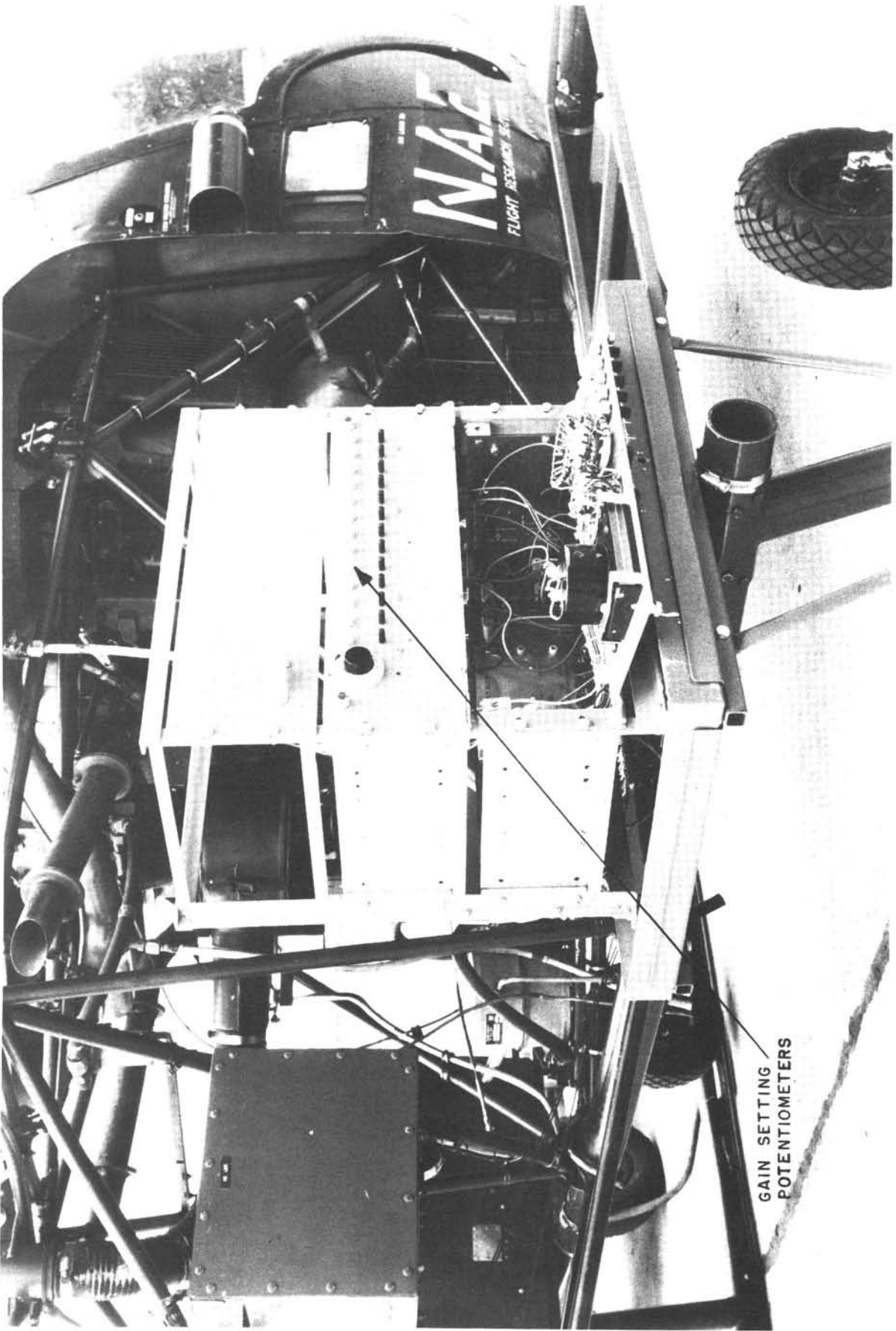
MOUNTING OF RATE GYROS AND PRESSURE TRANSDUCERS





CALIBRATION BOX IN POSITION





GAIN SETTING
POTENTIOMETERS

MOUNTING OF ANALOGUE COMPUTER

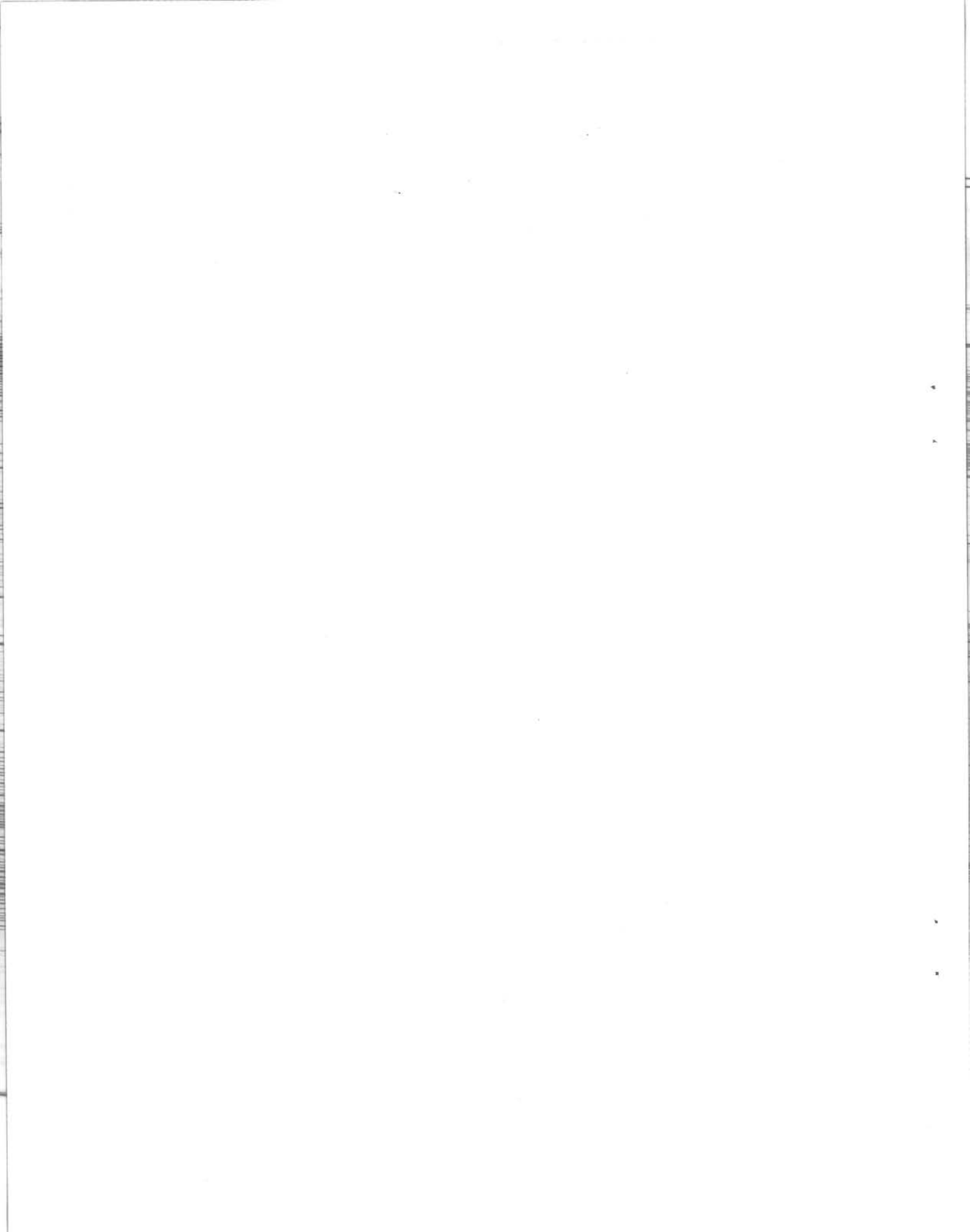
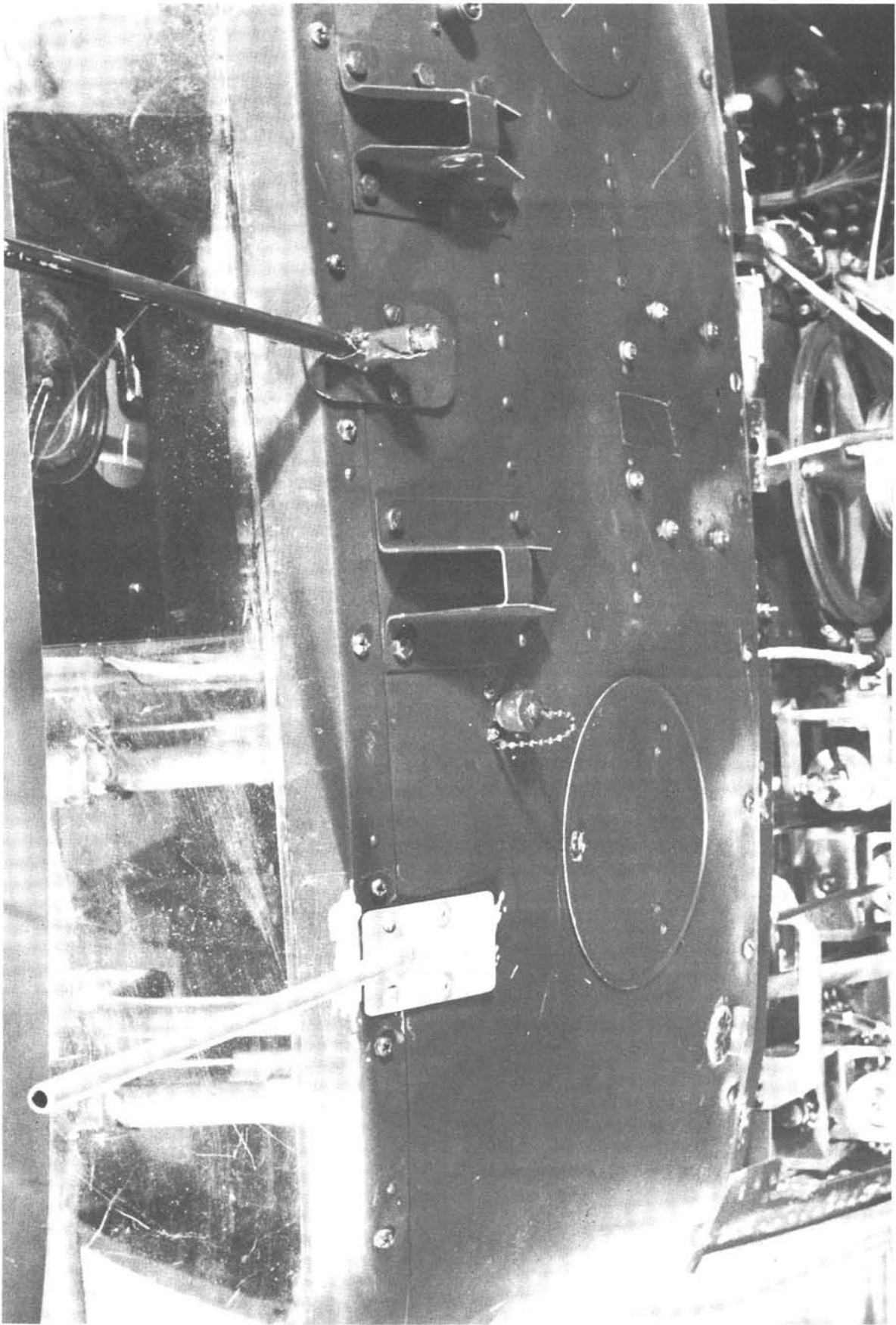


FIG. 18
LR-352

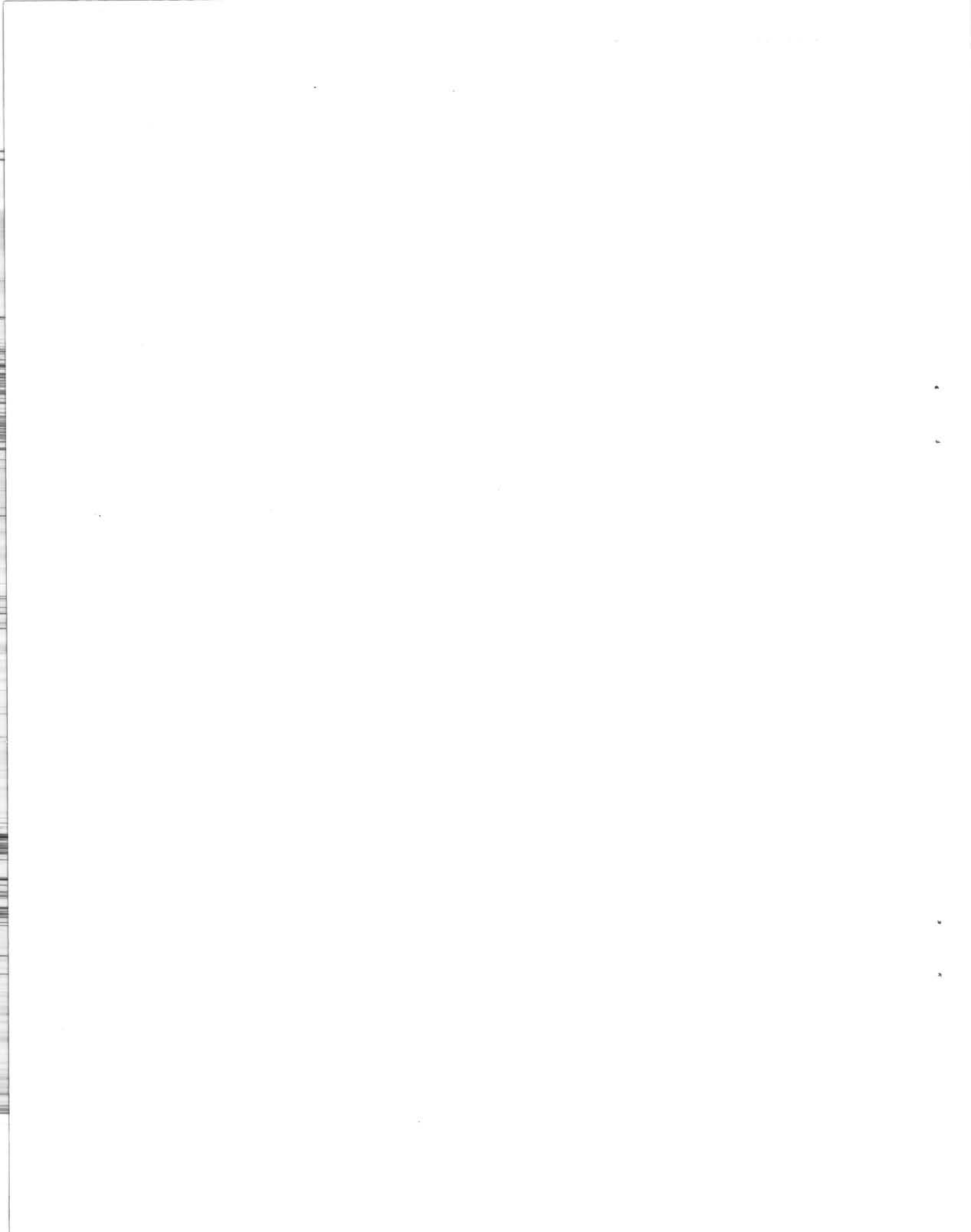


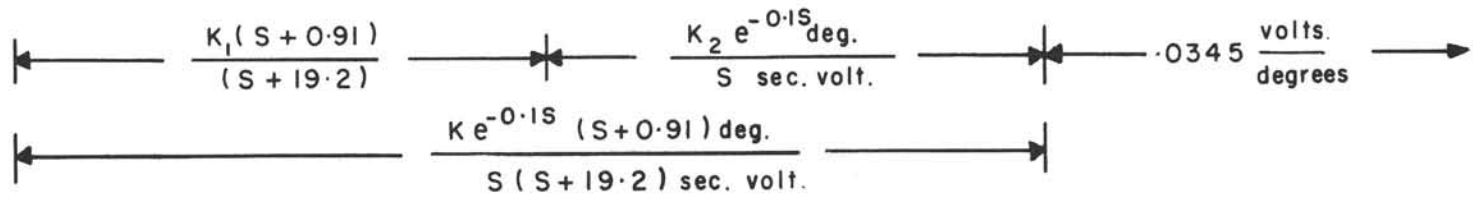
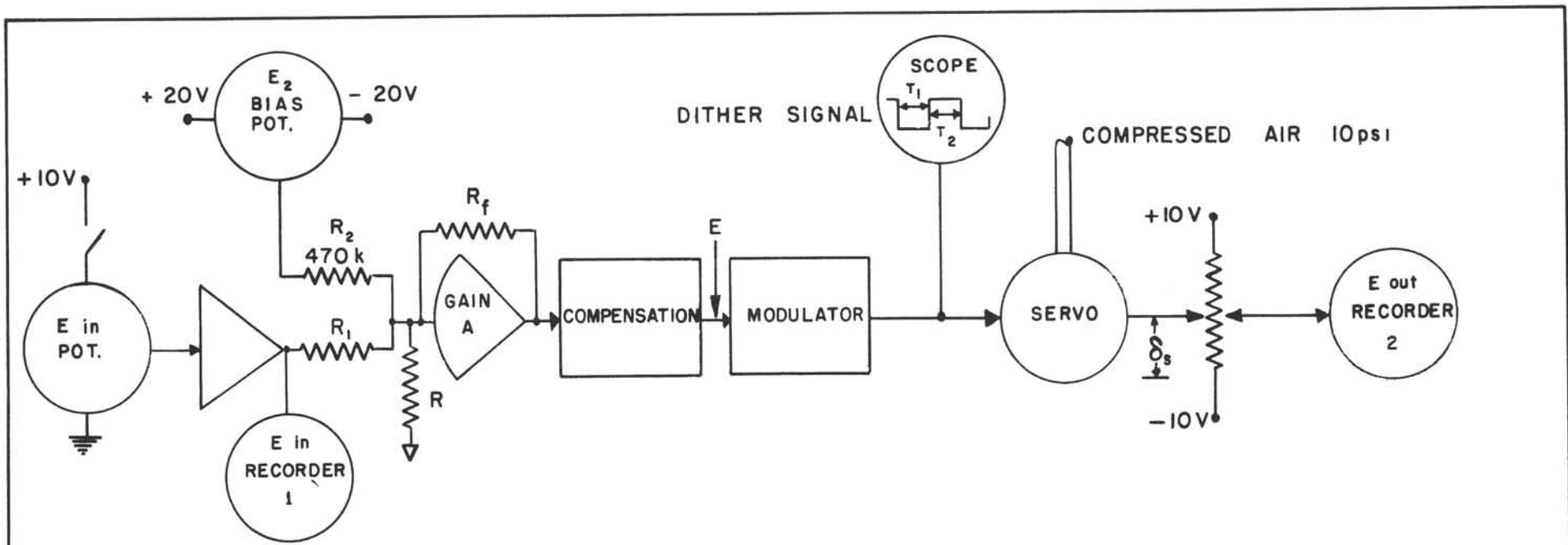
CONTROL SPRING FEEL UNIT

FIG. 19
LR-352



INSTALLATION OF TOTAL HEAD PRESSURE PROBES





← INPUT SIGNAL AND RECORDER AUTOPILOT COMPONENTS OUTPUT POTENTIOMETER AND RECORDER →

$$E = \left(\frac{E_{in}}{R_1} + \frac{E_2}{R_2} \right) \frac{ARR_f}{\left[R(1-A) + R_f + \frac{RR_f(R_1+R_2)}{R_1R_2} \right]} = \left[\frac{E_{in}}{R_1} + \frac{E_2}{R_2} \right] \frac{-1.815 \times 10^7}{\left[9 \times 10^3 + \frac{8.41 \times 10^7(R_1+R_2)}{R_1R_2} \right]}$$

SIMPLIFIED BLOCK DIAGRAM OF THE AUTOPILOT

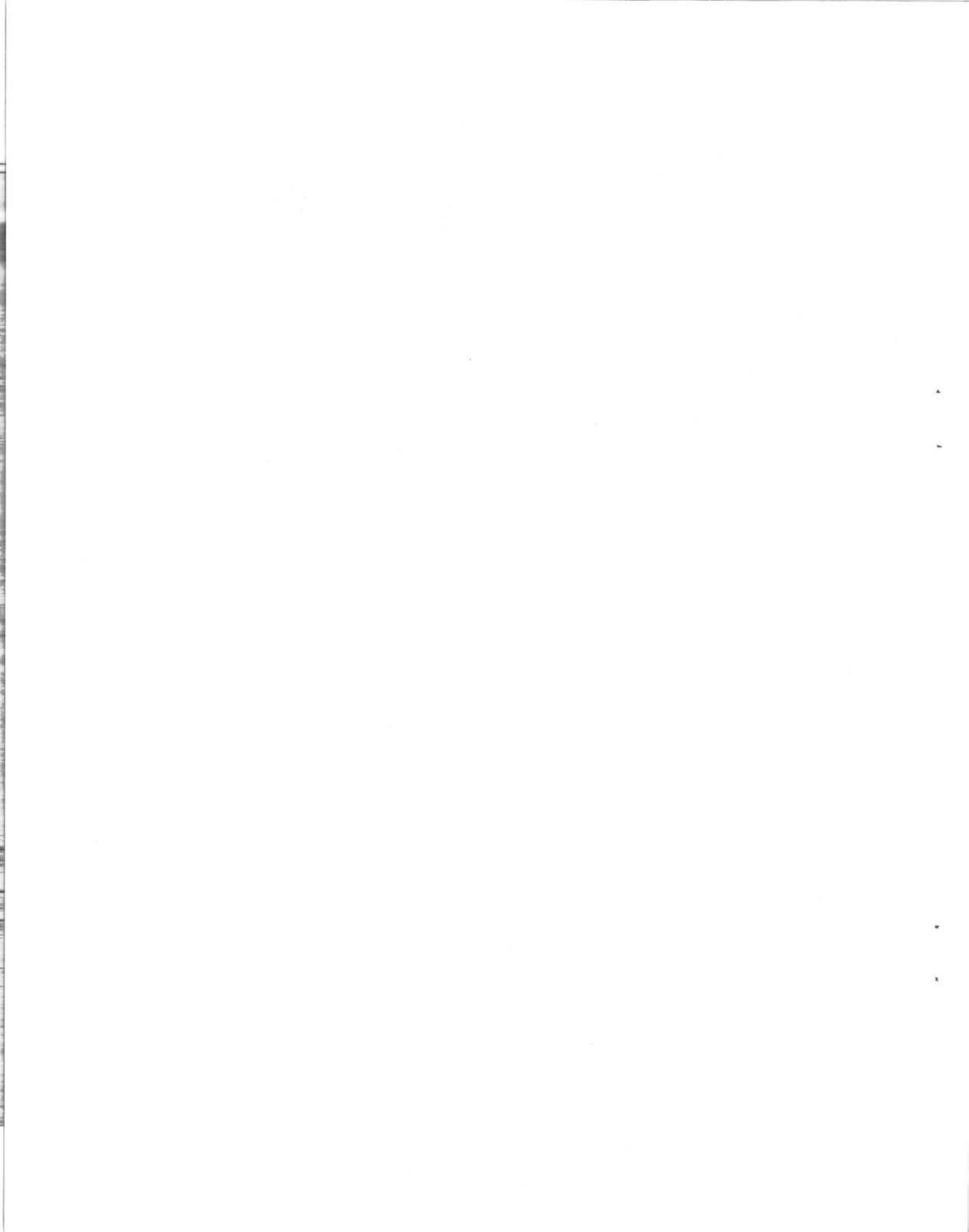
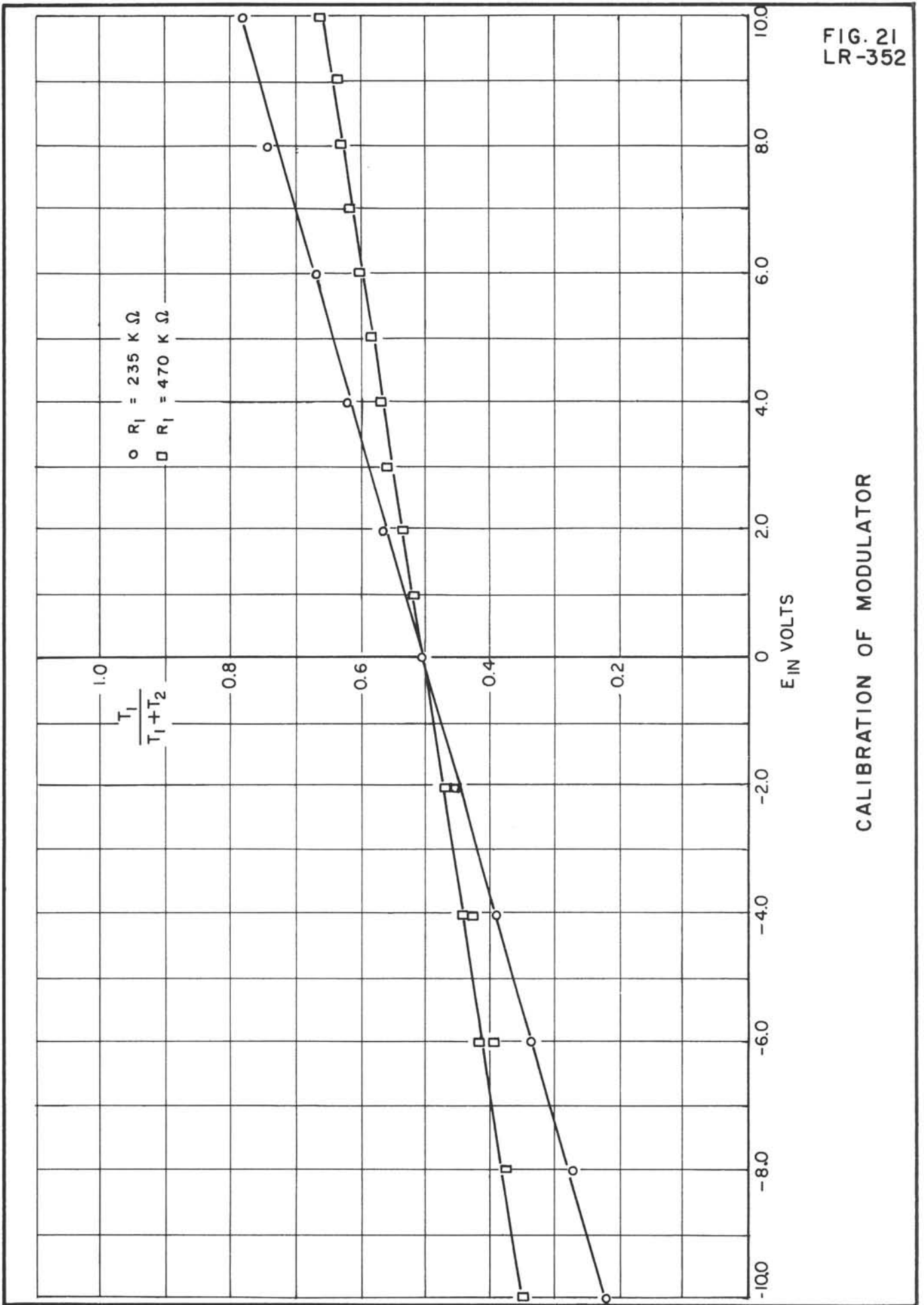
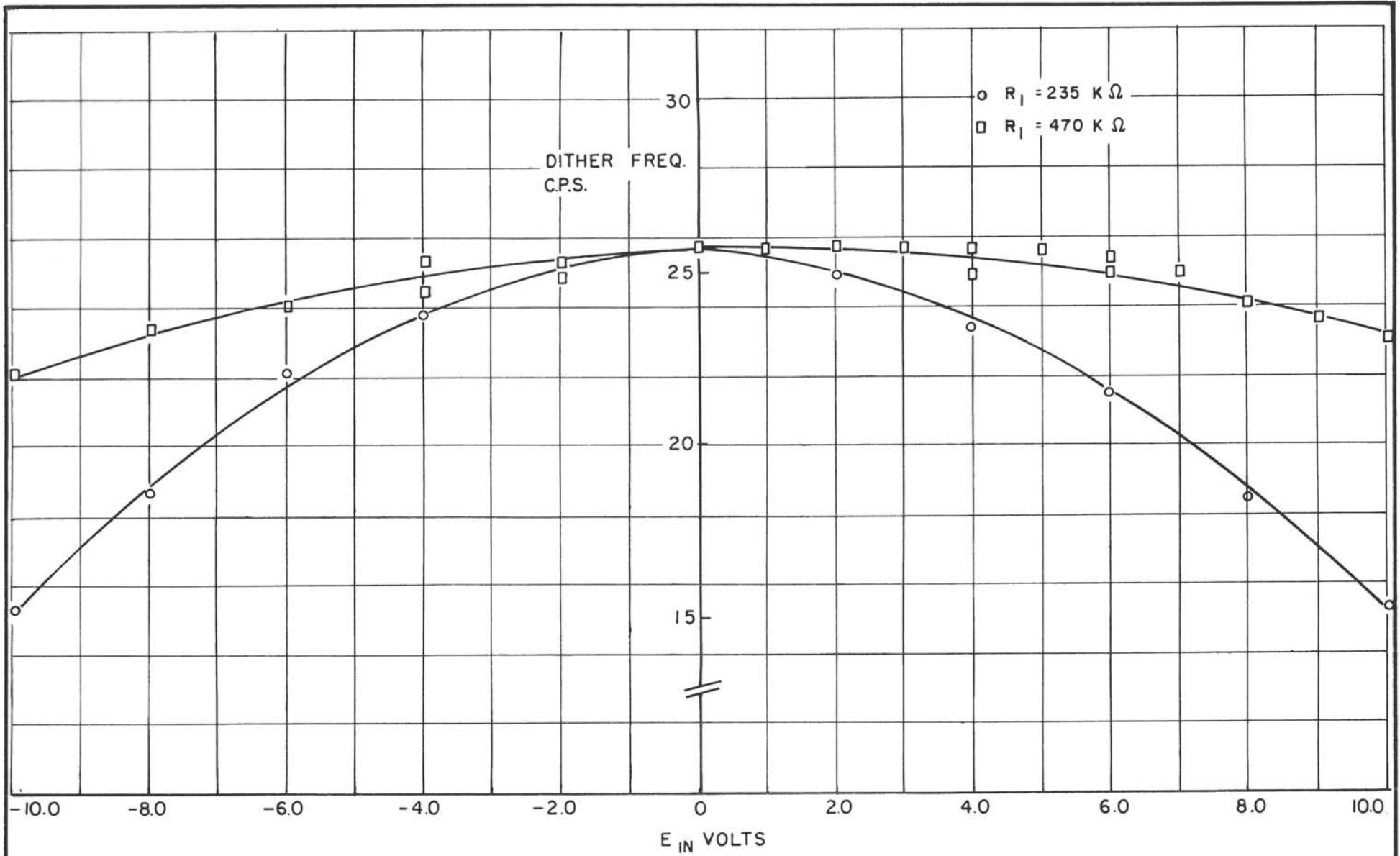


FIG. 21
LR-352



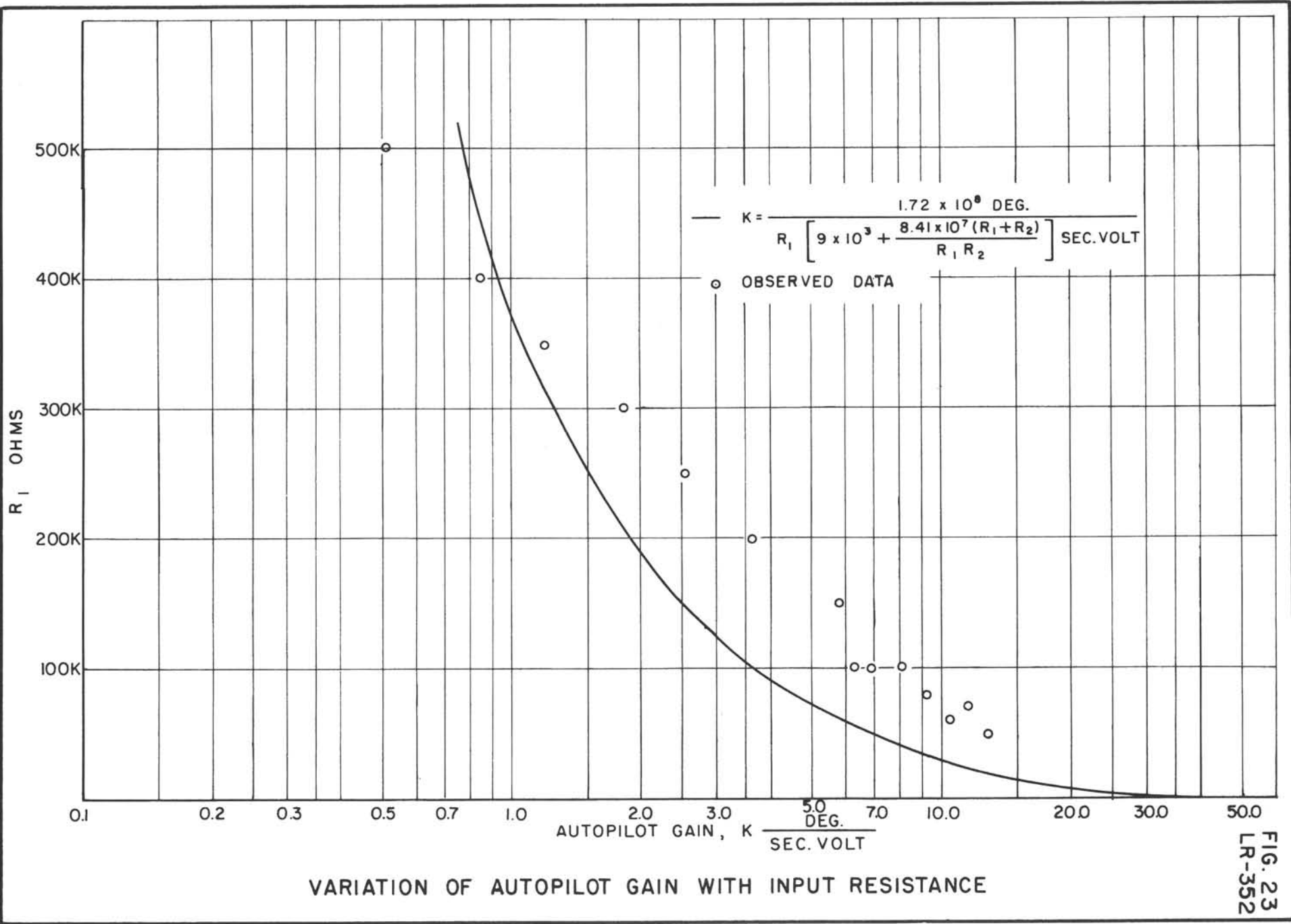
CALIBRATION OF MODULATOR





VARIATION OF DITHER FREQUENCY WITH E_{IN} AND R_{IN}





VARIATION OF AUTOPILOT GAIN WITH INPUT RESISTANCE



→ ← 1.0 SEC.

↓
↑ 1.0 VOLT

RECORDER NO. 1 E_{IN}

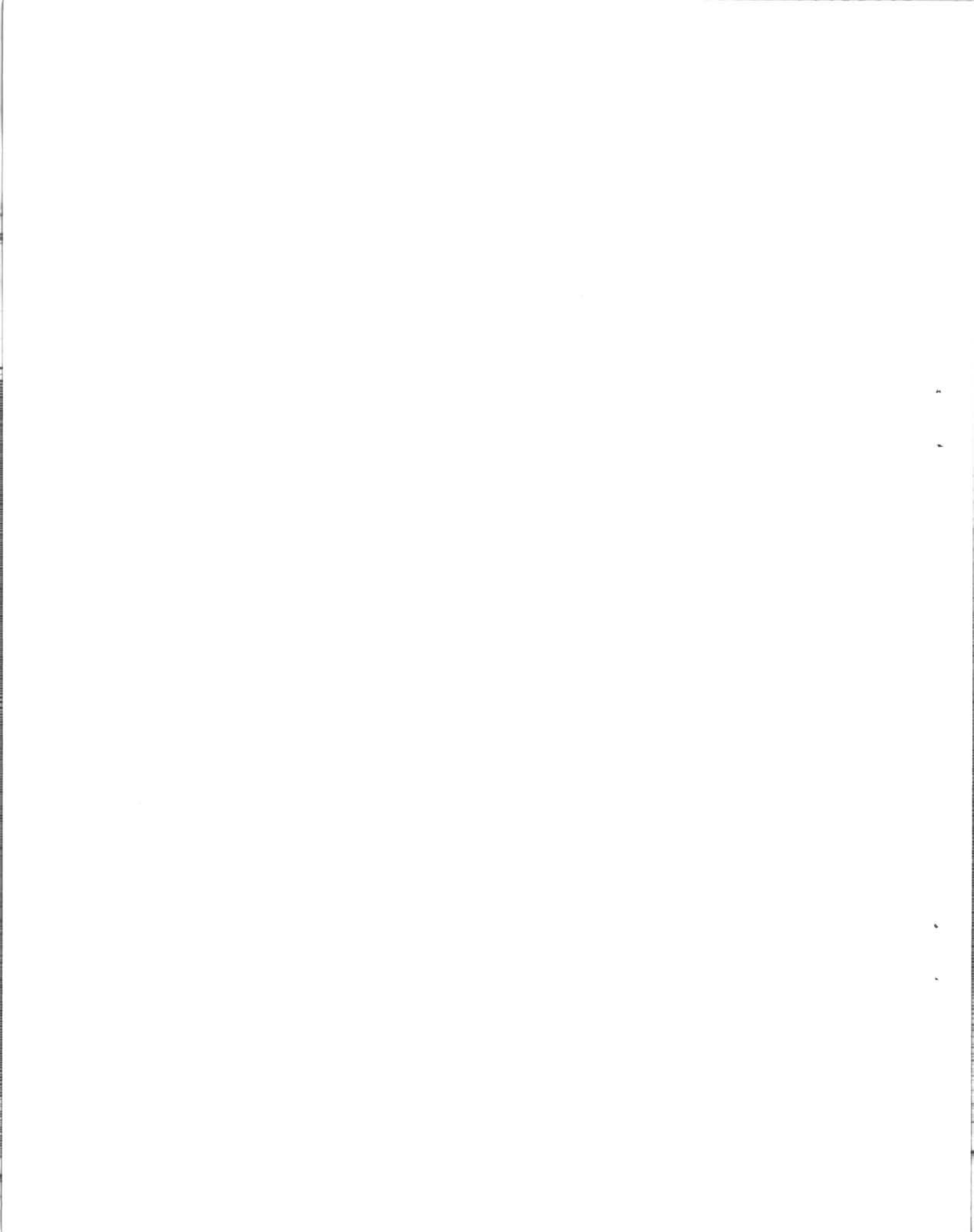
← 16.75 SECS. →
← APPARENT LAG 0.13 SEC. →

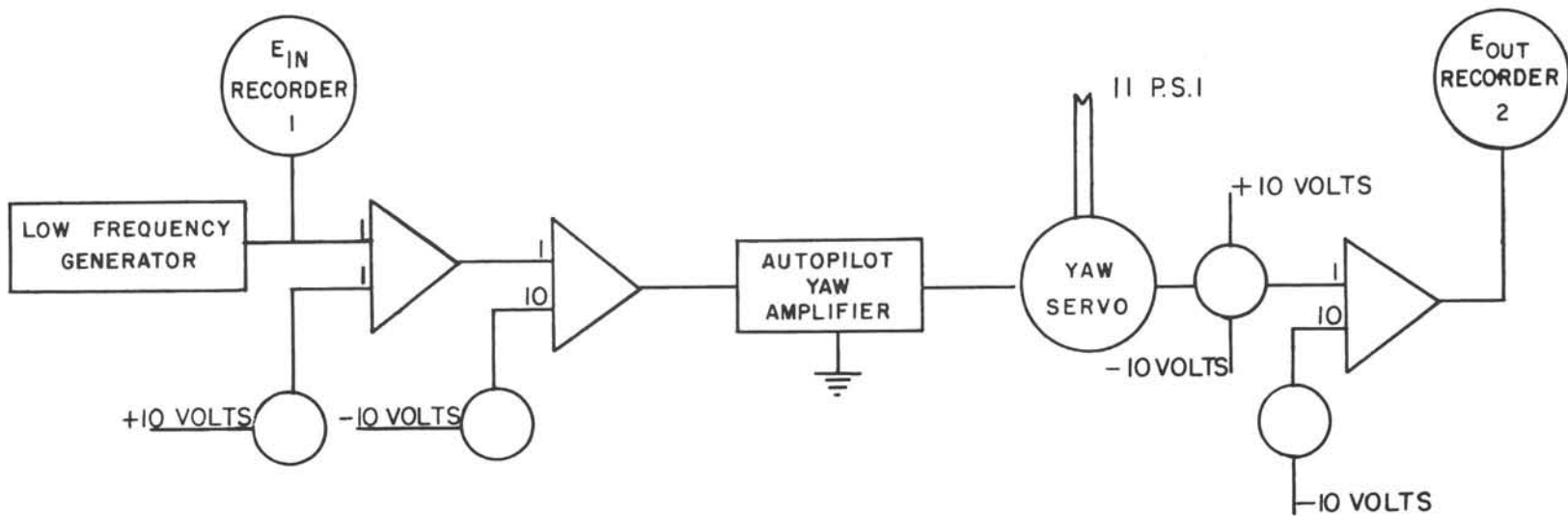
RECORDER NO. 2 E_{OUT}

+
0.5 VOLT

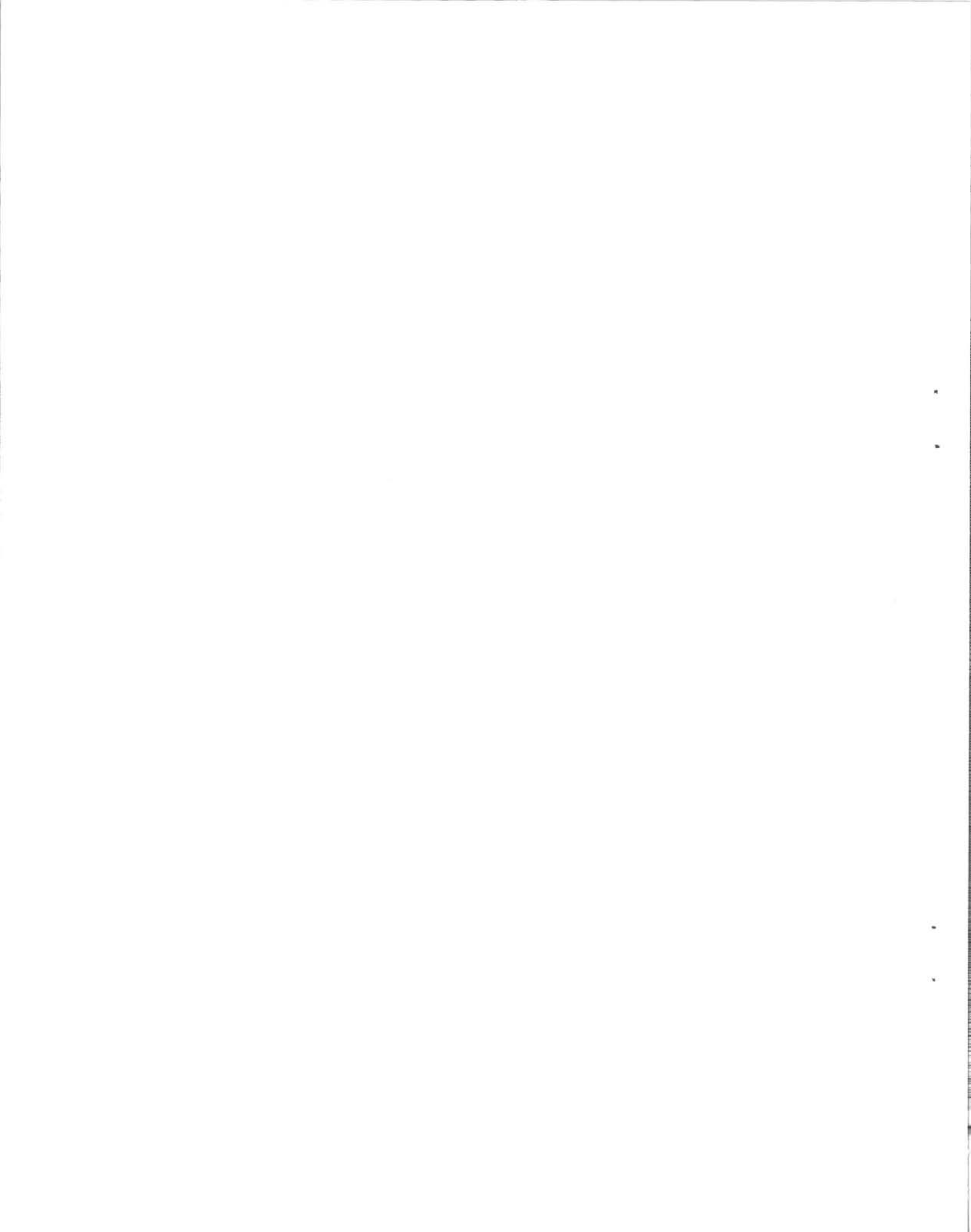
$$K = \frac{0.5}{16.75 \text{ SEC}} \cdot \frac{\text{deg.}}{(0.0345) \text{ VOLTS}} = 0.86 \frac{\text{deg.}}{\text{SEC. VOLT}} \text{ for } R_1 = 400K \Omega \quad 10\text{PSI}$$

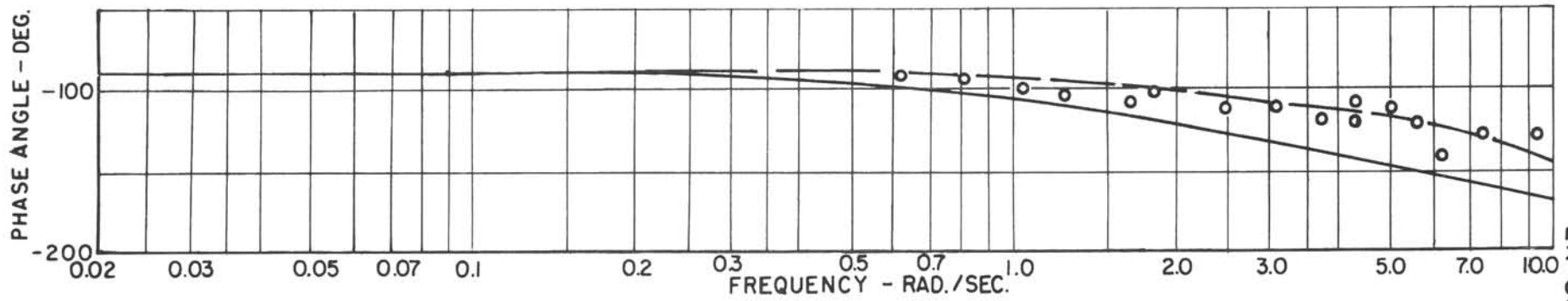
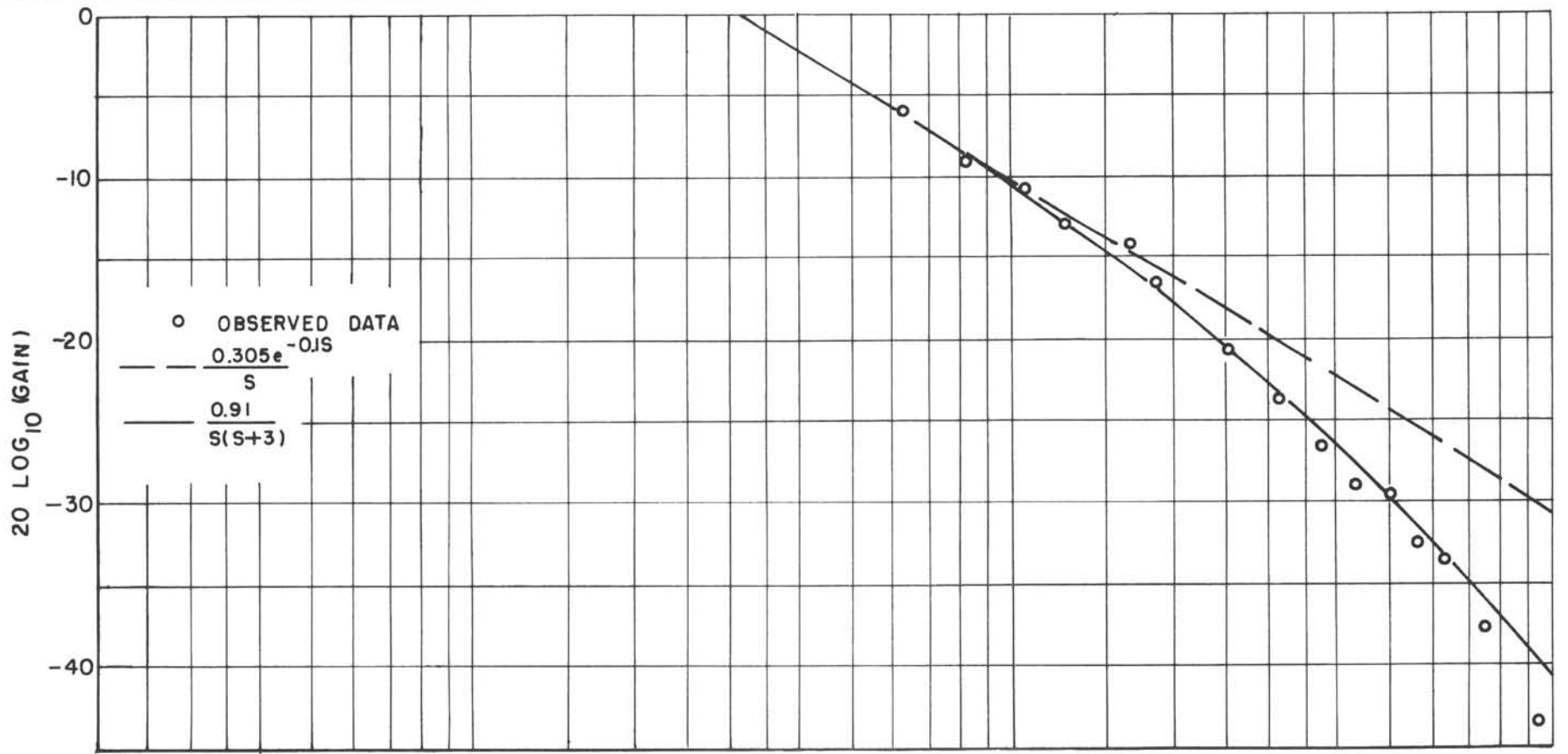
SAMPLE OF AUTOPILOT RESPONSE TO A STEP INPUT



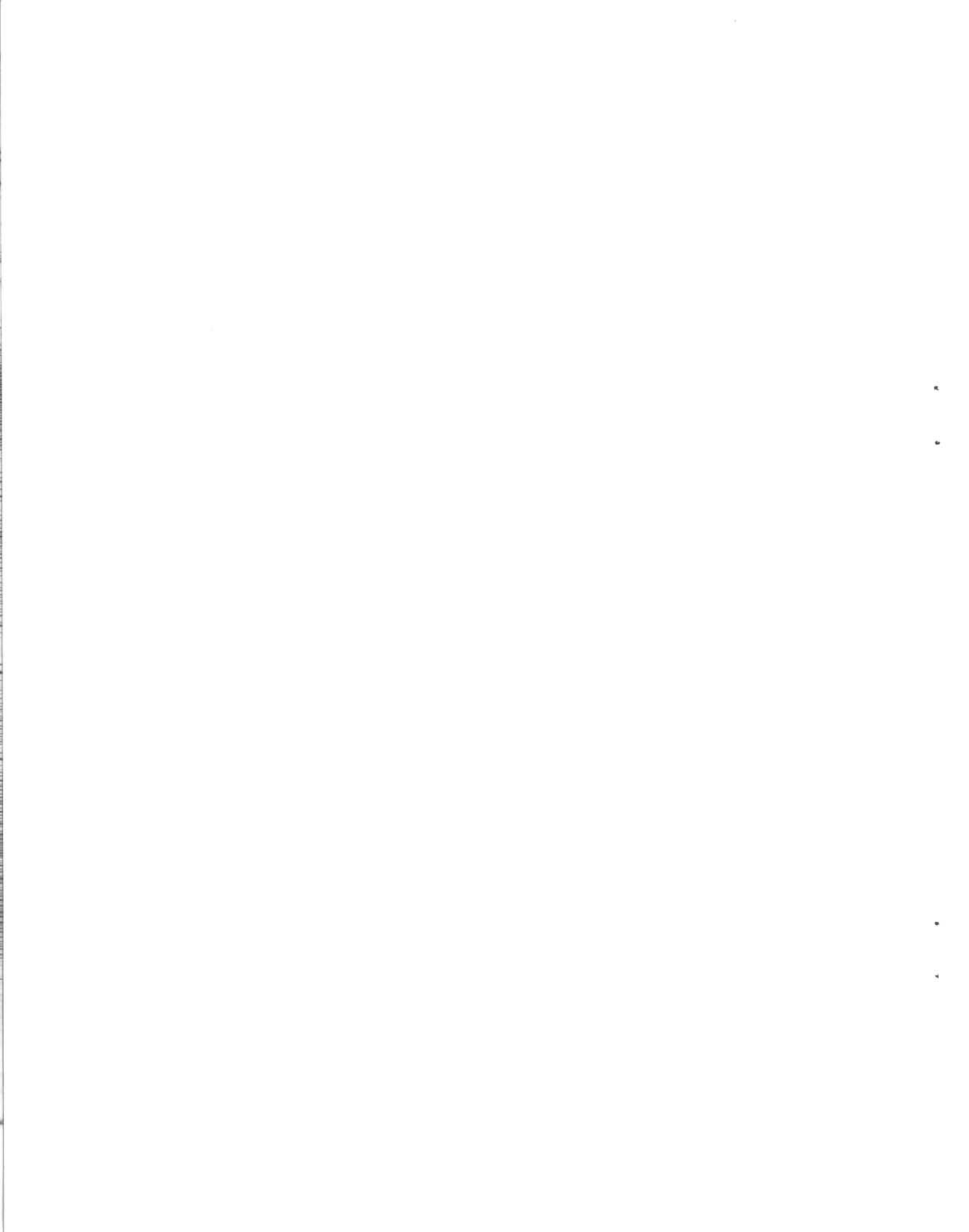


CIRCUIT FOR FREQUENCY RESPONSE TEST





PNEUMATIC SERVO TRANSFER FUNCTION



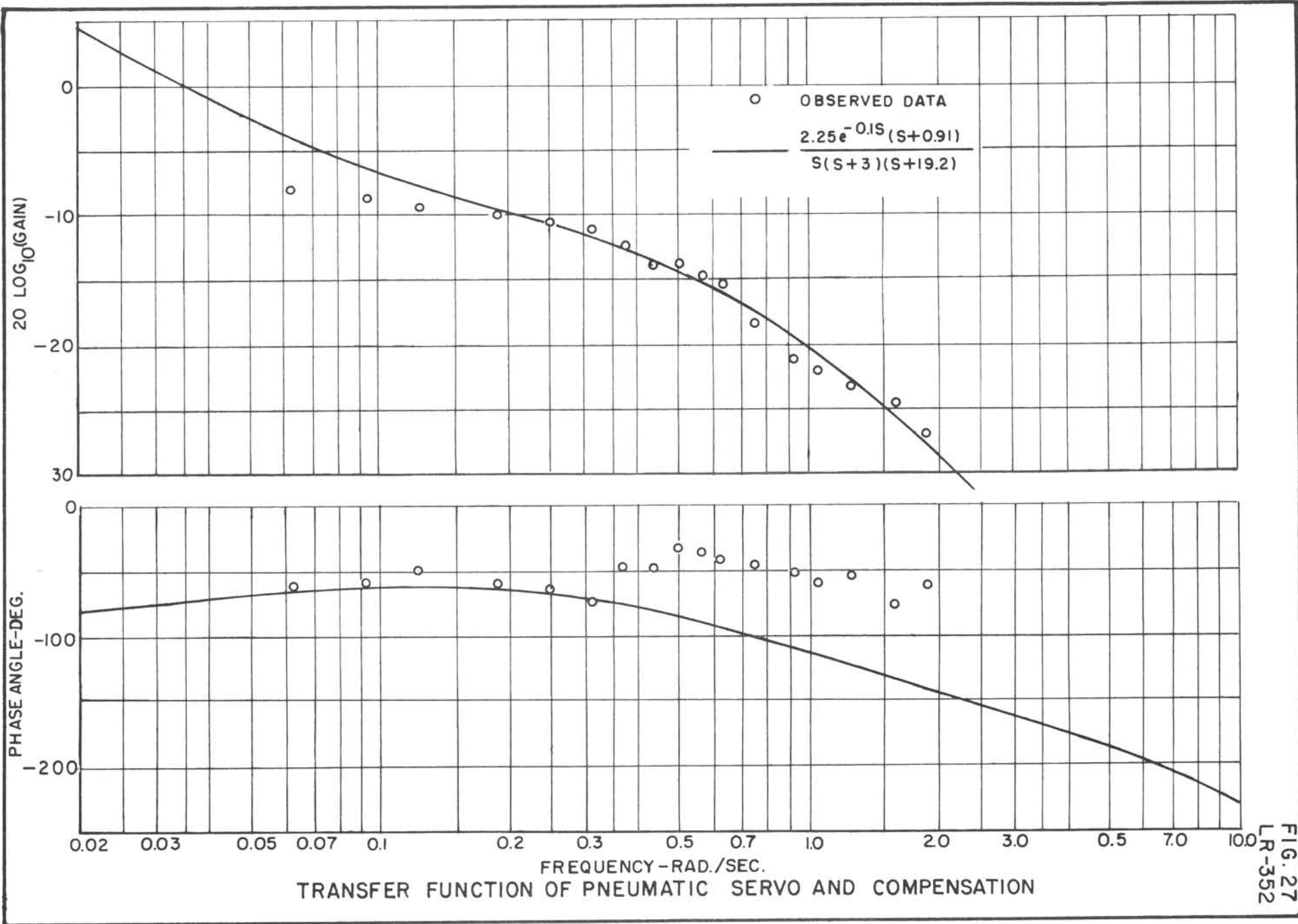
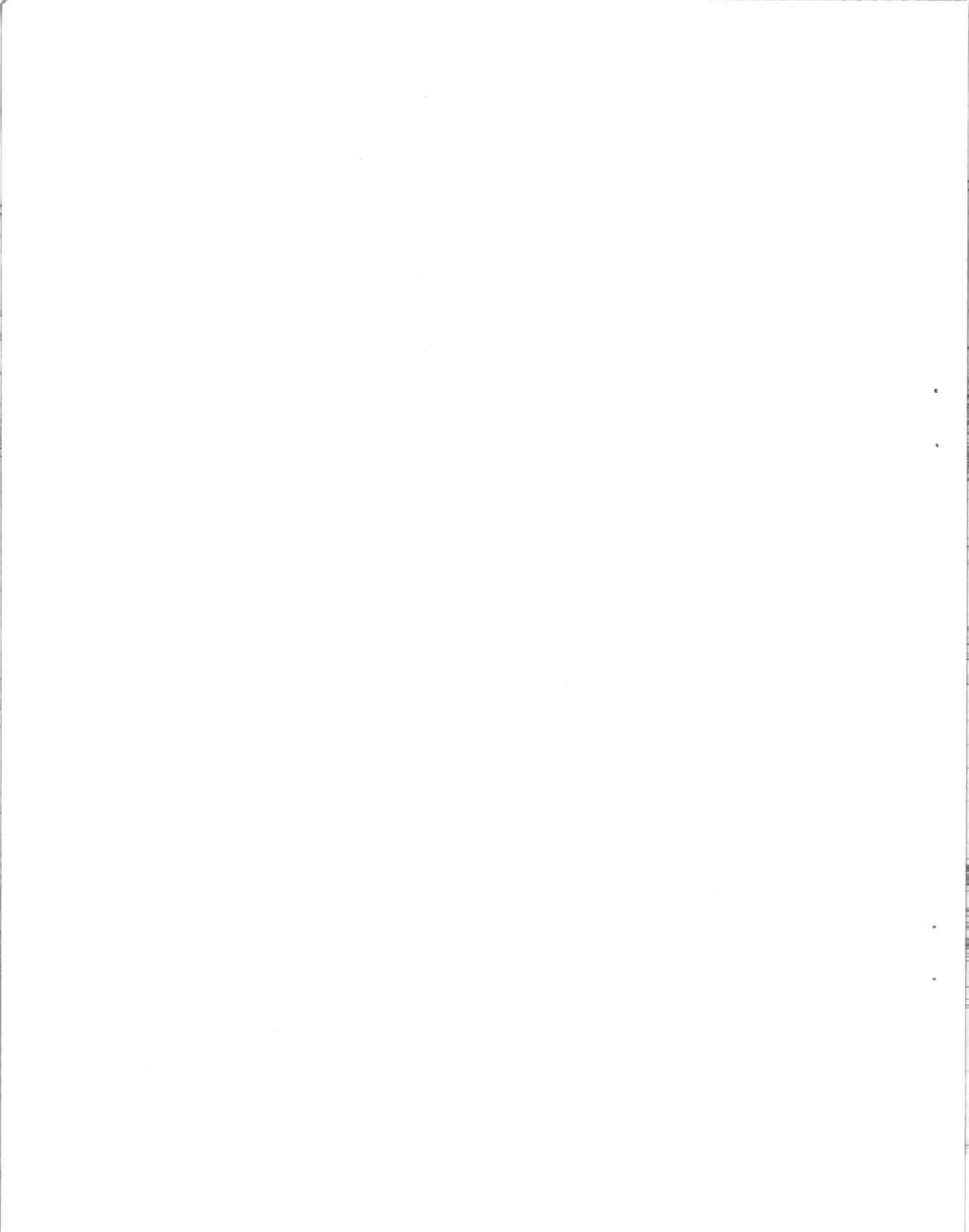
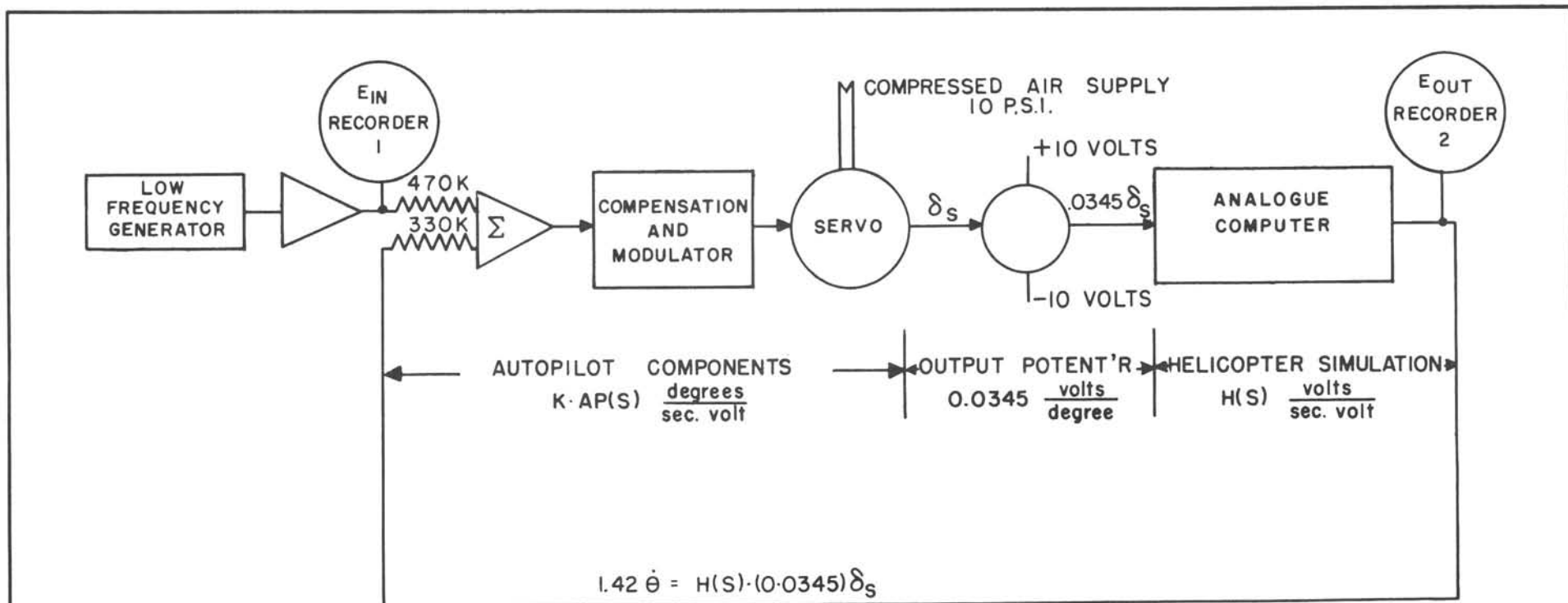


FIG. 27
LR-352



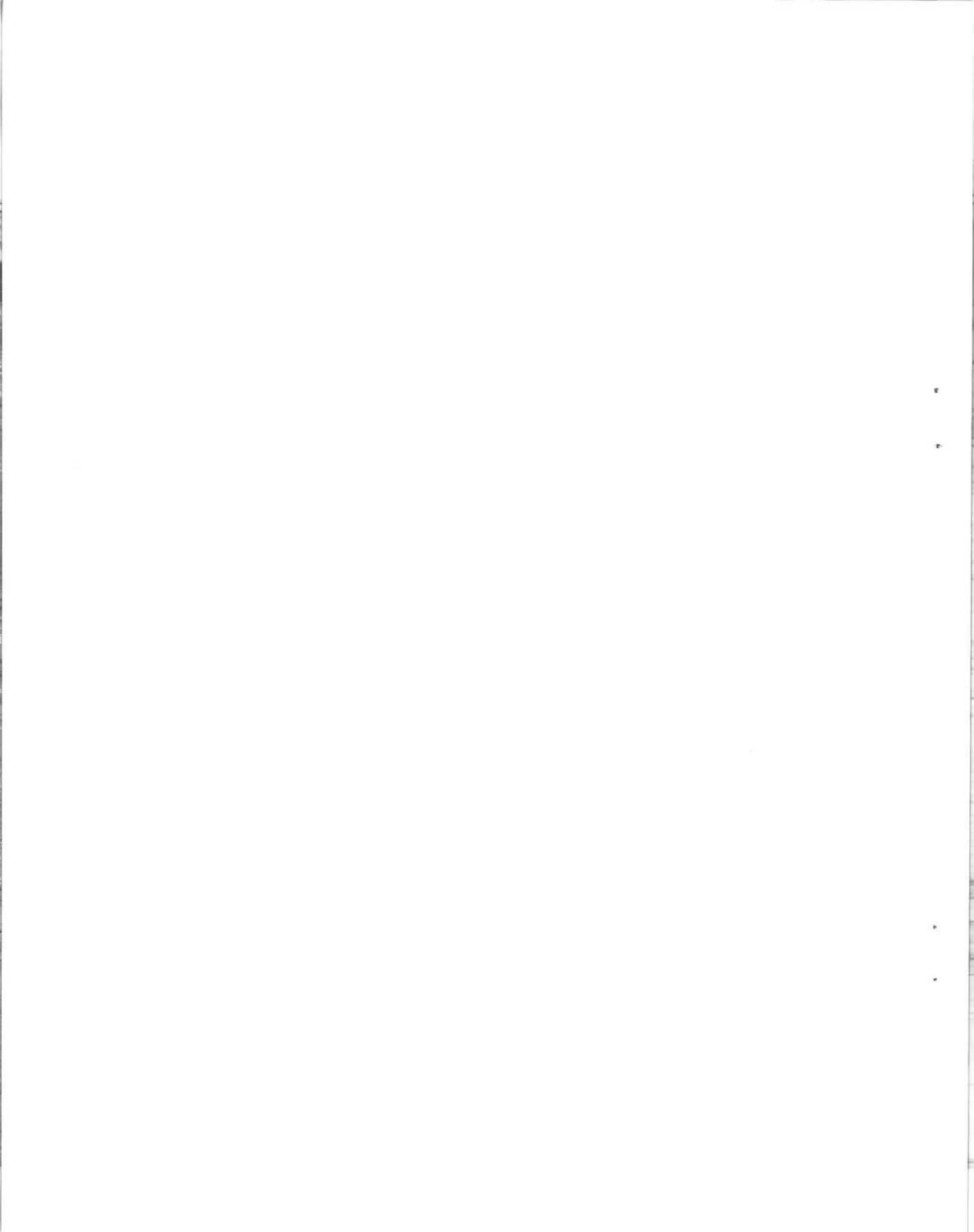


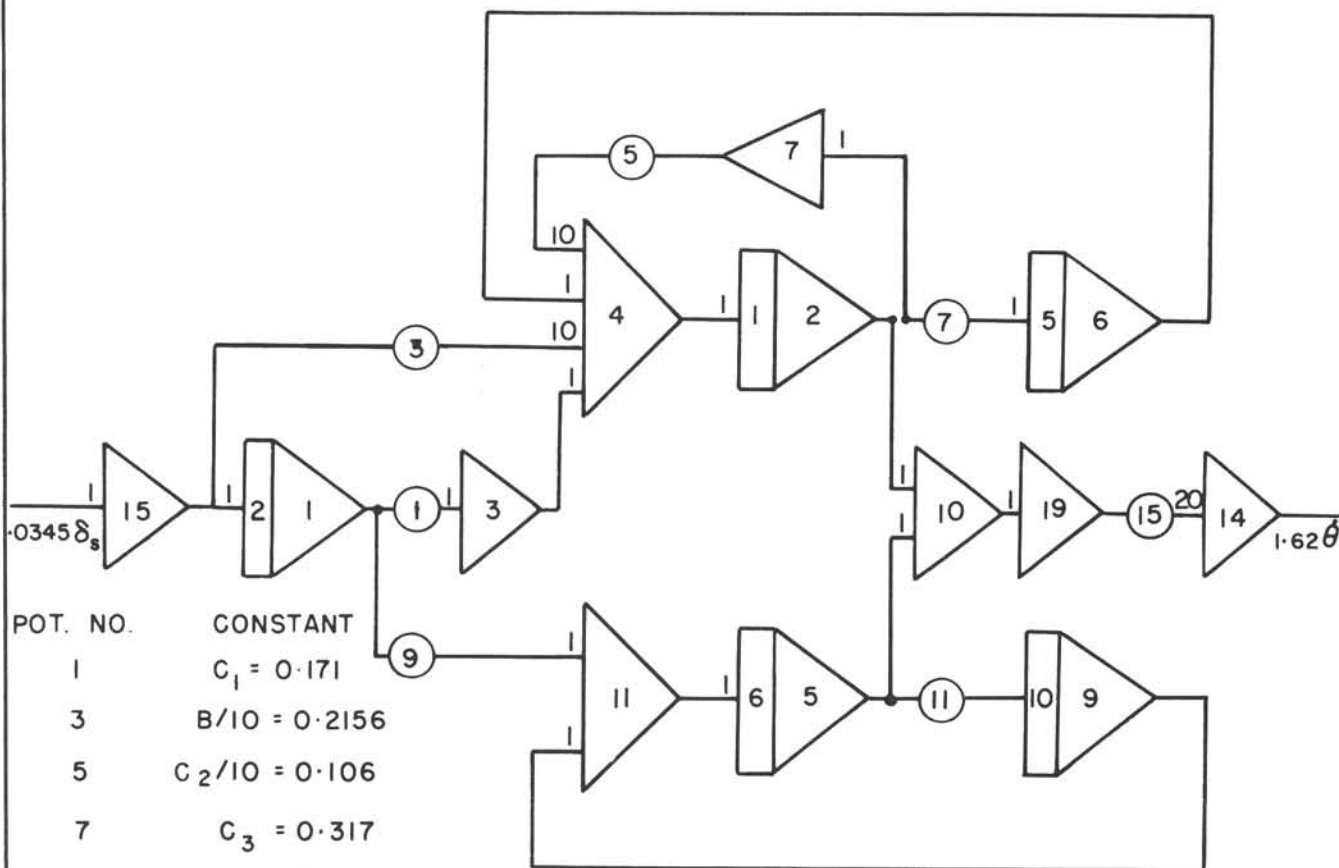
$$\text{LOOP GAIN} = [K \cdot AP(S) \cdot (0.0345) H(S)]_{S=0} = [(0.867)(0.0345)(77.7)] = 2.32$$

$$\frac{E_{OUT}}{E_{IN}} = \left[\frac{K \cdot AP(S) \cdot (0.0345) H(S)}{1 + K \cdot AP(S) \cdot (0.0345) H(S)} \right] \left(\frac{330}{470} \right)$$

$$H(S) = \frac{33.6 S(S^2 + .0401S + .115)}{(S^2 + 1.06S + .317)(S^2 + .157)}$$

CLOSED LOOP - AUTOPILOT WITH SIMULATED HELICOPTER RESPONSE





POT. NO.	CONSTANT
1	$C_1 = 0.171$
3	$B/10 = 0.2156$
5	$C_2/10 = 0.106$
7	$C_3 = 0.317$
9	$b = 0.0845$
11	$\omega_n^2 = 0.157$
15	0.780

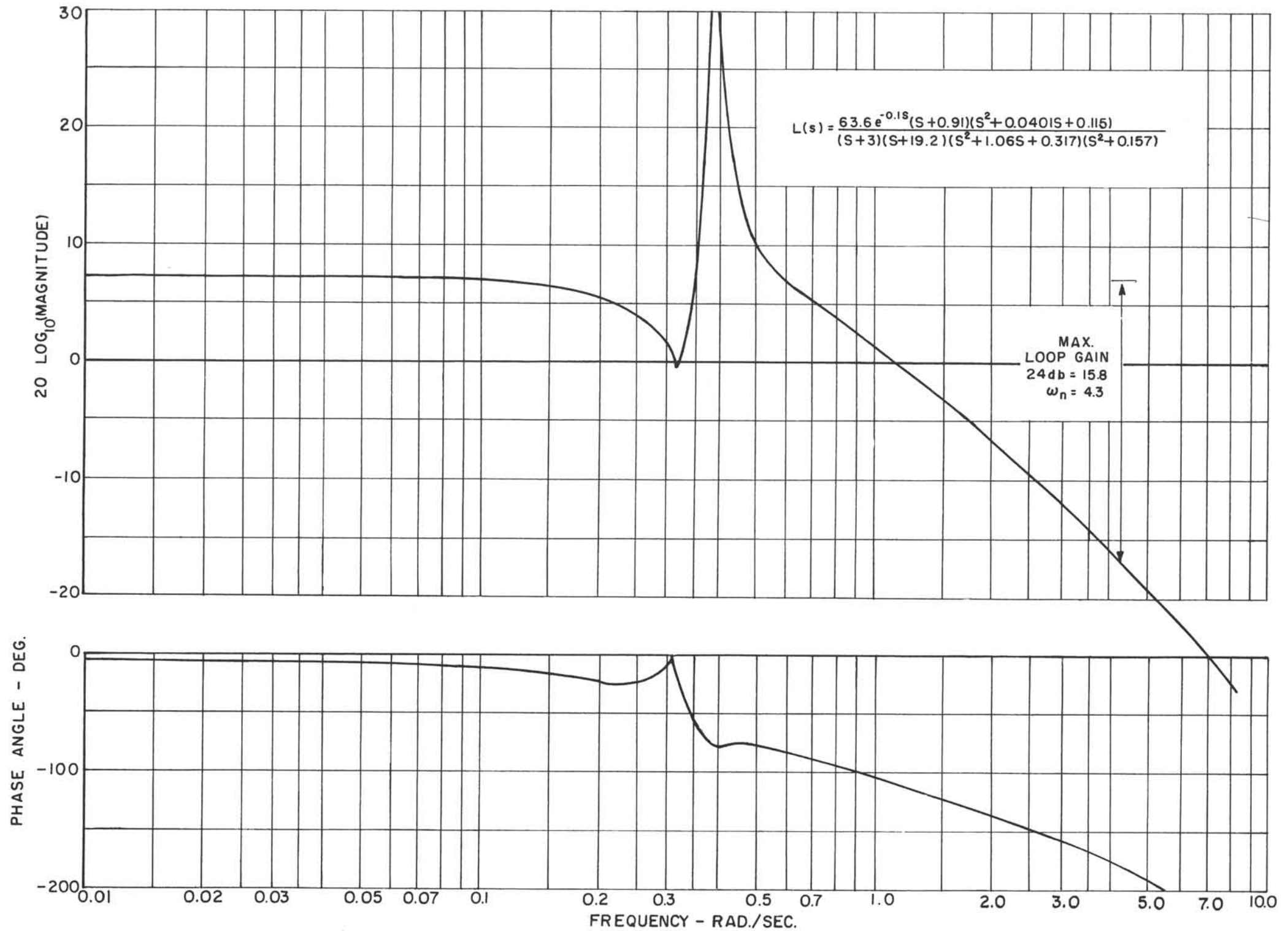
$$H(S) = 15.6 \left[\frac{BS + C_1}{S^2 + C_2S + C_3} - \frac{b}{S^2 + \omega_n^2} \right]$$

$$H(S) = \frac{33.6S(S^2 + 0.0401S + 0.115)}{(S^2 + 1.06S + 0.317)(S^2 + 0.157)}$$

$$\frac{\dot{\theta}}{\delta_s} = \frac{0.715S(S^2 + 0.0401S + 0.115)}{(S^2 + 1.06S + 0.317)(S^2 + 0.157)}$$

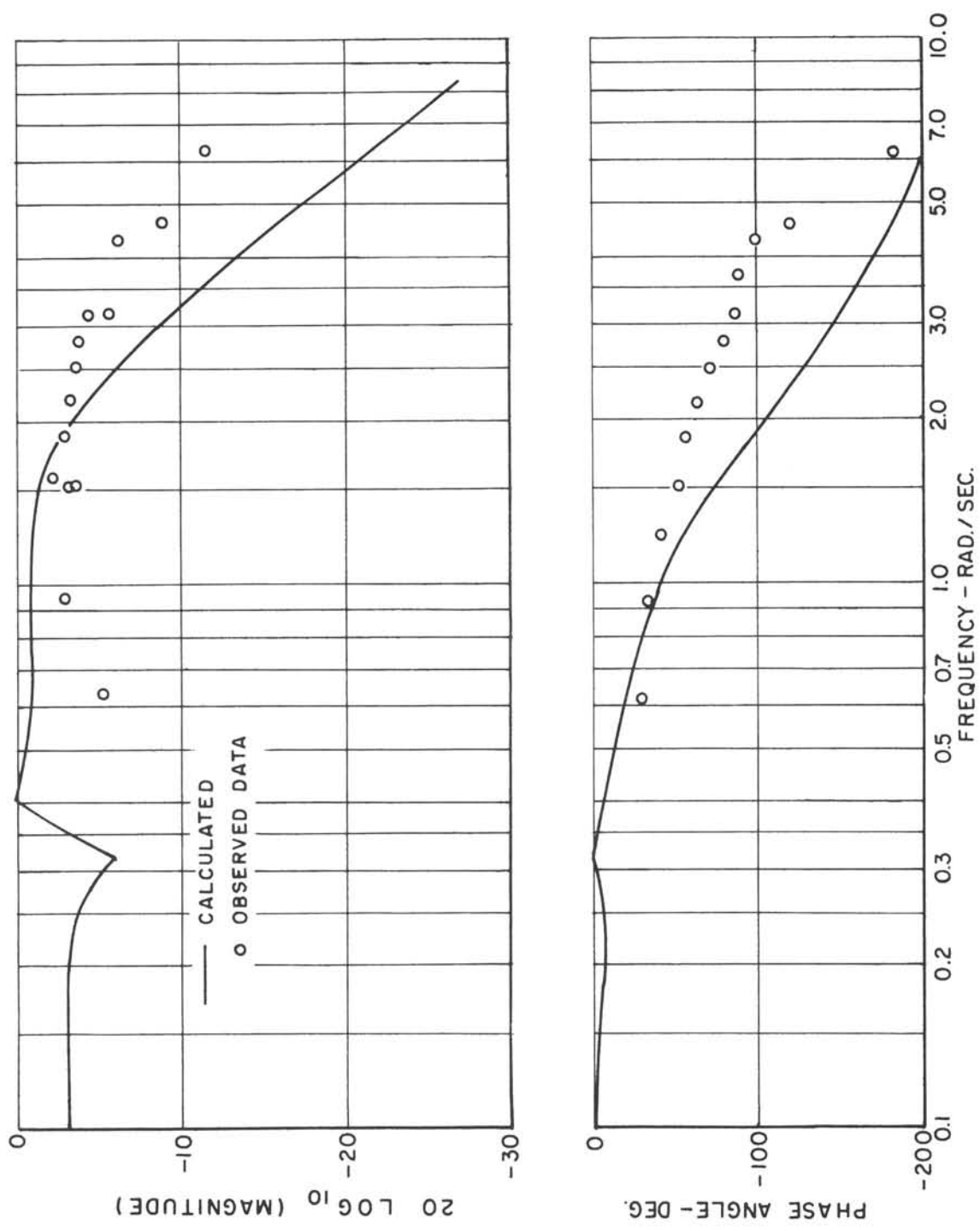
SIMULATION OF HELICOPTER
PITCH RATE RESPONSE



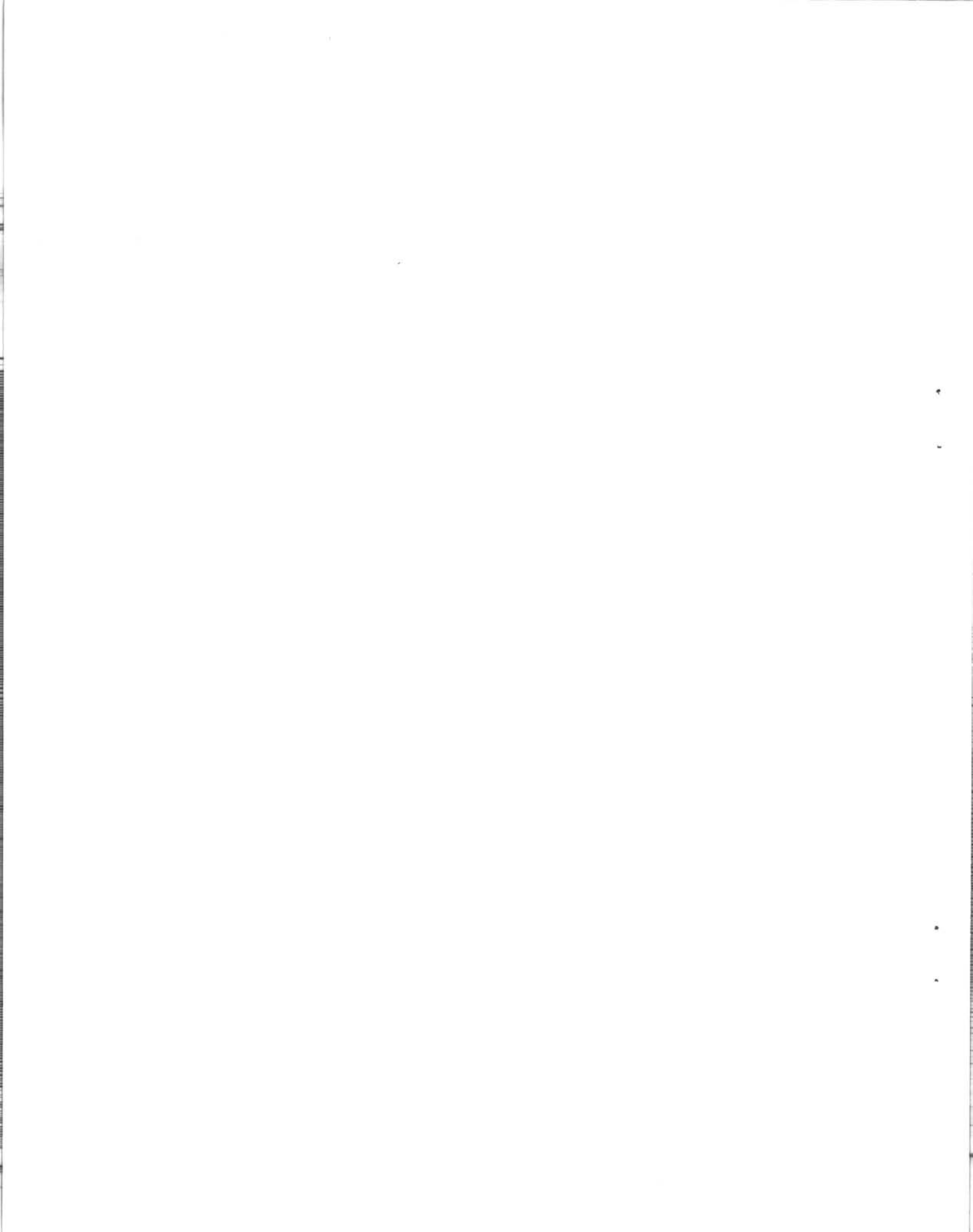


CALCULATED OPEN LOOP RESPONSE
LS = (0.0345)K · AP(S) · H(S)





CLOSED LOOP RESPONSE
(LOOP GAIN = 2.32)

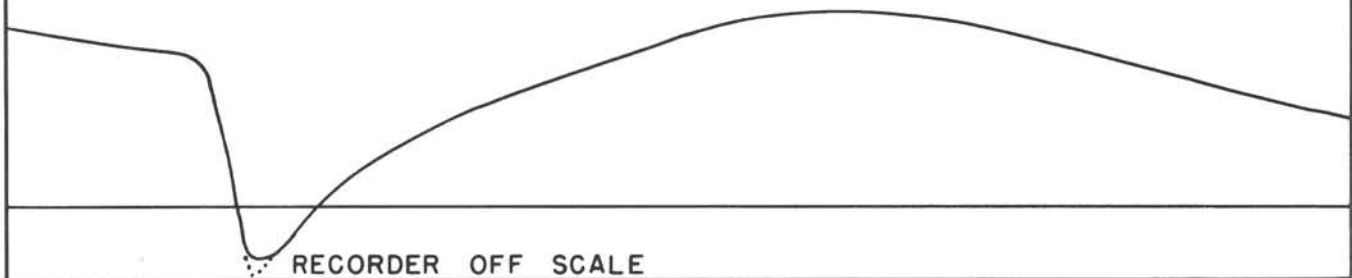


(a) TYPICAL CONTROL STICK INPUT

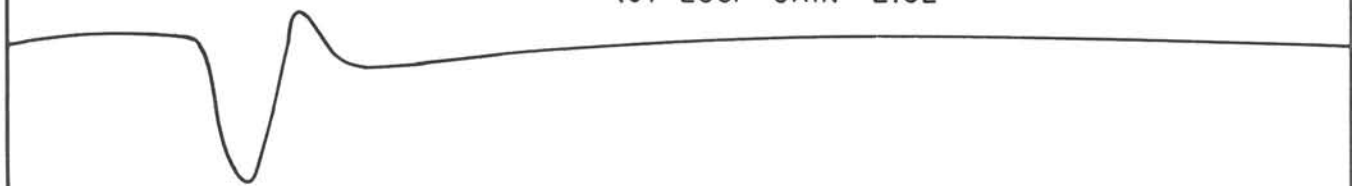


→ | ← 1.0 SEC.

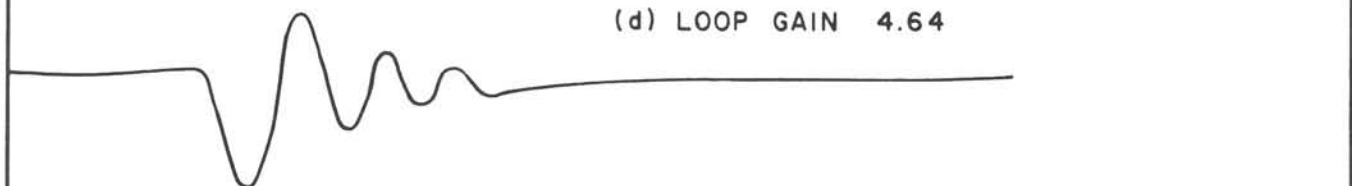
(b) LOOP GAIN ZERO (HELICOPTER RESPONSE)



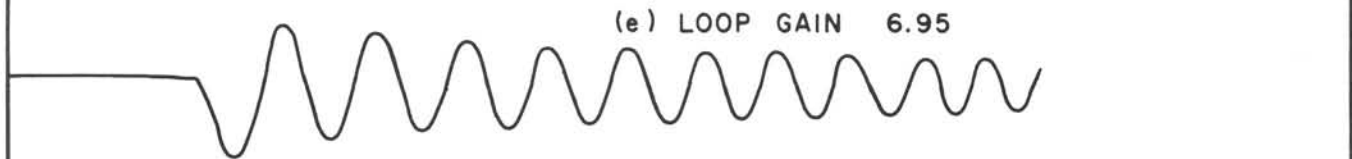
(c) LOOP GAIN 2.32



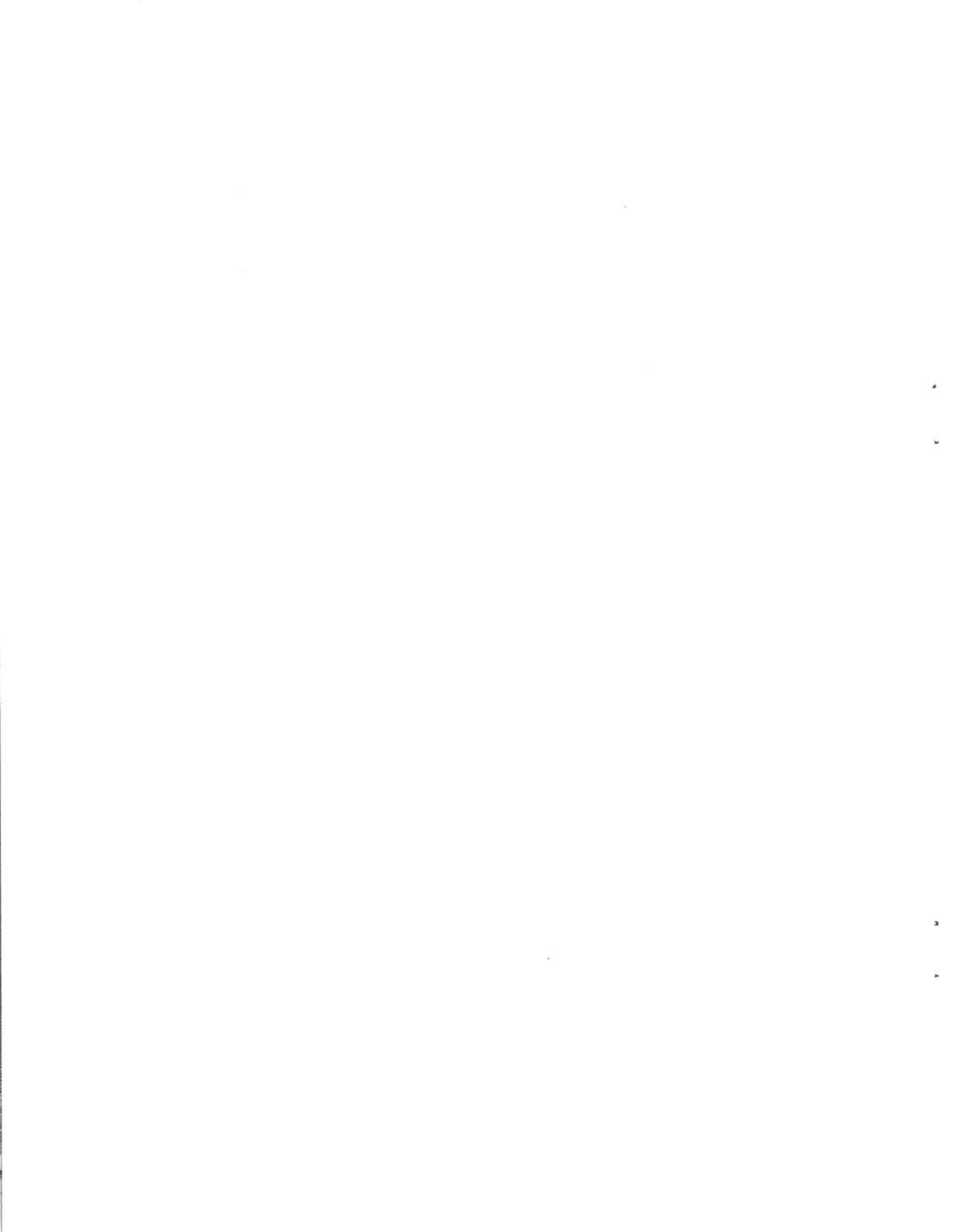
(d) LOOP GAIN 4.64

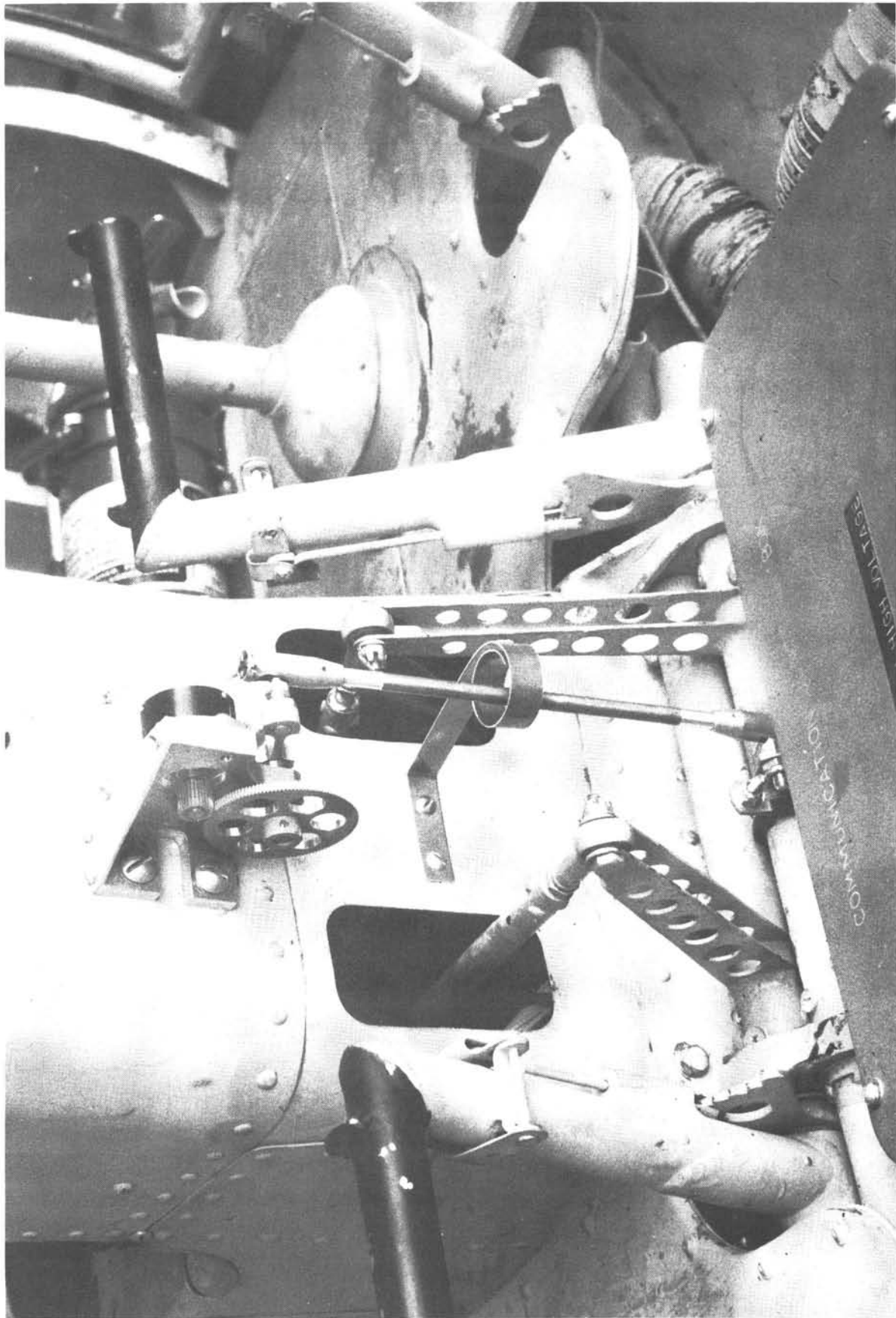


(e) LOOP GAIN 6.95



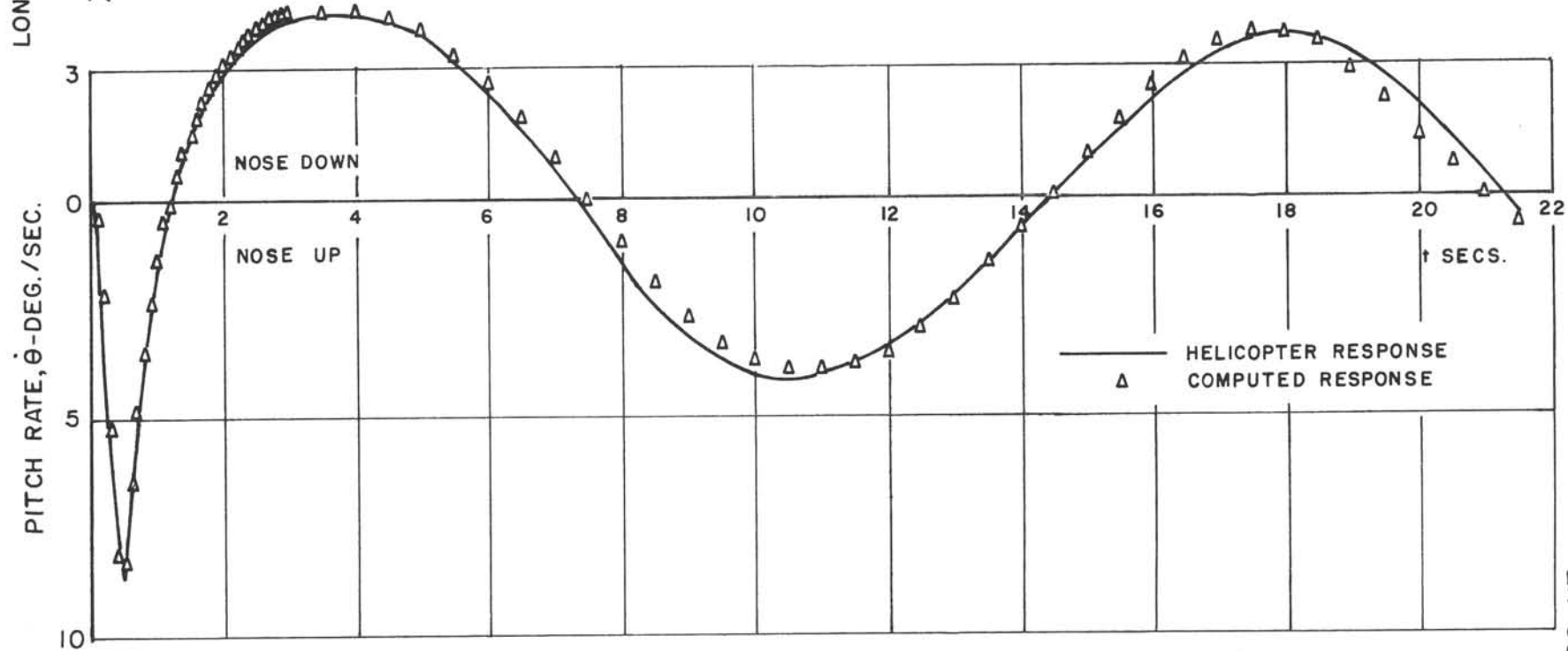
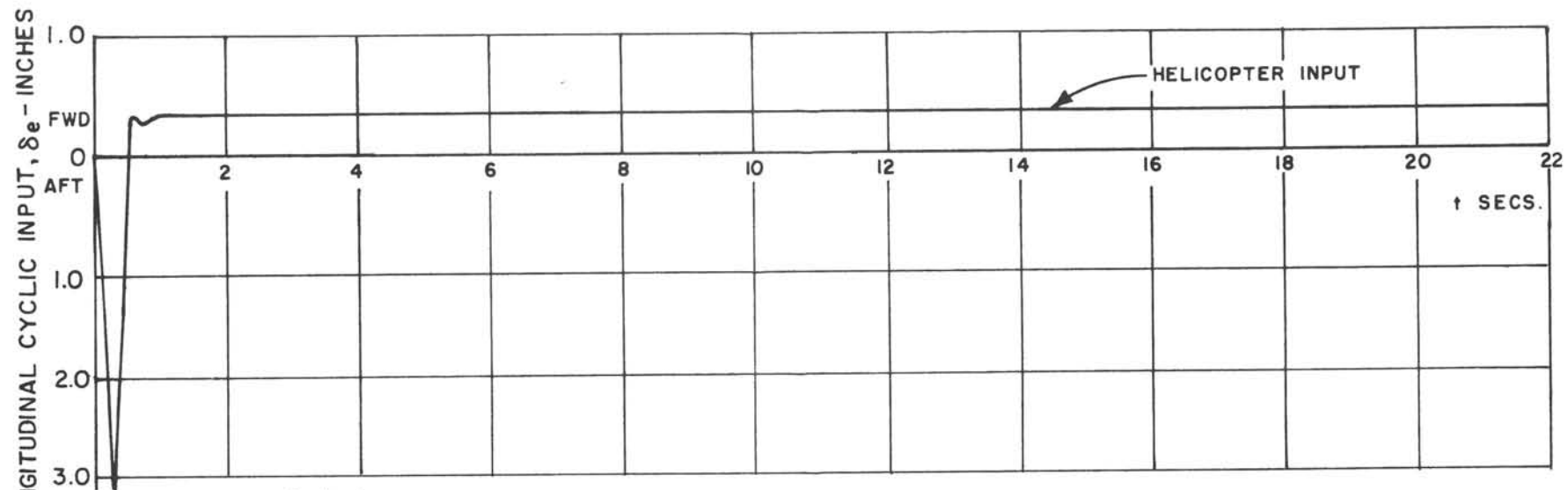
TYPICAL PITCH RATE RESPONSES TO A PULSE



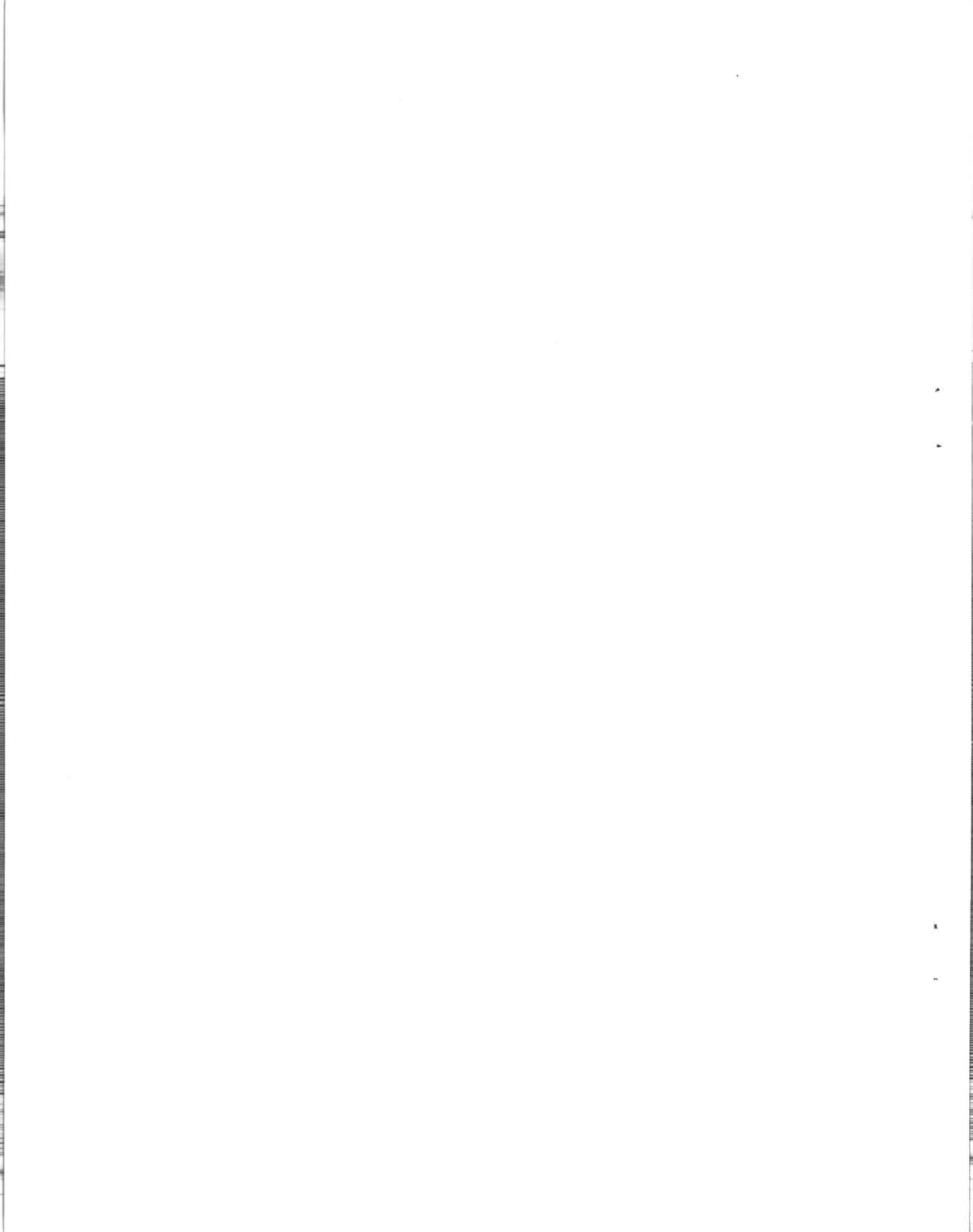


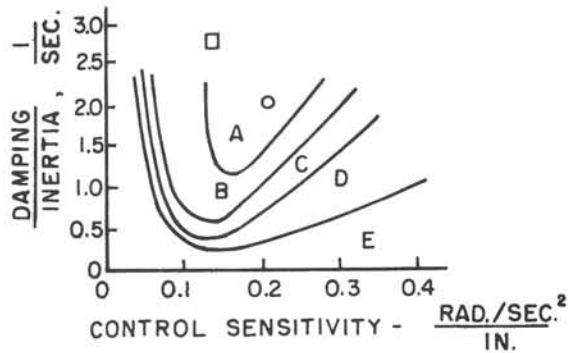
INSTALLATION OF TAIL ROTOR CONTROL POSITION POTENTIOMETER



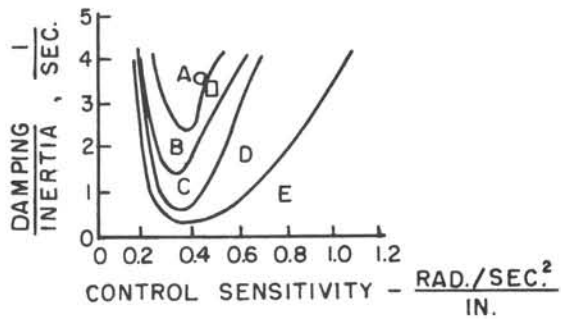


BASIC HELICOPTER FLIGHT TEST AND CALCULATED RESPONSES

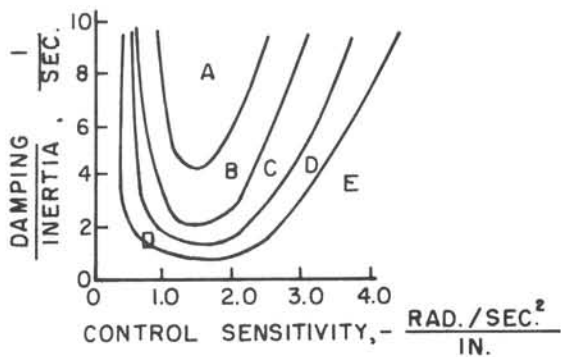




(a) PITCH AXIS



(b) ROLL AXIS



(c) YAW AXIS

PILOT'S RATING

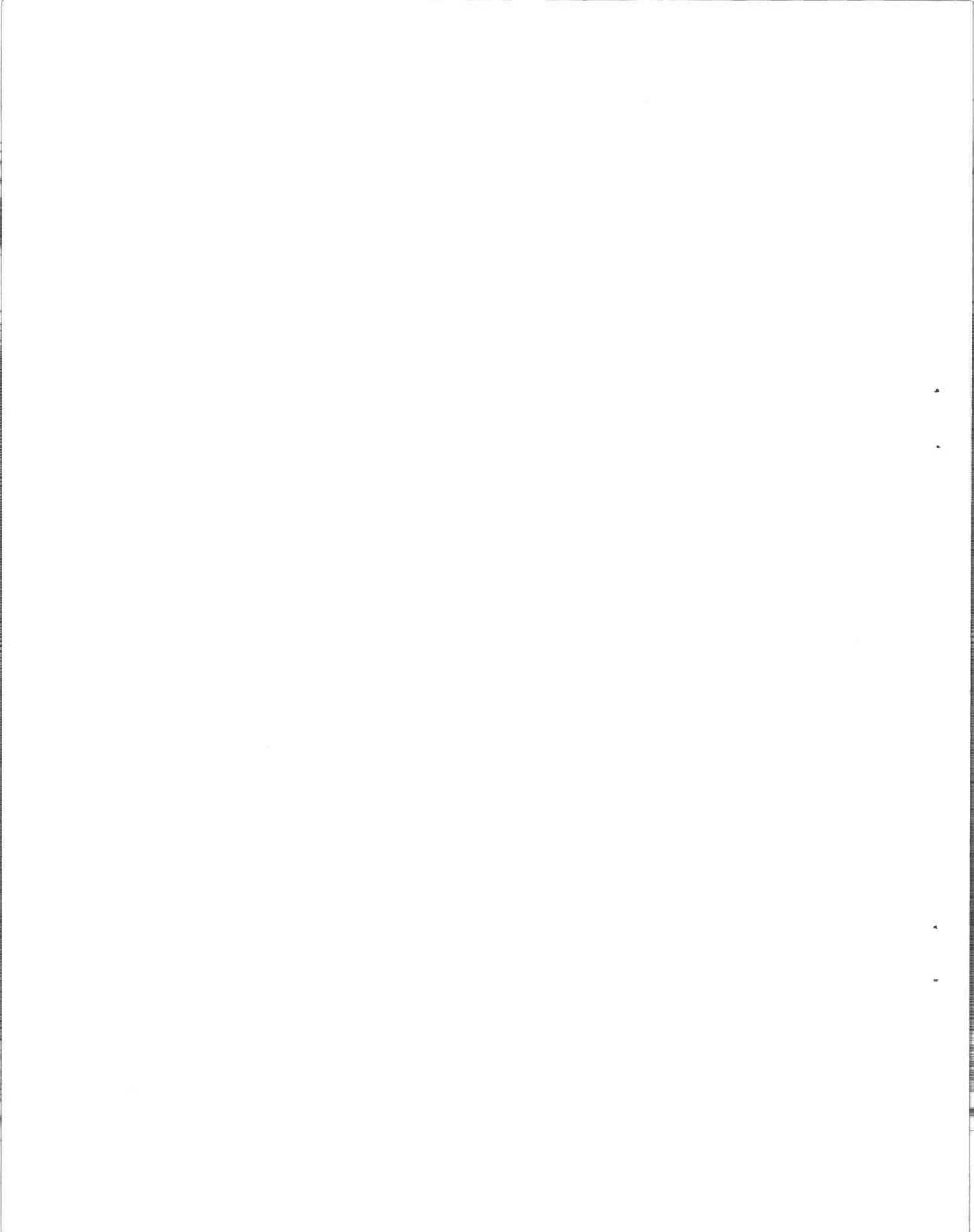
- A DESIRABLE
- B ACCEPTABLE
- C MINIMUM ACCEPTABLE
- D MARGINAL
- E UNACCEPTABLE

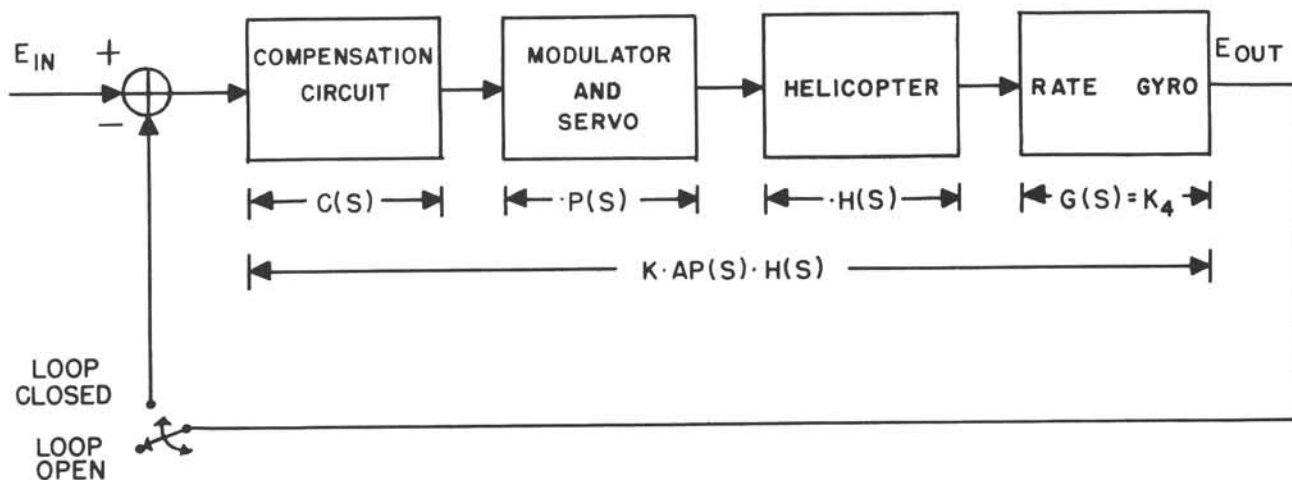
H - 13 G.

○ - 20 KNOTS

□ - 60 KNOTS

HANDLING QUALITIES BOUNDARIES AS A FUNCTION OF DAMPING
AND CONTROL SENSITIVITY - FROM REFERECE II





OPEN LOOP TRANSFER FUNCTION :
$$\frac{E_{OUT}(S)}{E_{IN}(S)} = K \cdot AP(S) \cdot H(S)$$

CLOSED LOOP TRANSFER FUNCTION :
$$\frac{E_{OUT}(S)}{E_{IN}(S)} = \frac{K \cdot AP(S) \cdot H(S)}{1 + K \cdot AP(S) \cdot H(S)}$$

DEFINITIONS :

(a) NATURAL FREQUENCY (ω_n)

THE VALUE OF ω FOR WHICH $K \cdot AP(S) \cdot H(S) = \text{CONSTANT} \angle -180$ degrees

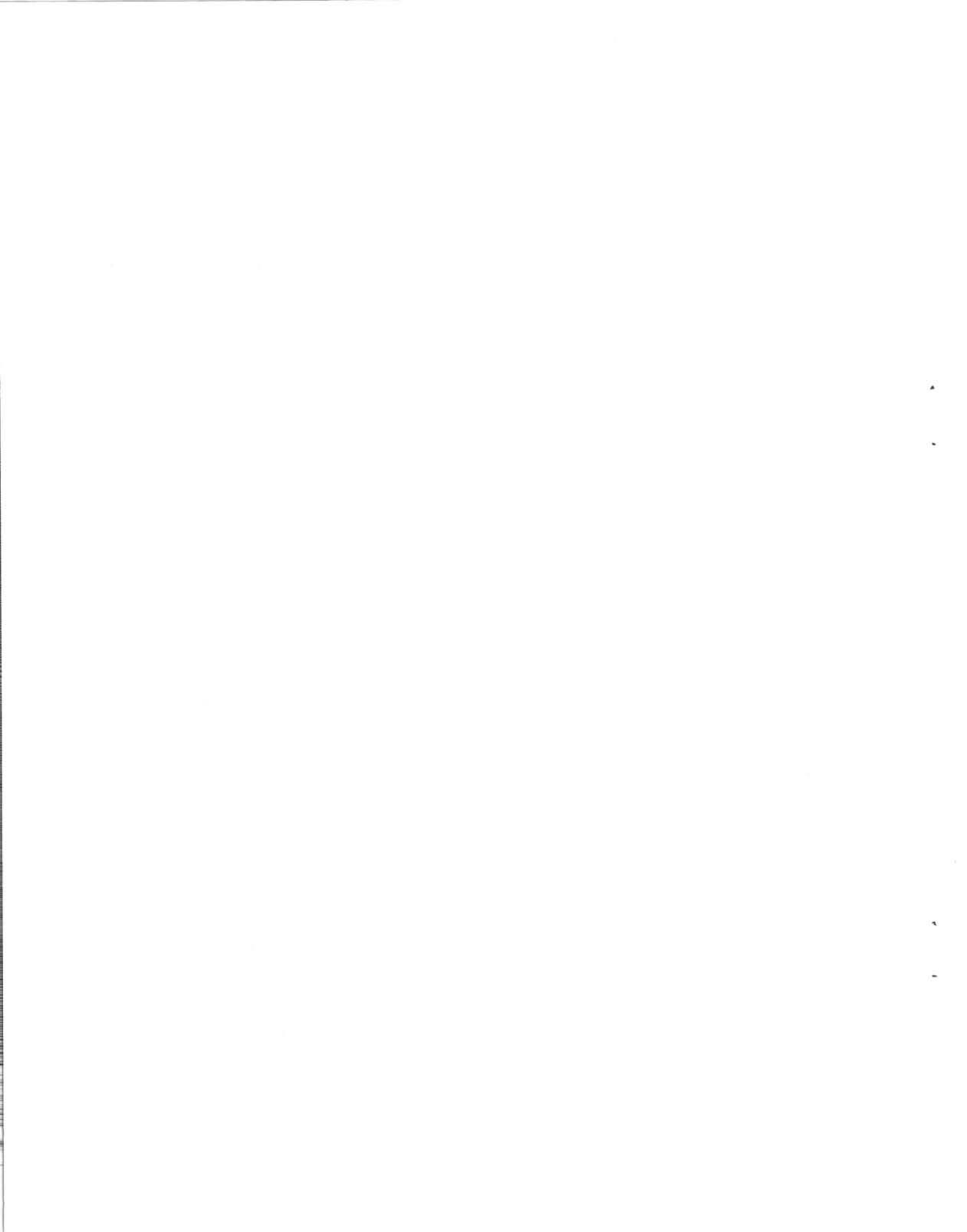
(b) MAXIMUM GAIN ($K_{MAX.}$)

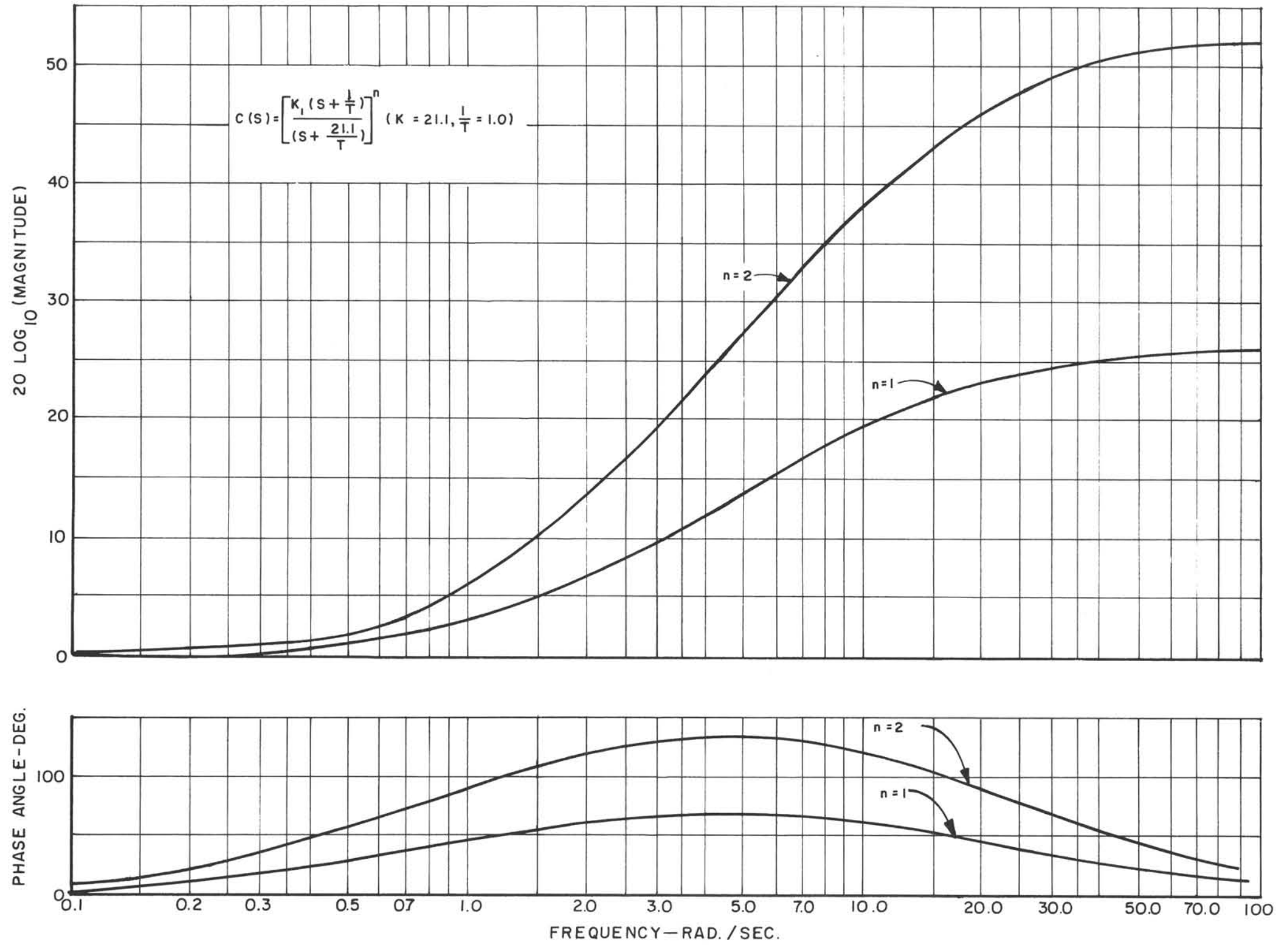
THE VALUE OF K FOR WHICH $K \cdot AP(S) \cdot H(S) = 1 \angle -180$ degrees

(c) OPTIMUM GAIN ($K_{OPT.}$)

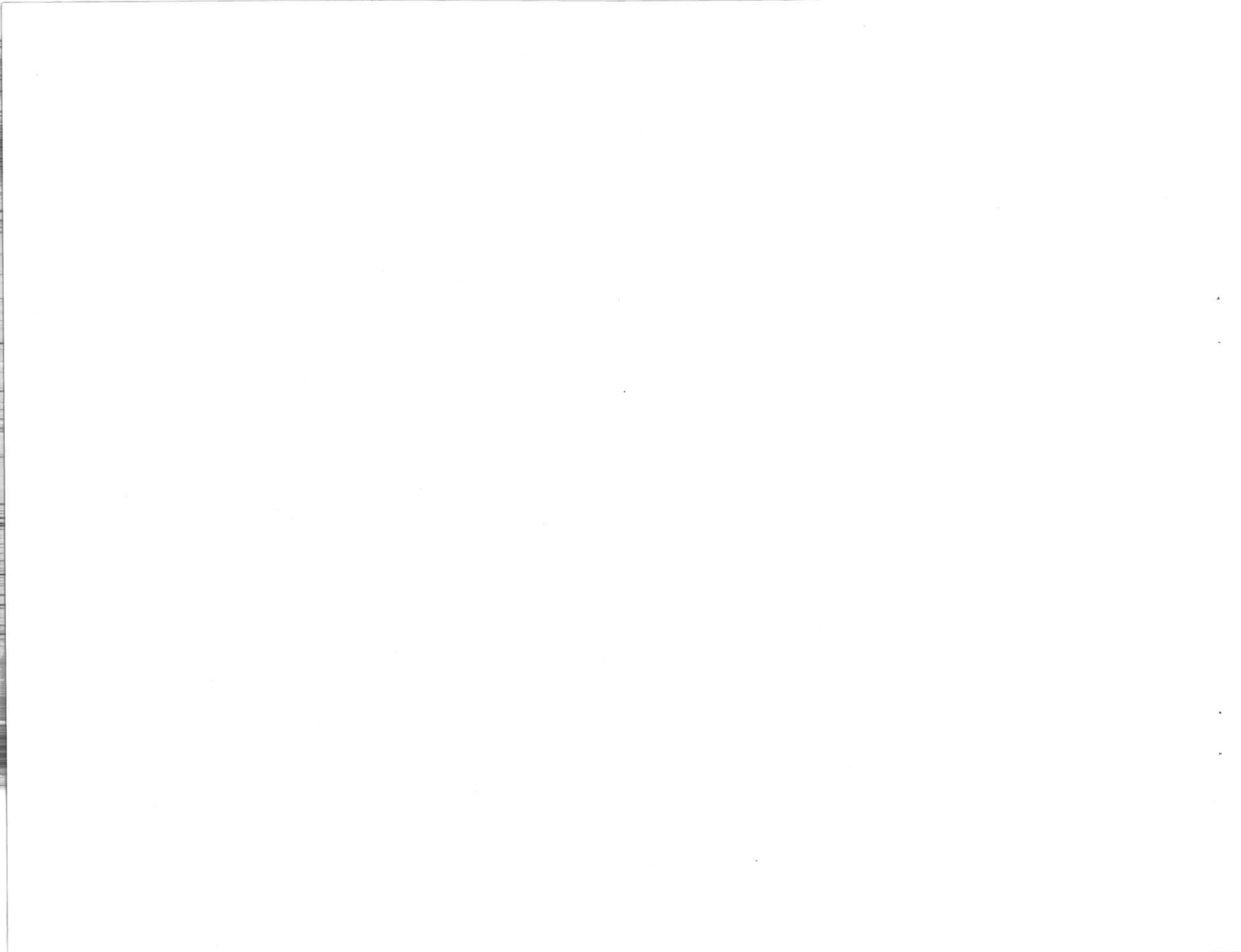
THE VALUE OF K FOR WHICH $K \cdot AP(S) \cdot H(S) = 1 \angle -150$ degrees

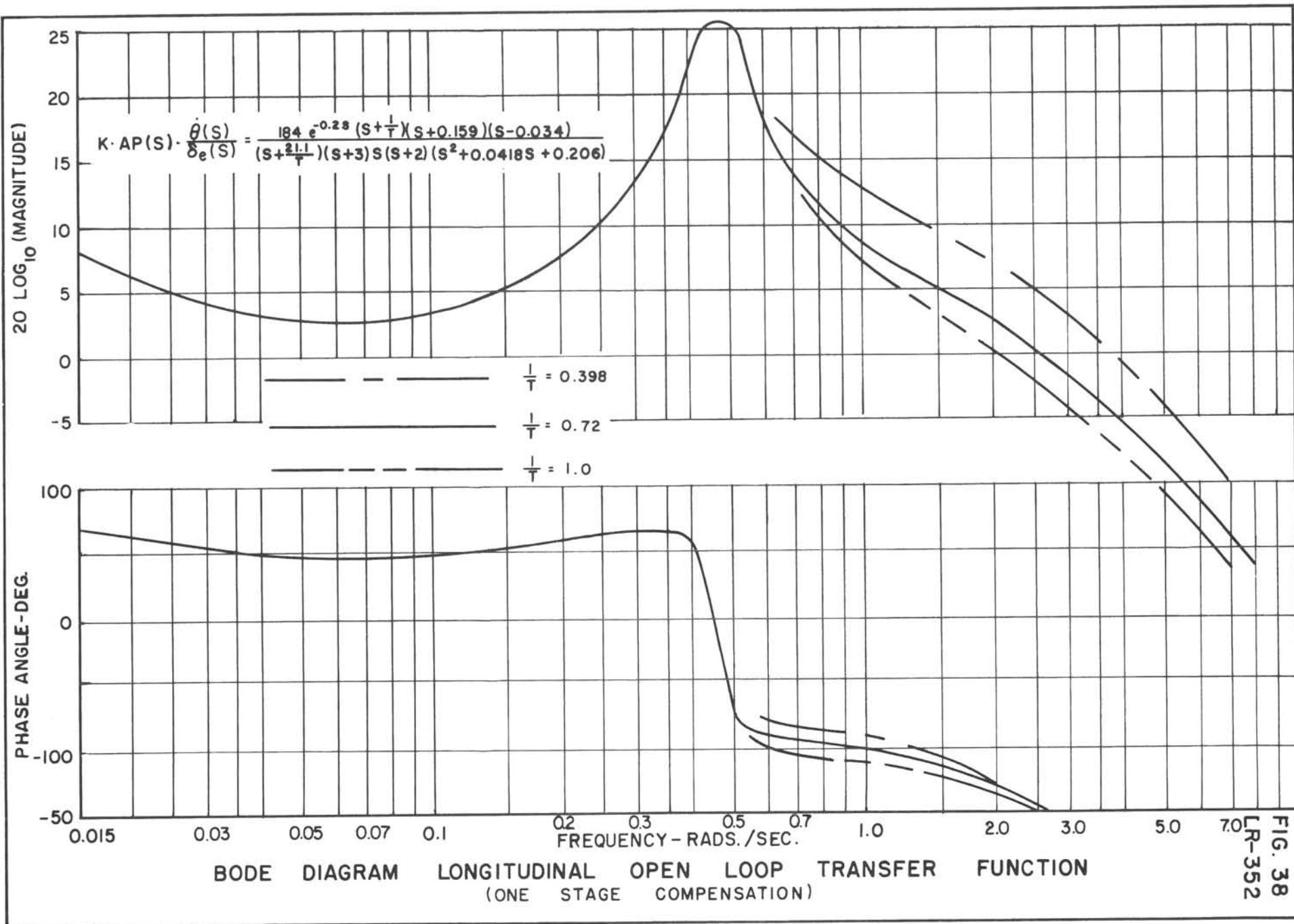
TYPICAL CONTROL LOOP

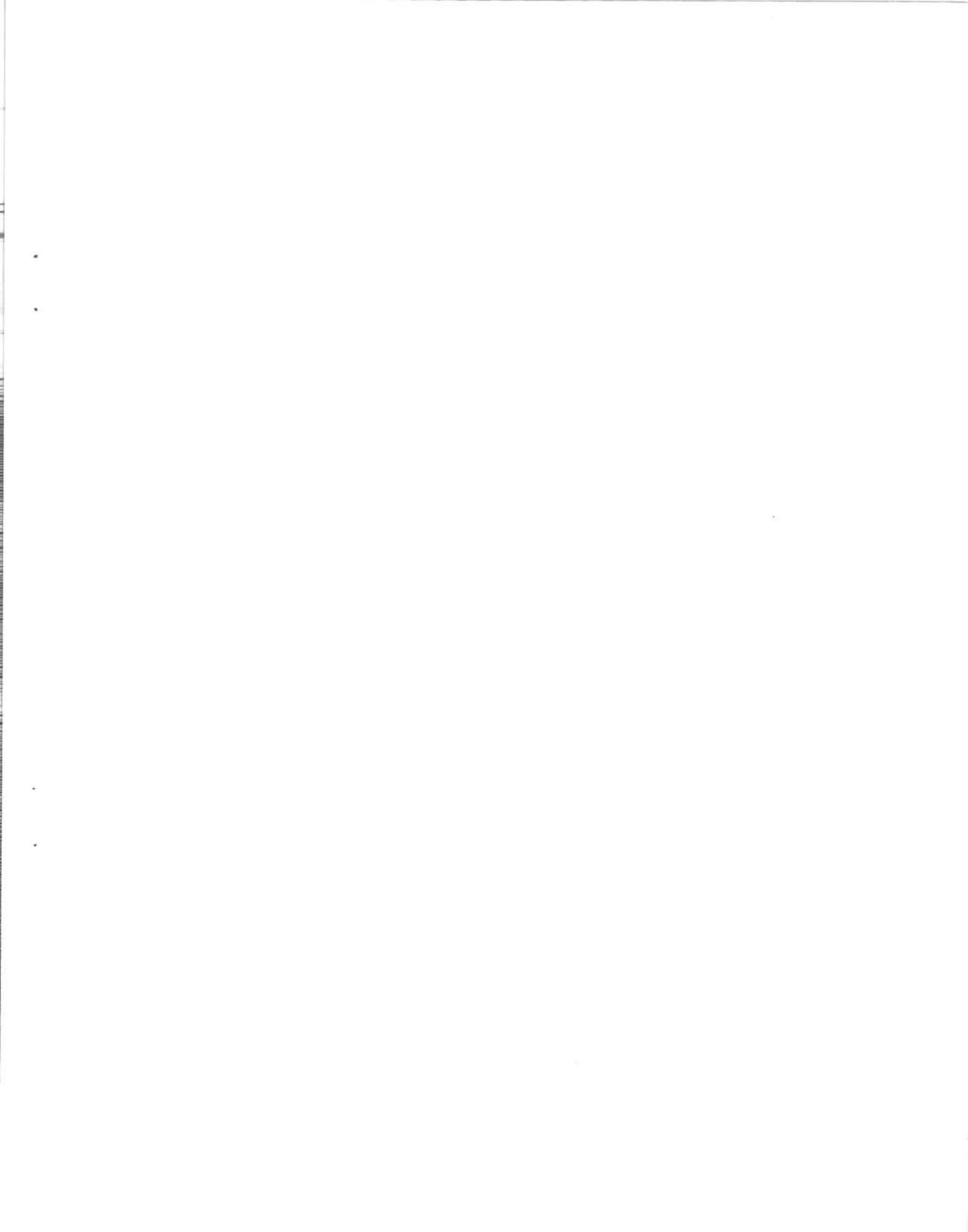


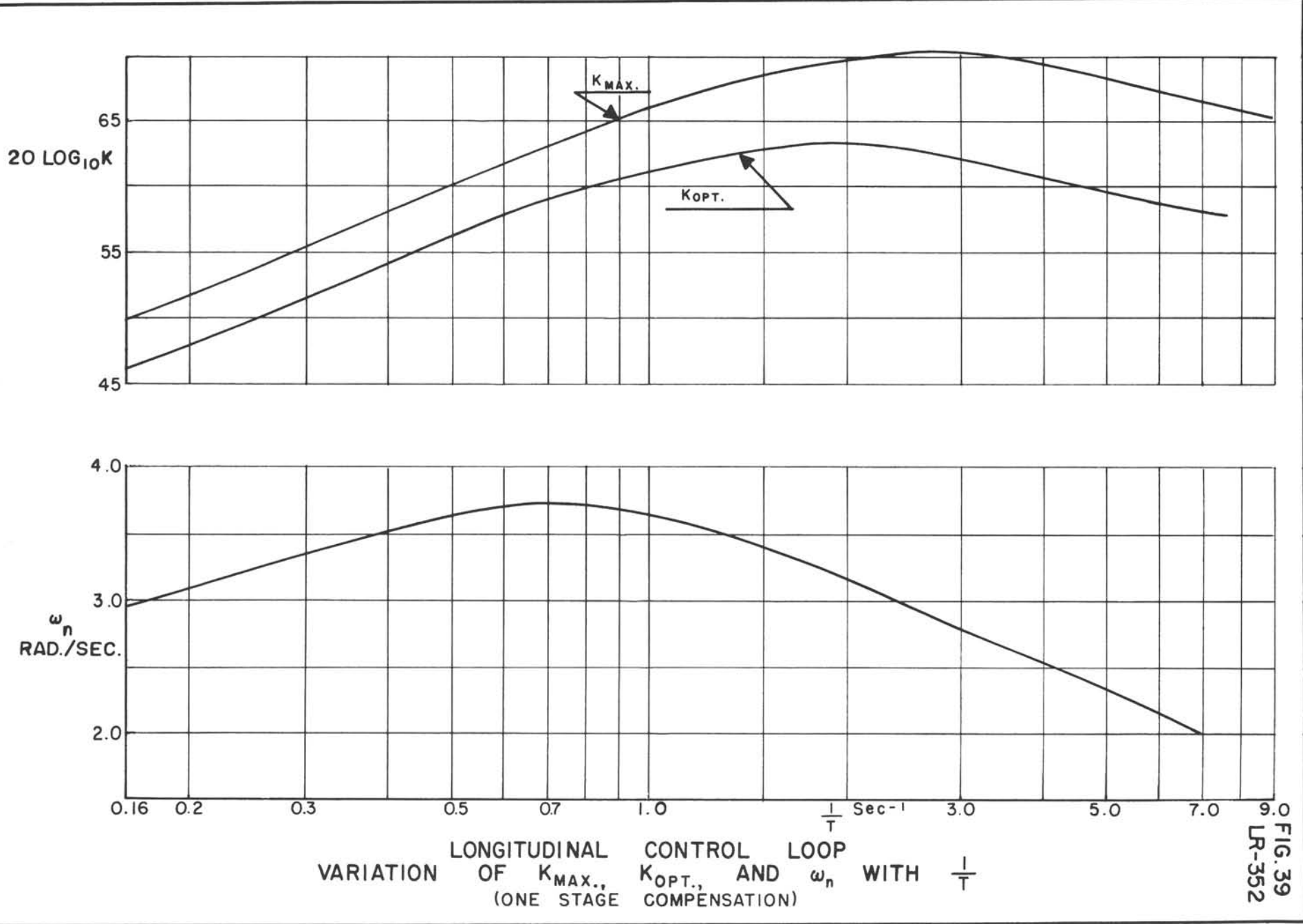


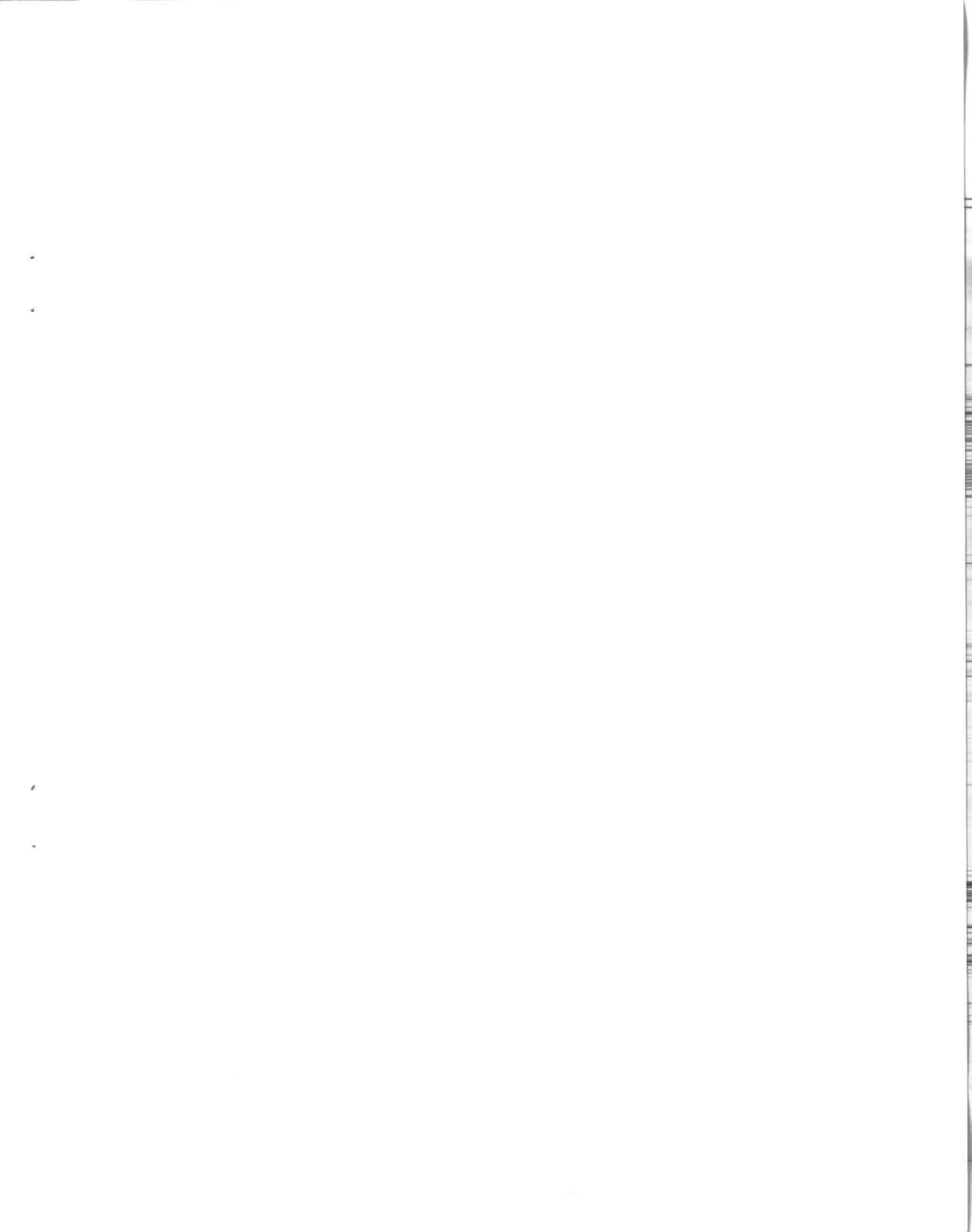
BODE DIAGRAM FOR COMPENSATION CIRCUIT

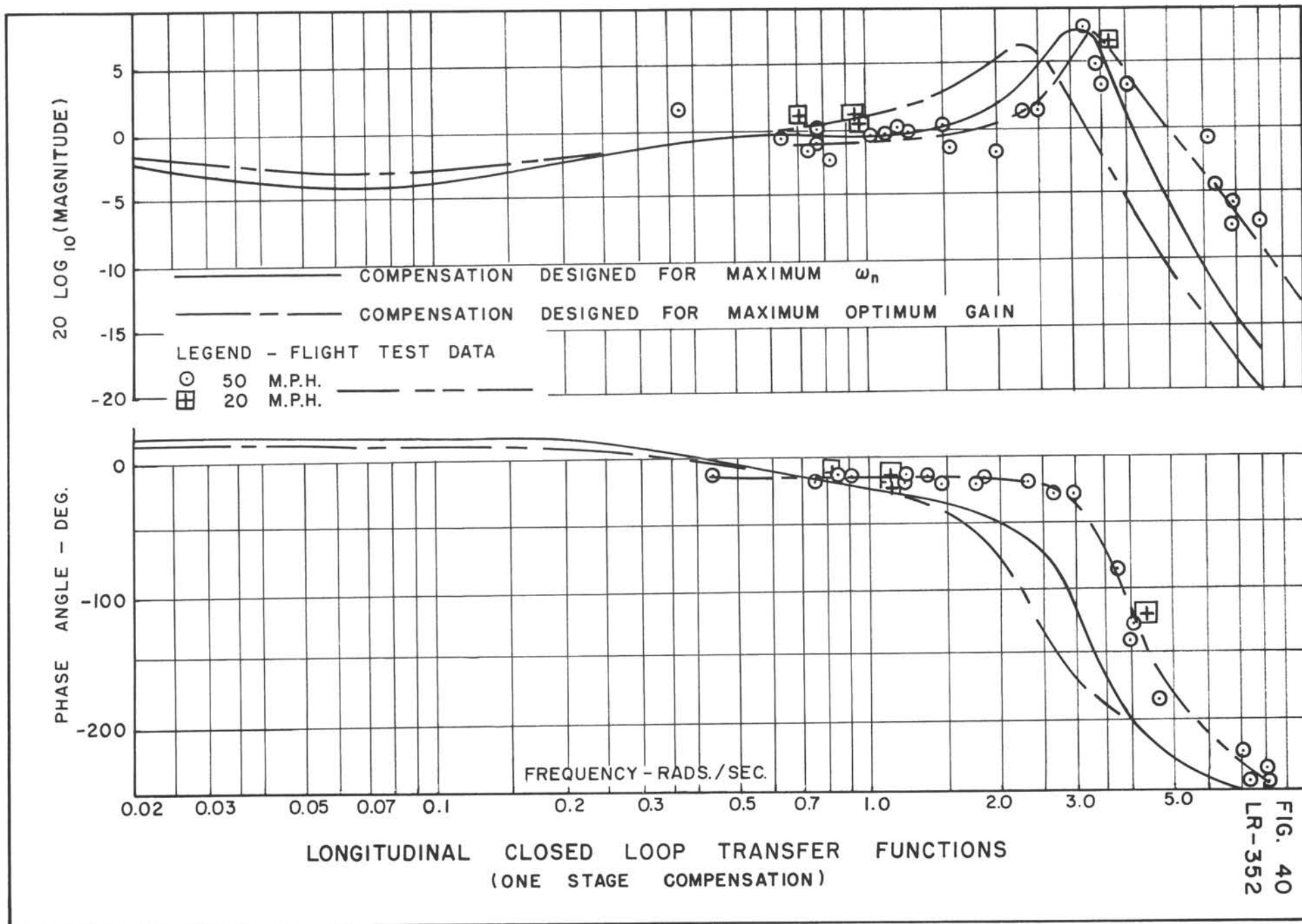


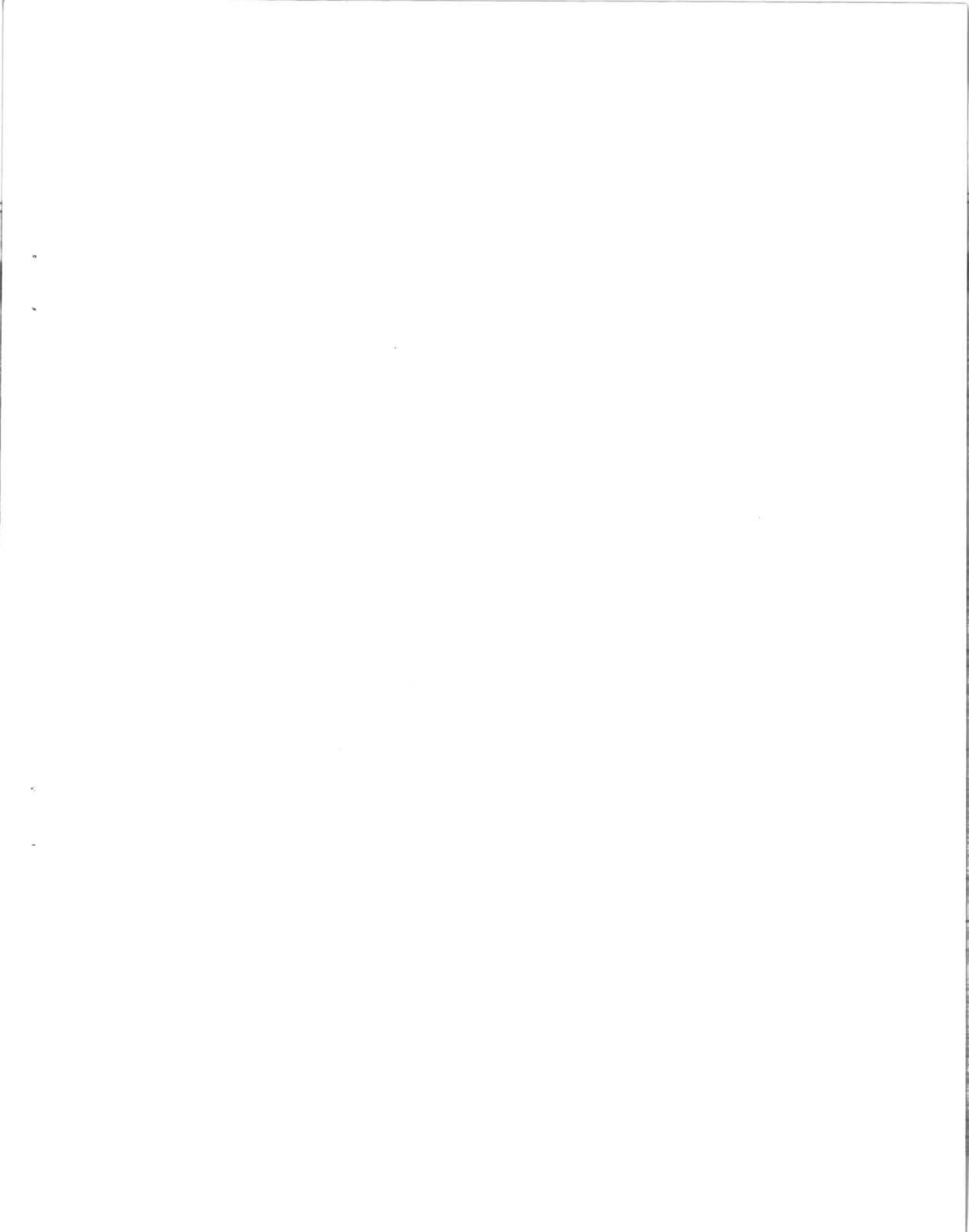


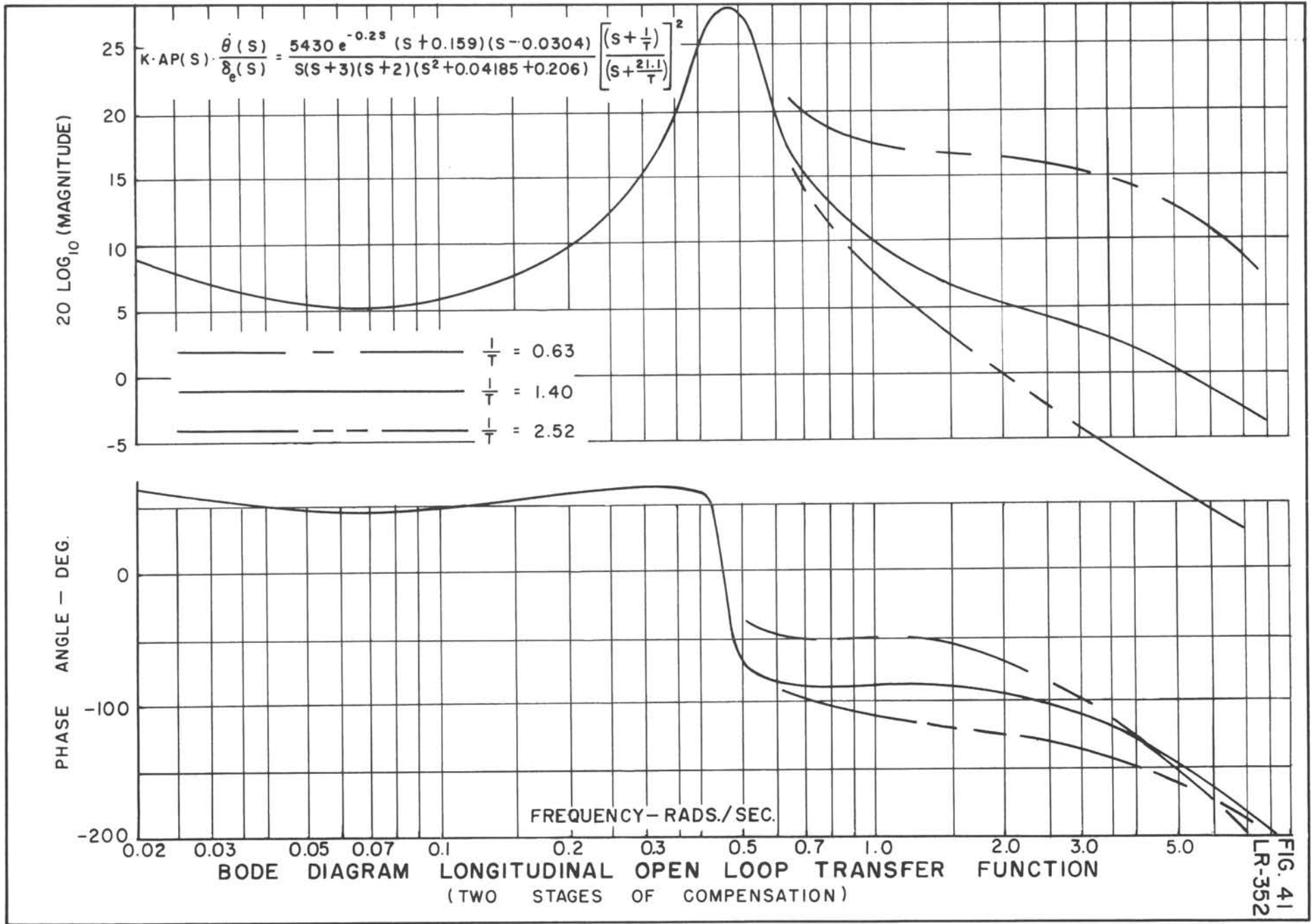


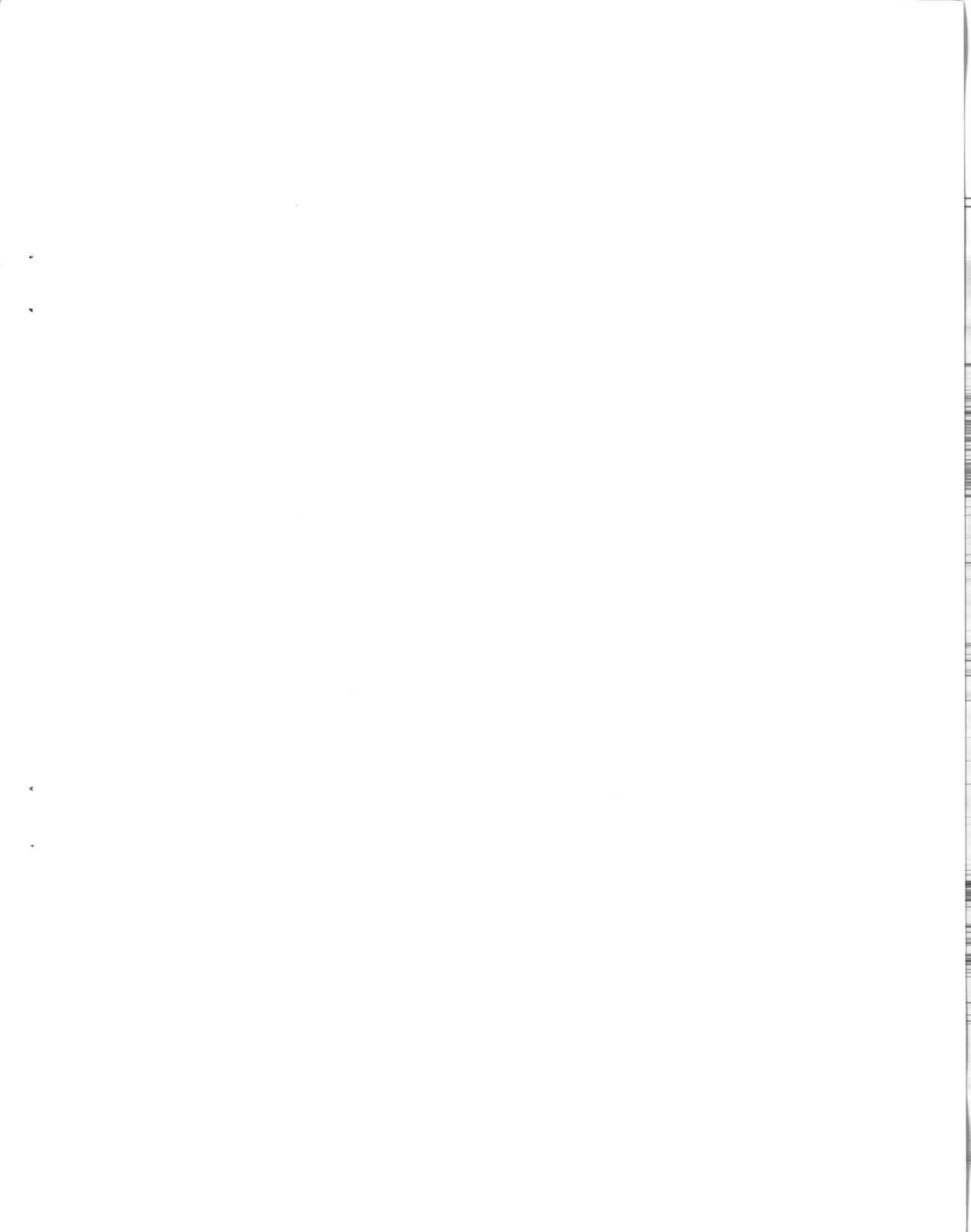


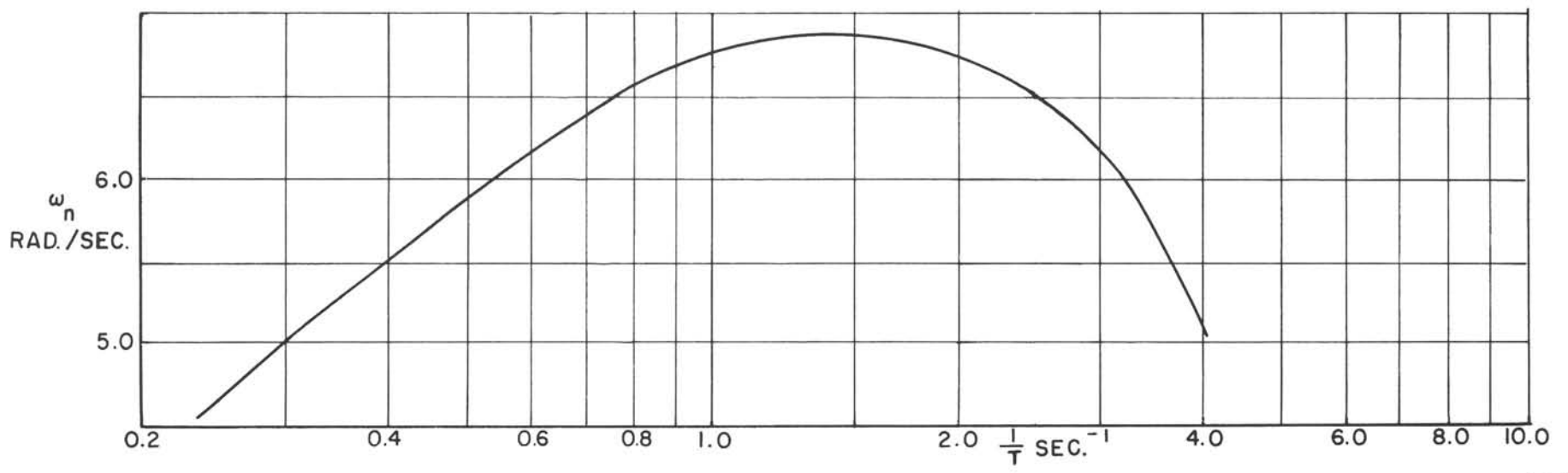
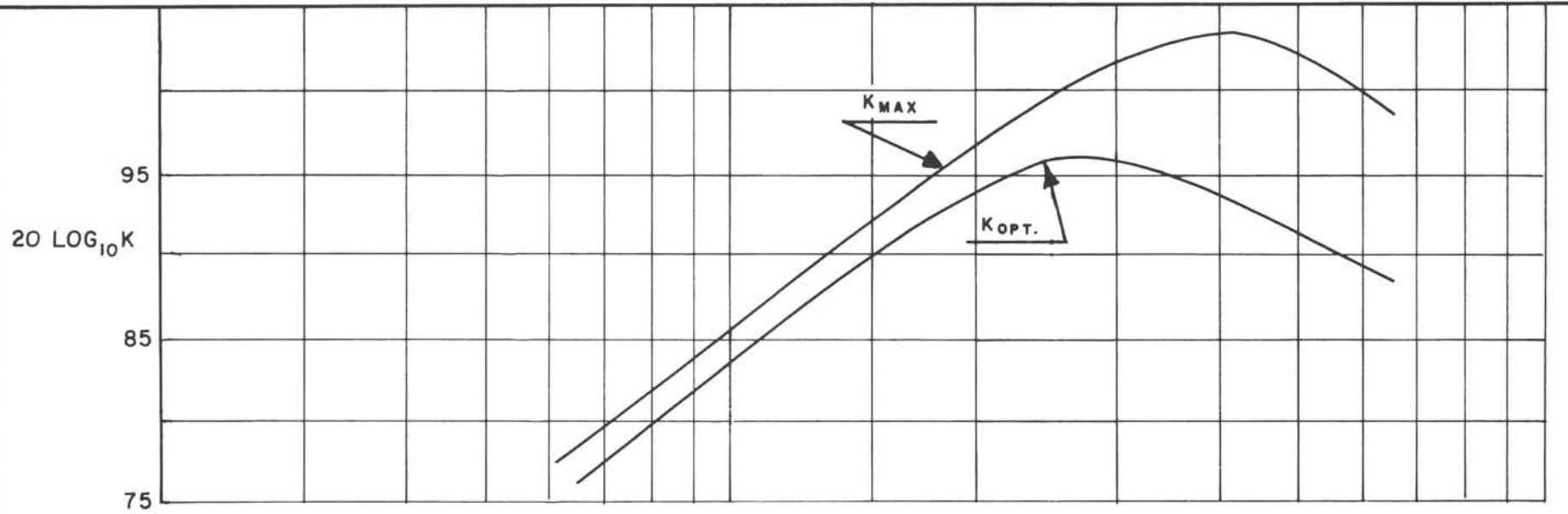




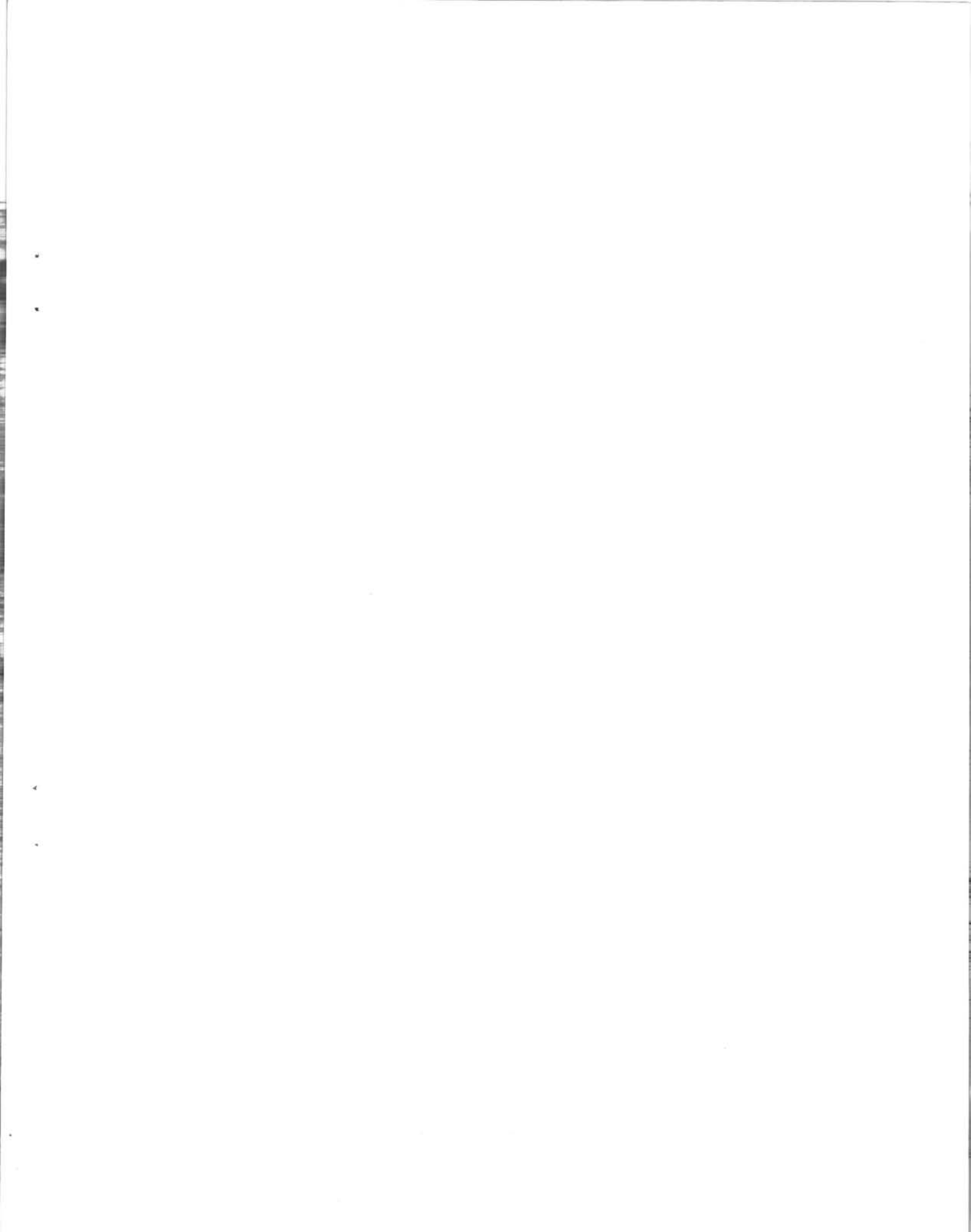


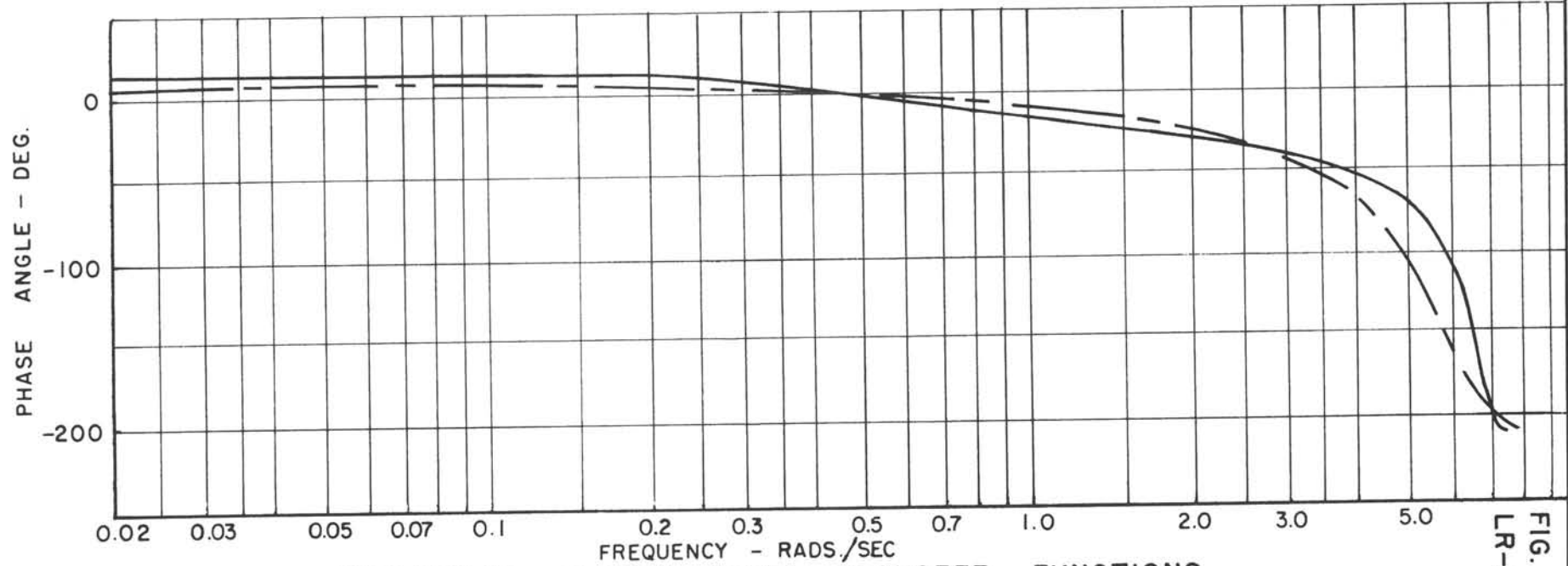
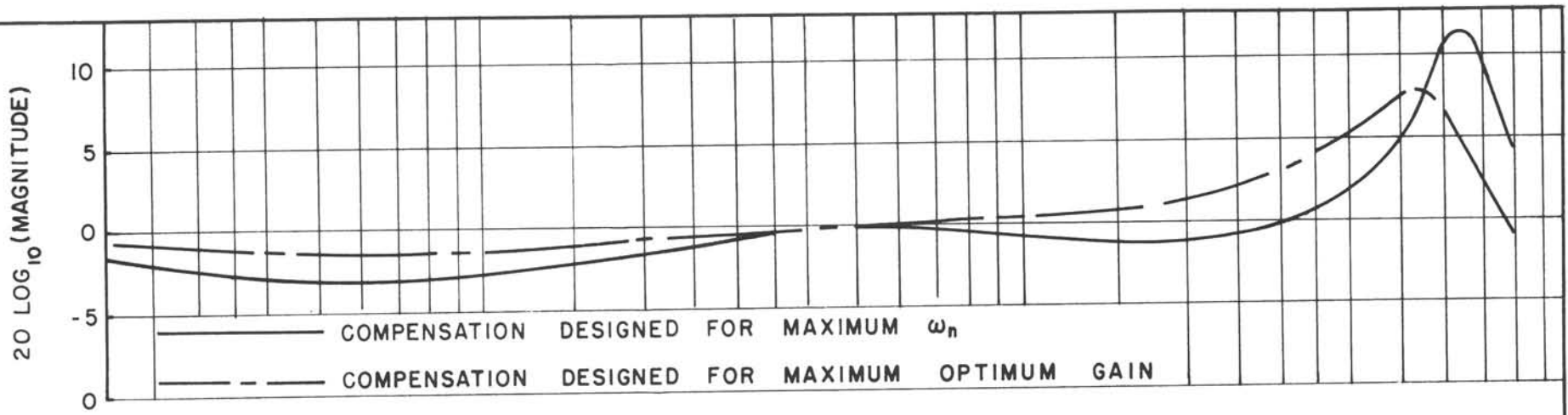




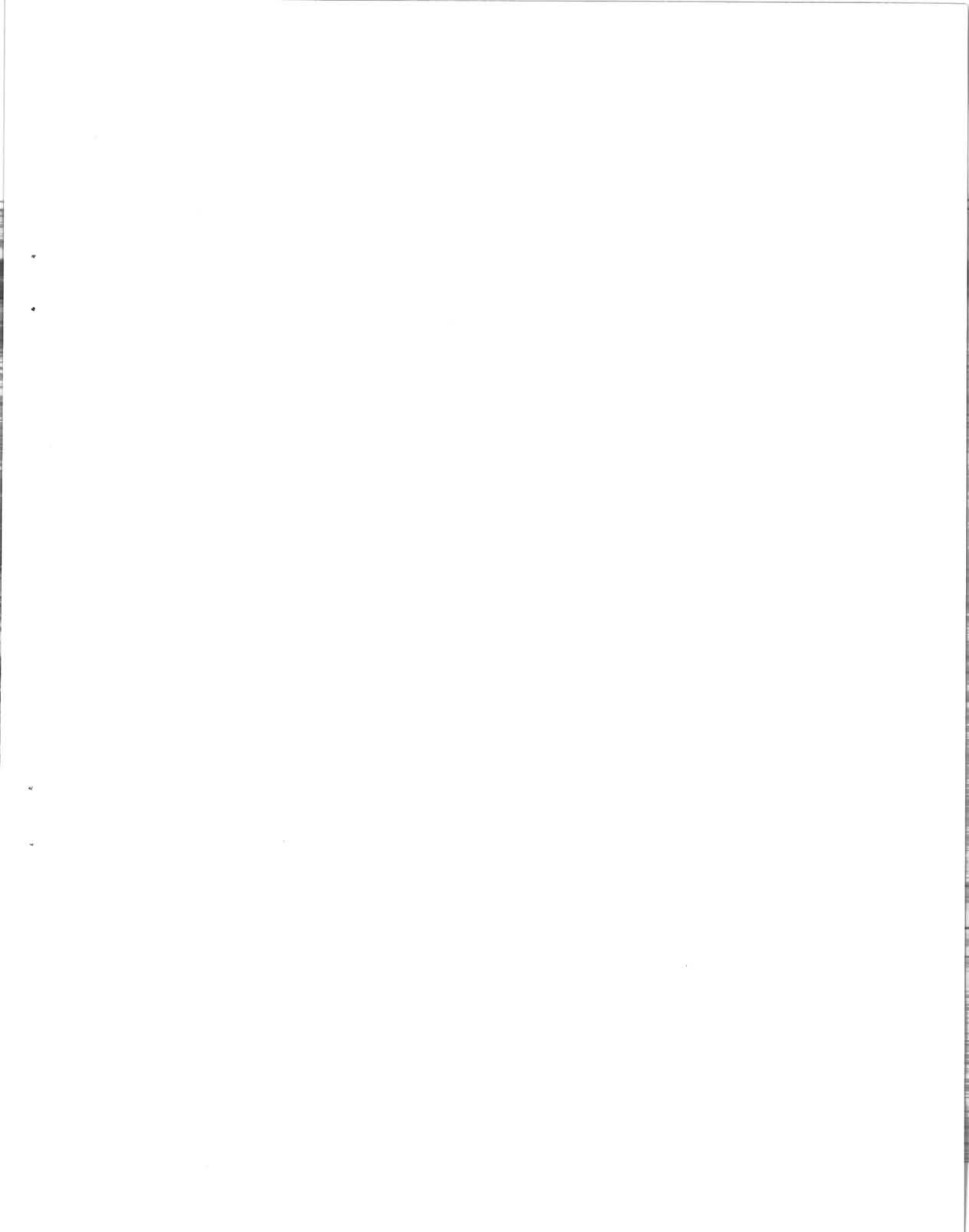


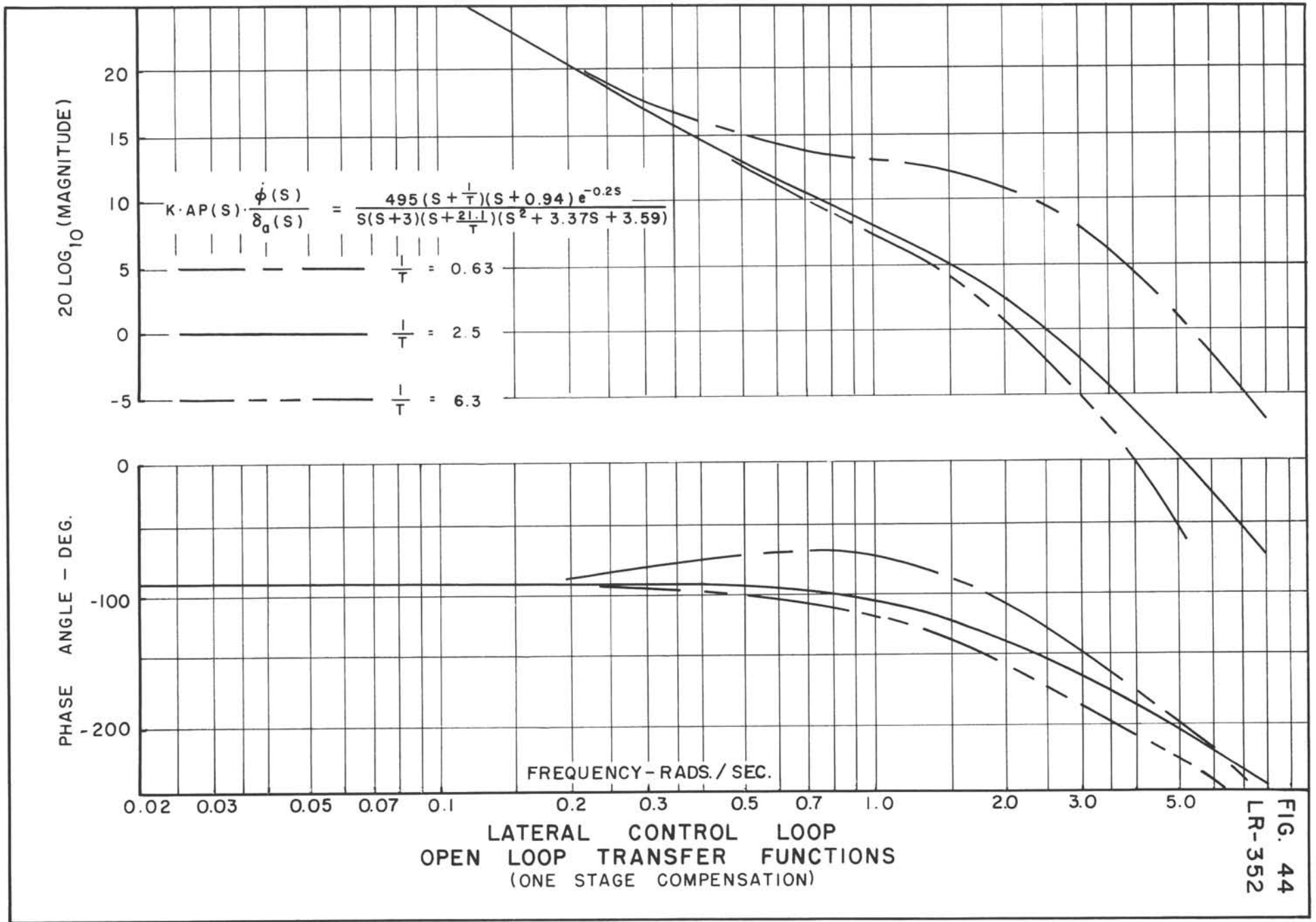
LONGITUDINAL CONTROL LOOP
 VARIATION OF K_{MAX} , K_{OPT} , AND ω_n WITH $\frac{1}{T}$
 (TWO STAGES OF COMPENSATION)





LONGITUDINAL CLOSED LOOP TRANSFER FUNCTIONS
(TWO STAGES OF COMPENSATION)







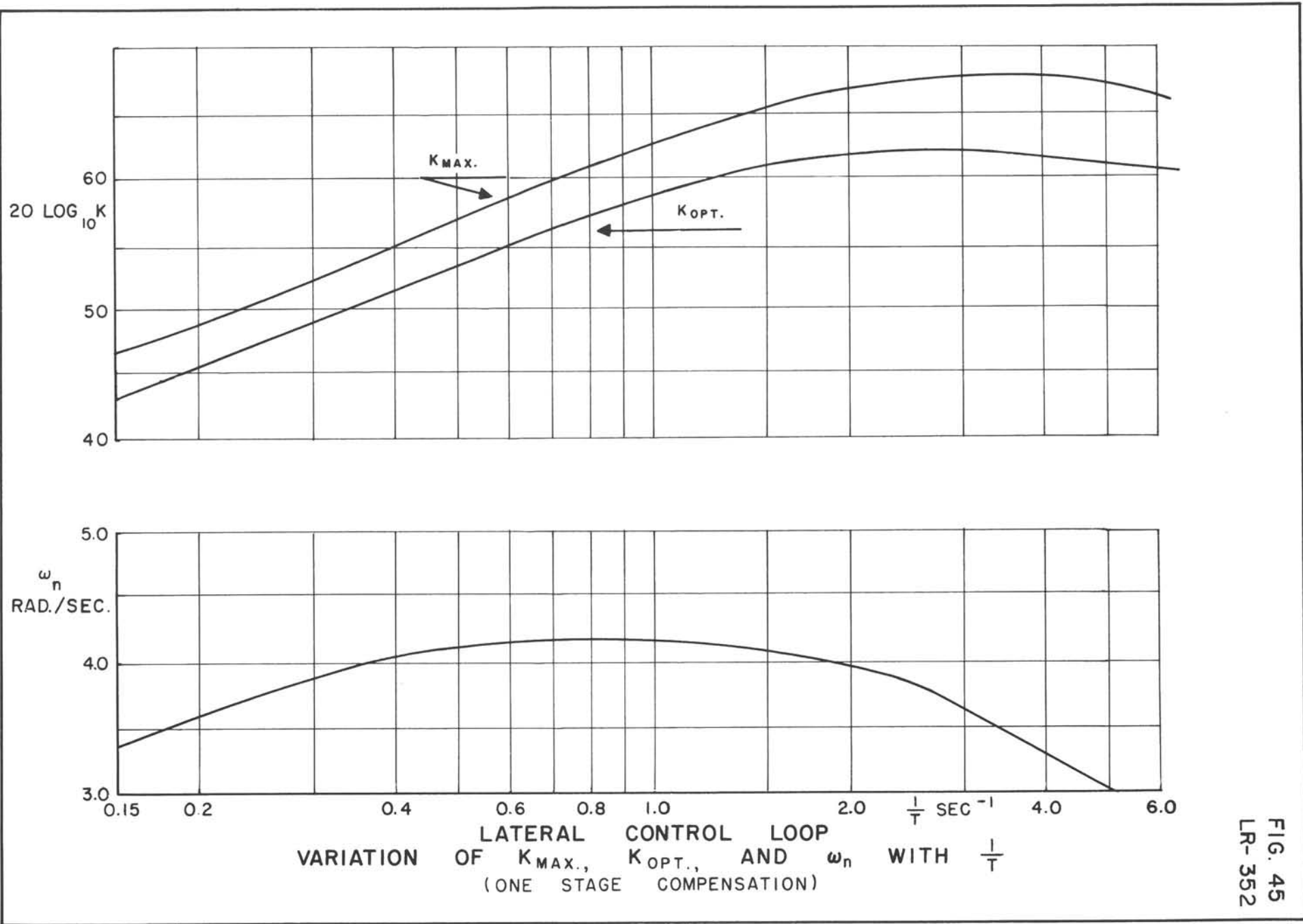
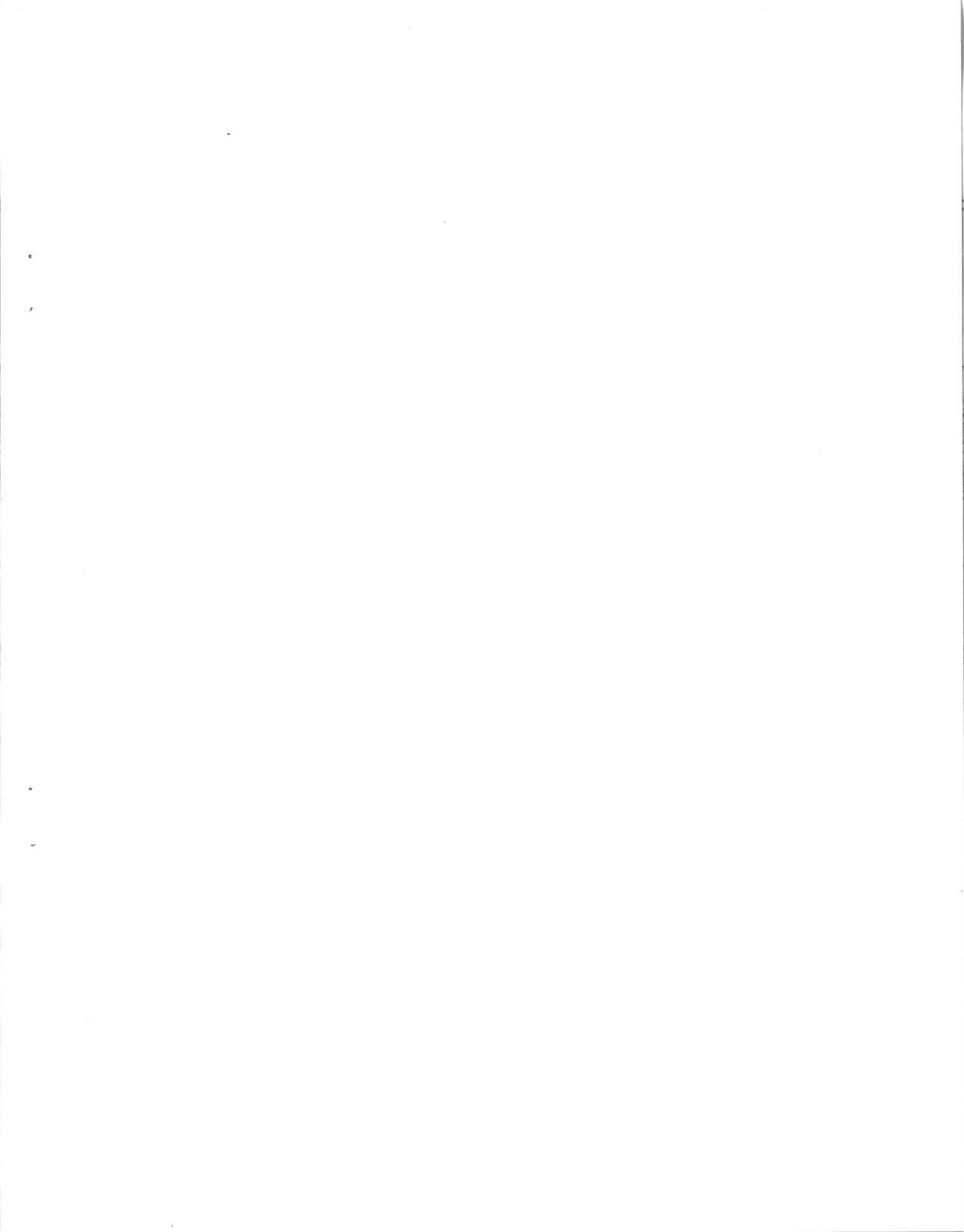
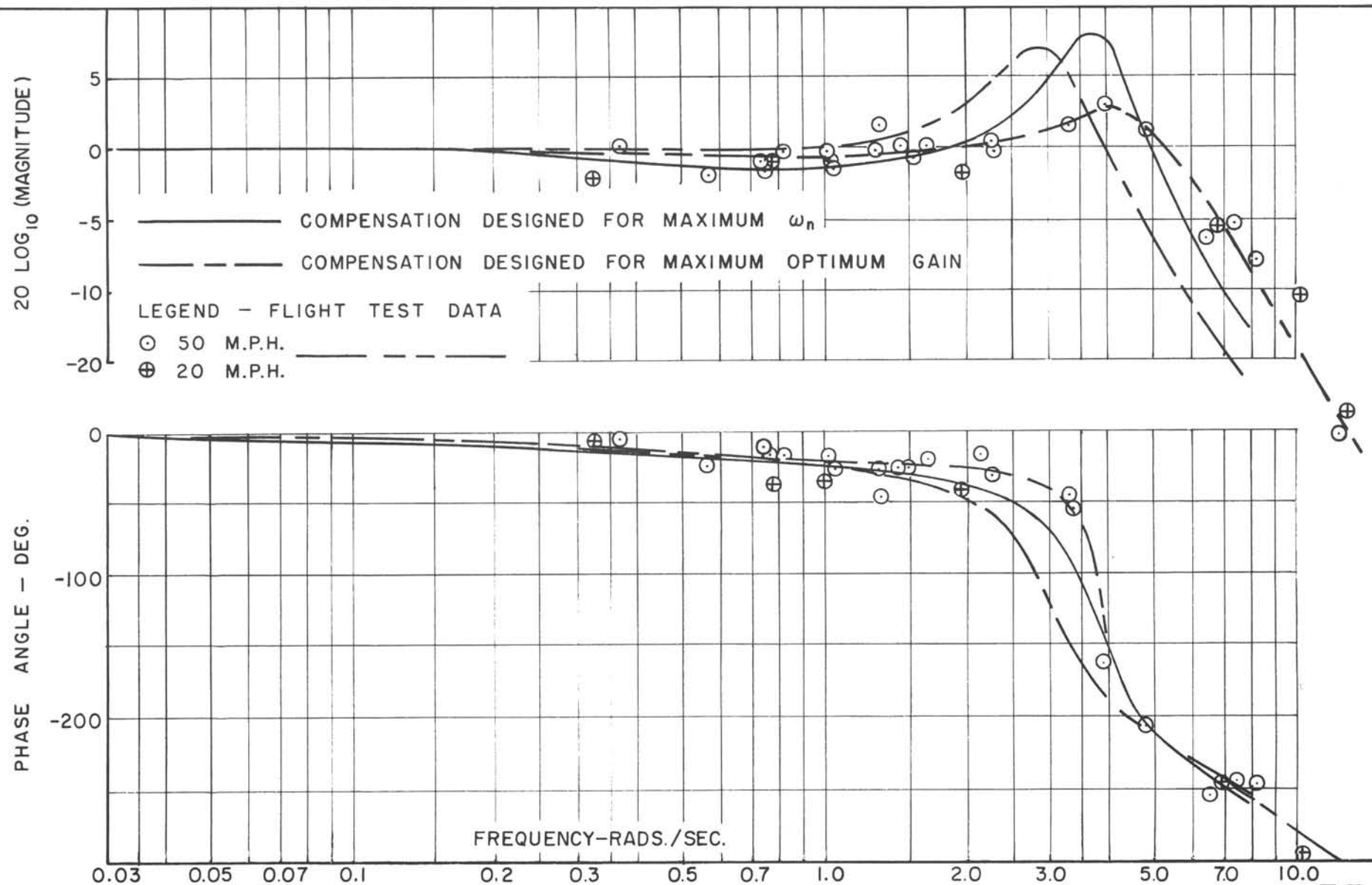


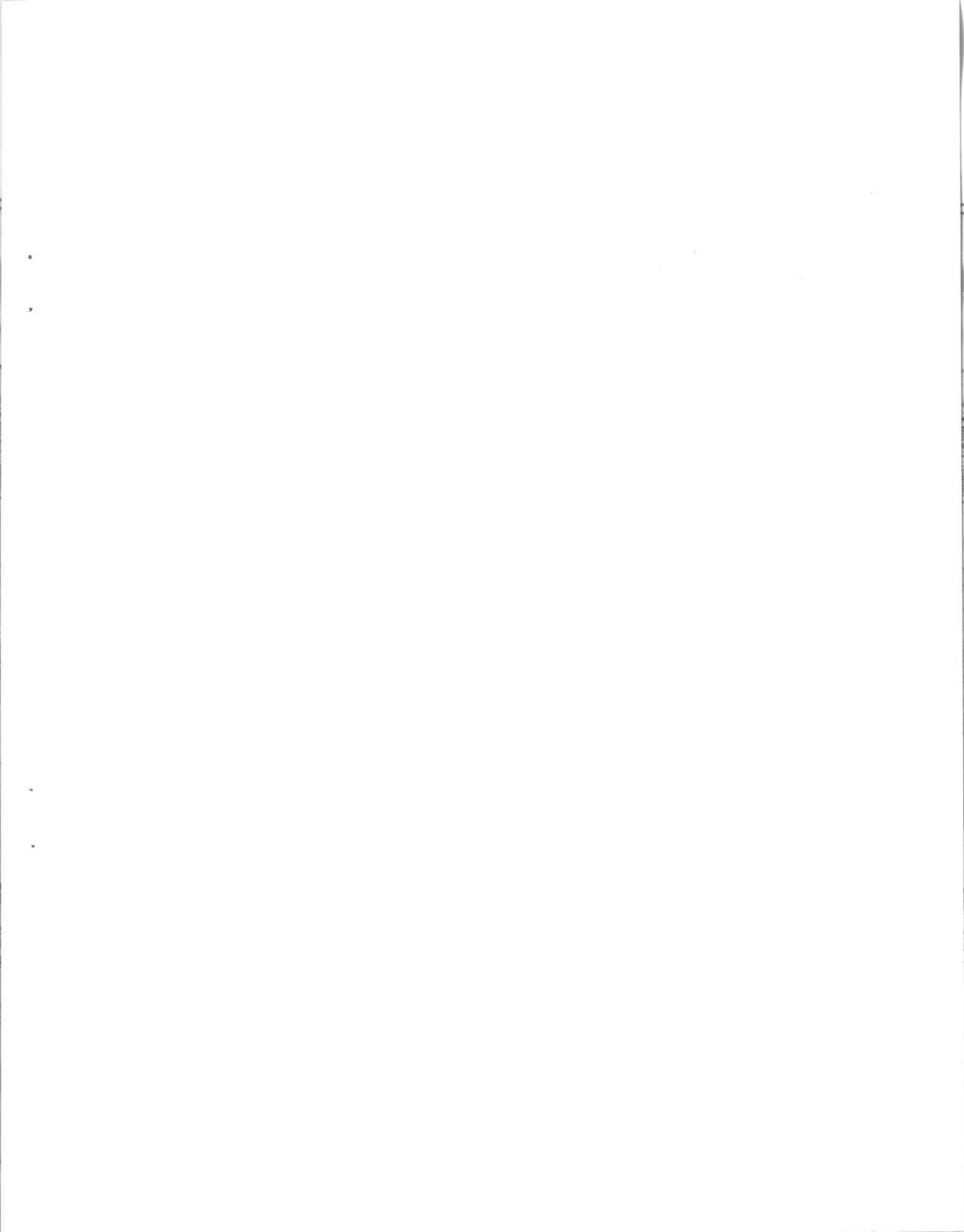
FIG. 45
LR-352

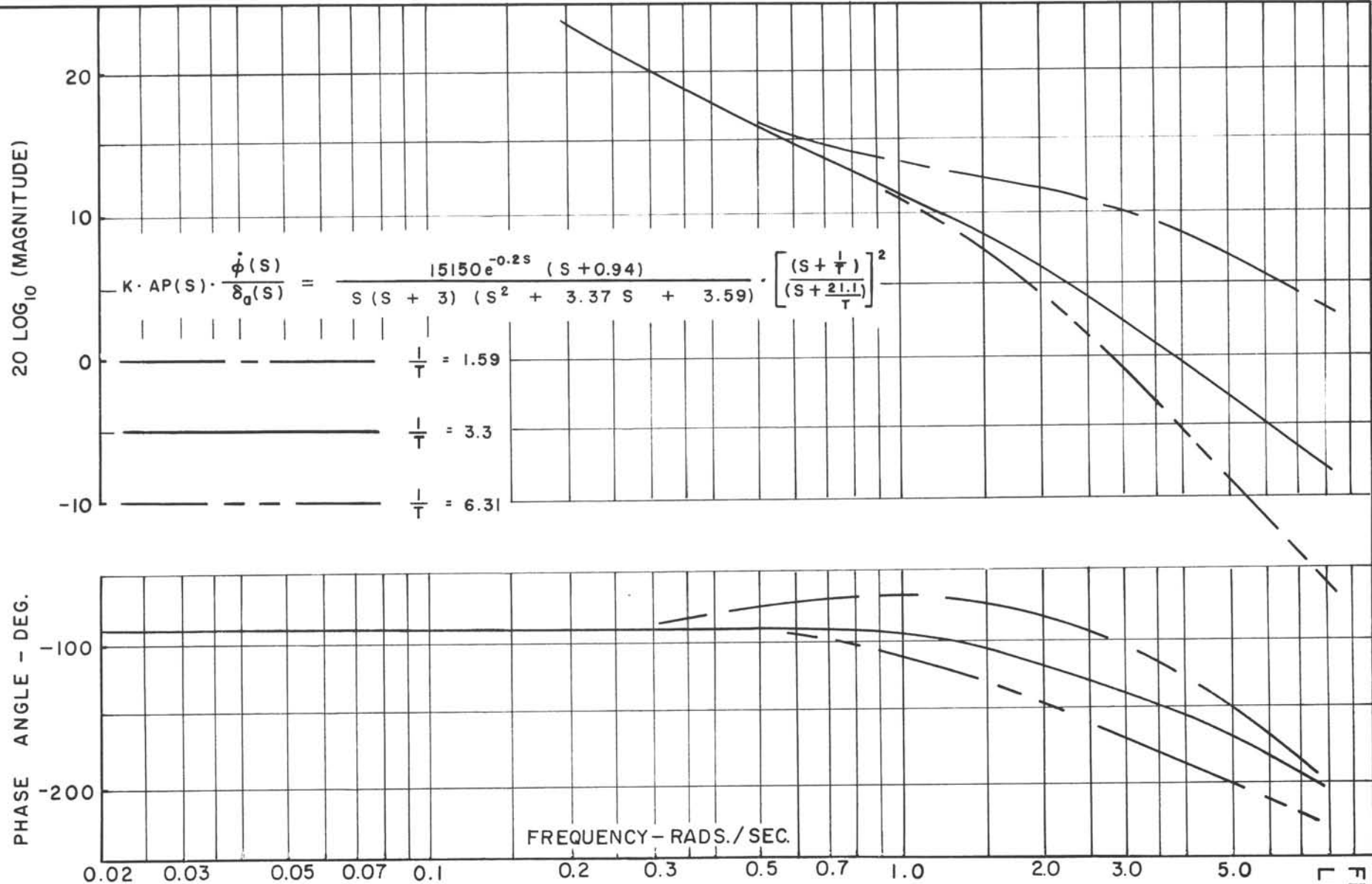




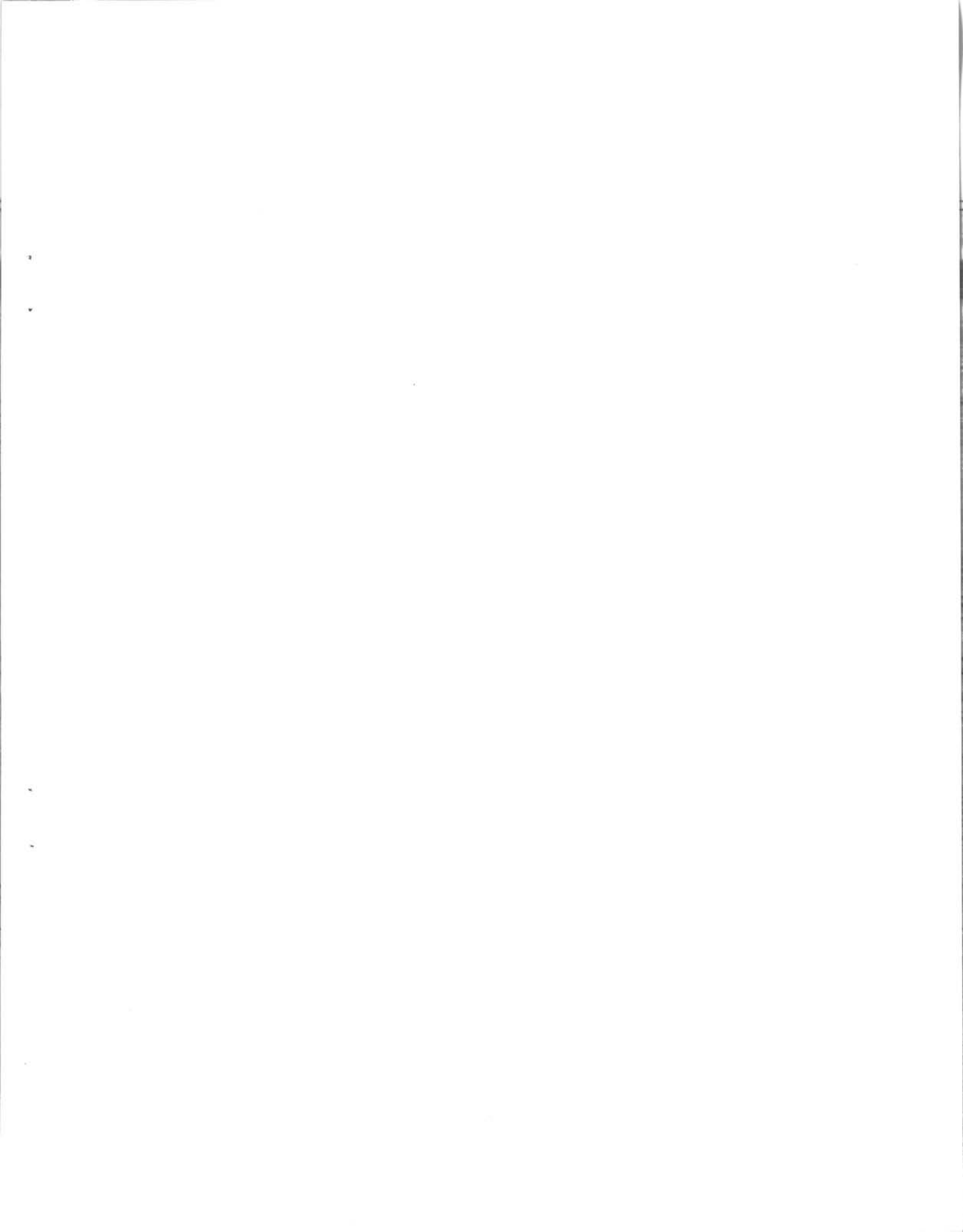
LATERAL CONTROL LOOP
 CLOSED LOOP TRANSFER FUNCTIONS
 (ONE STAGE COMPENSATION)

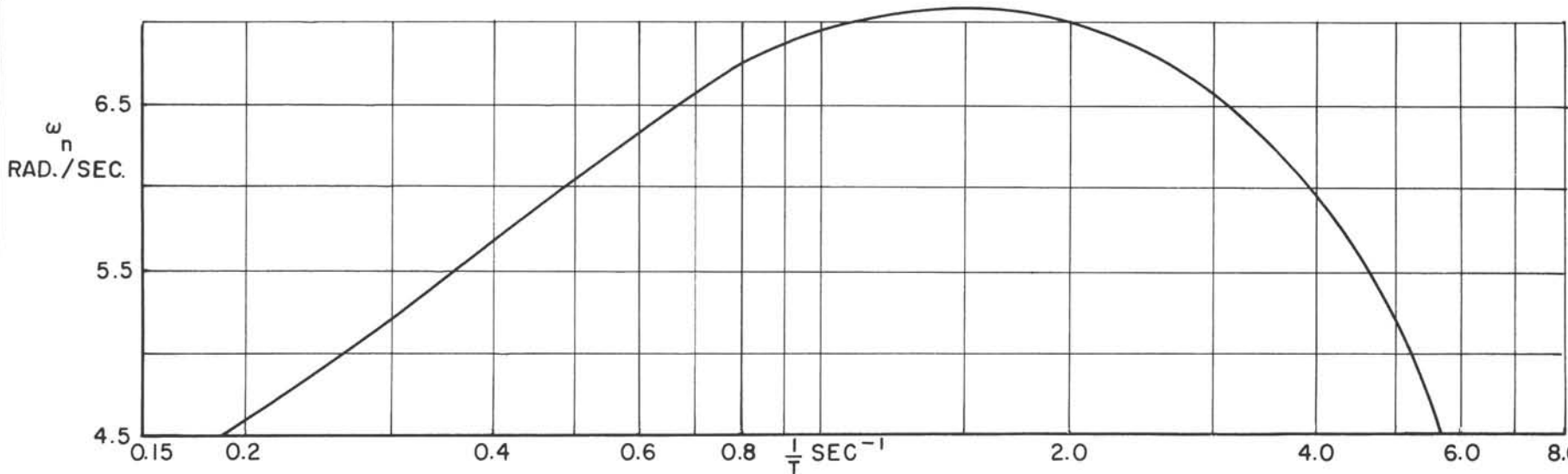
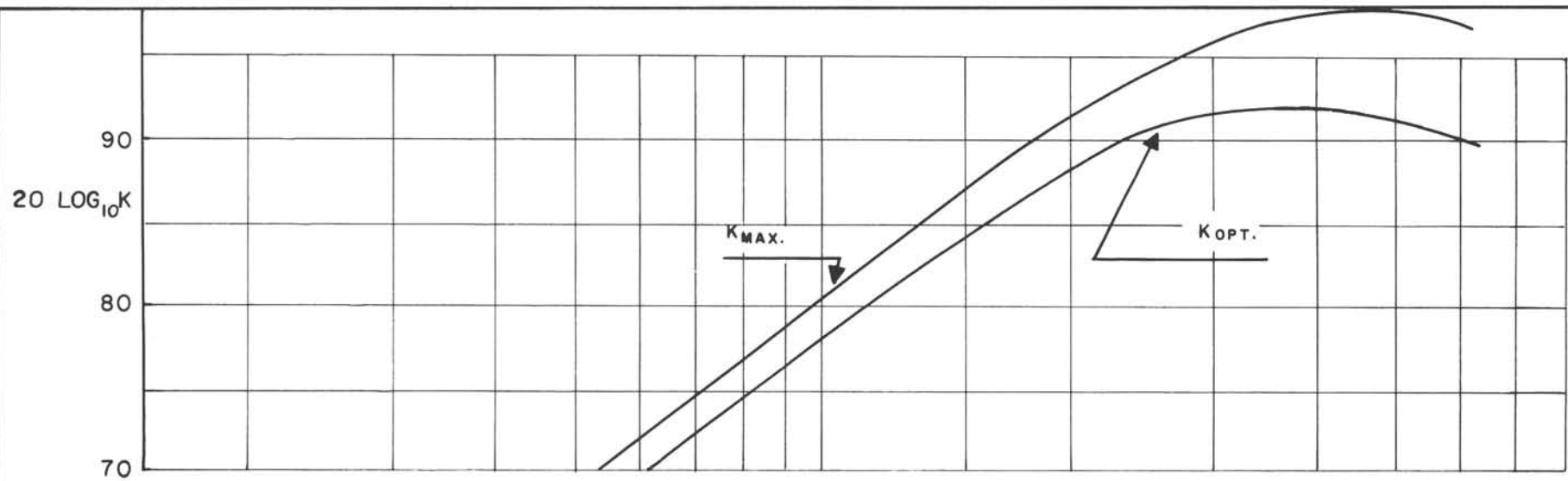
FIG. 46
 LR-352



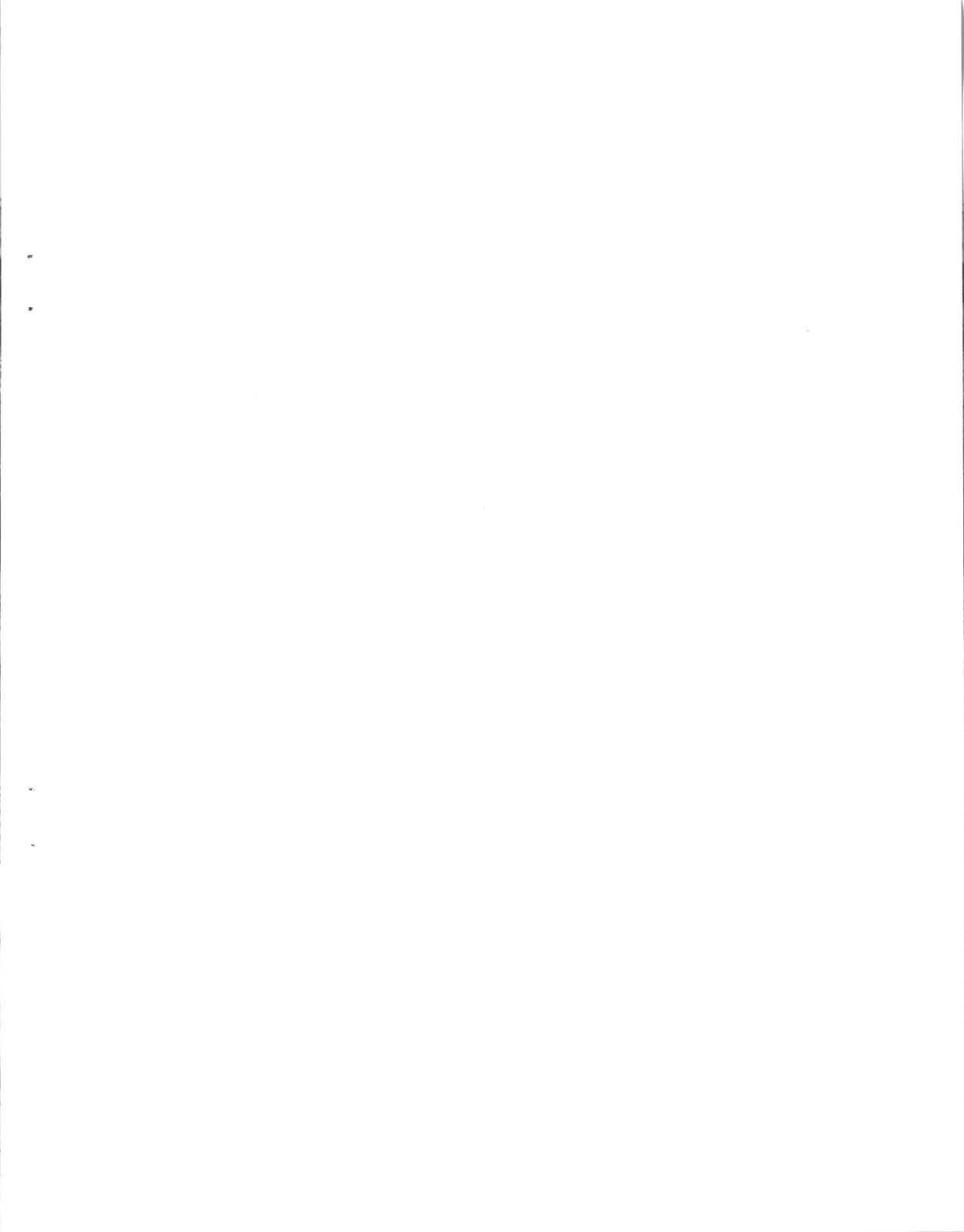


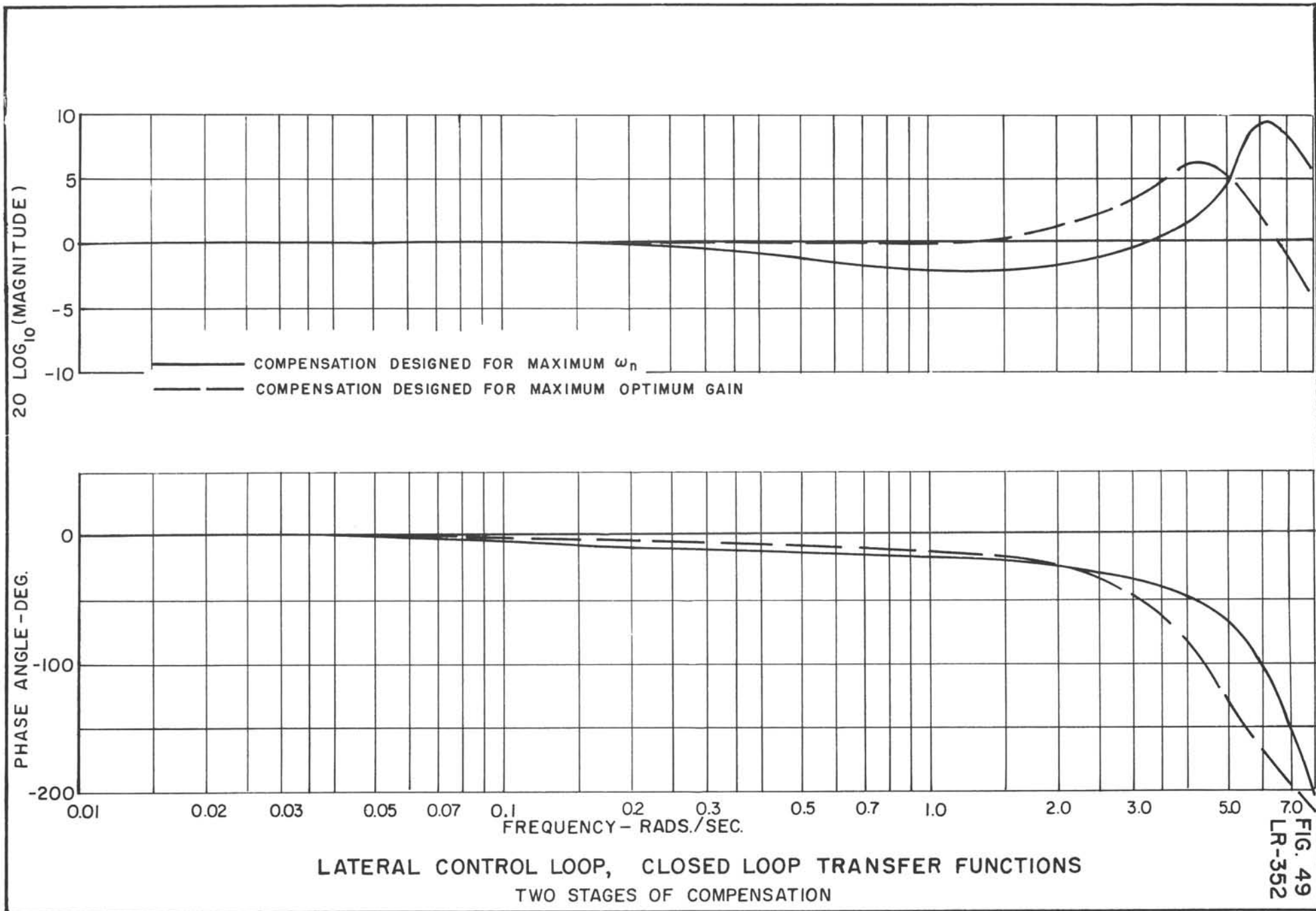
LATERAL CONTROL LOOP
 OPEN LOOP TRANSFER FUNCTIONS
 (TWO STAGES OF COMPENSATION)

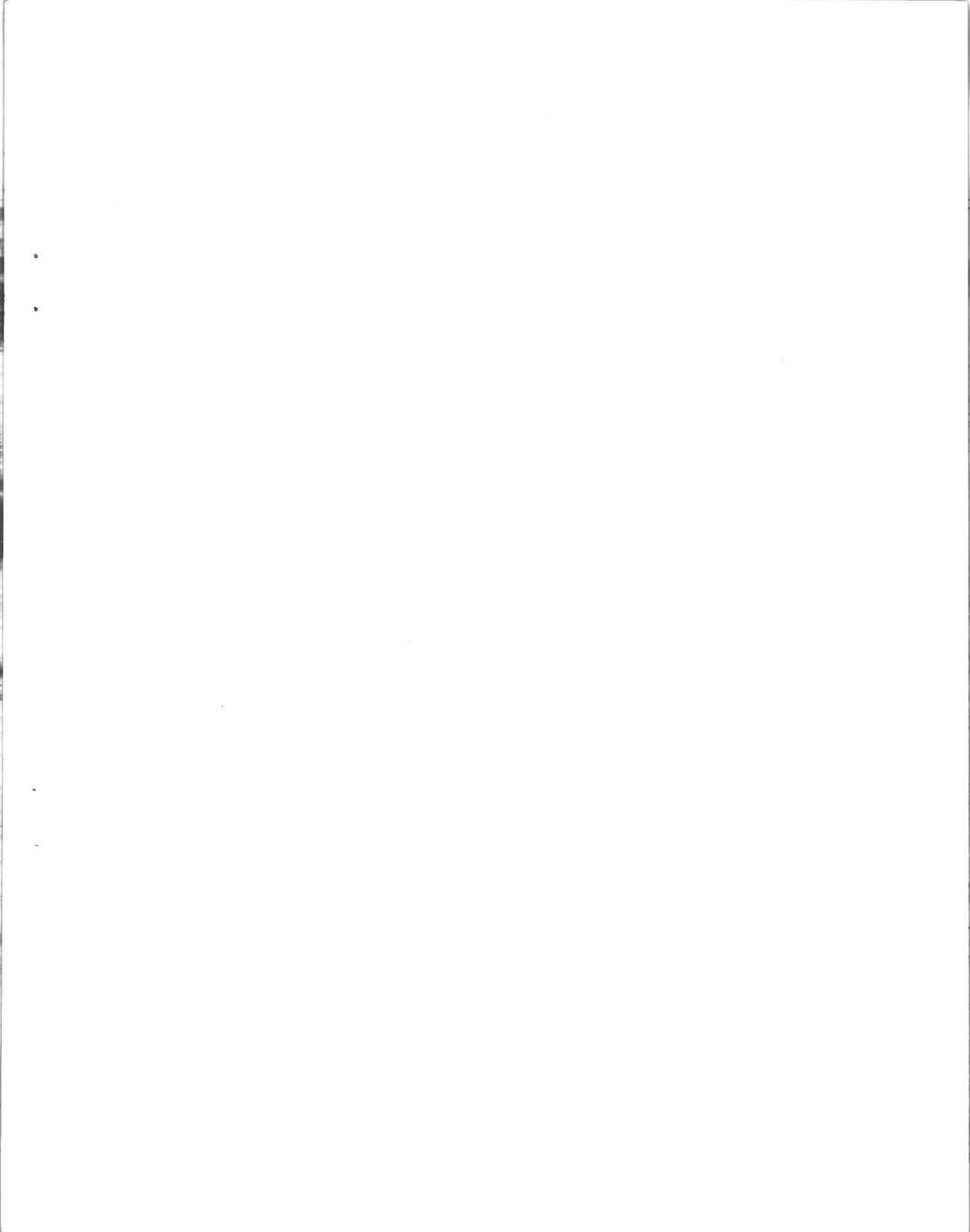


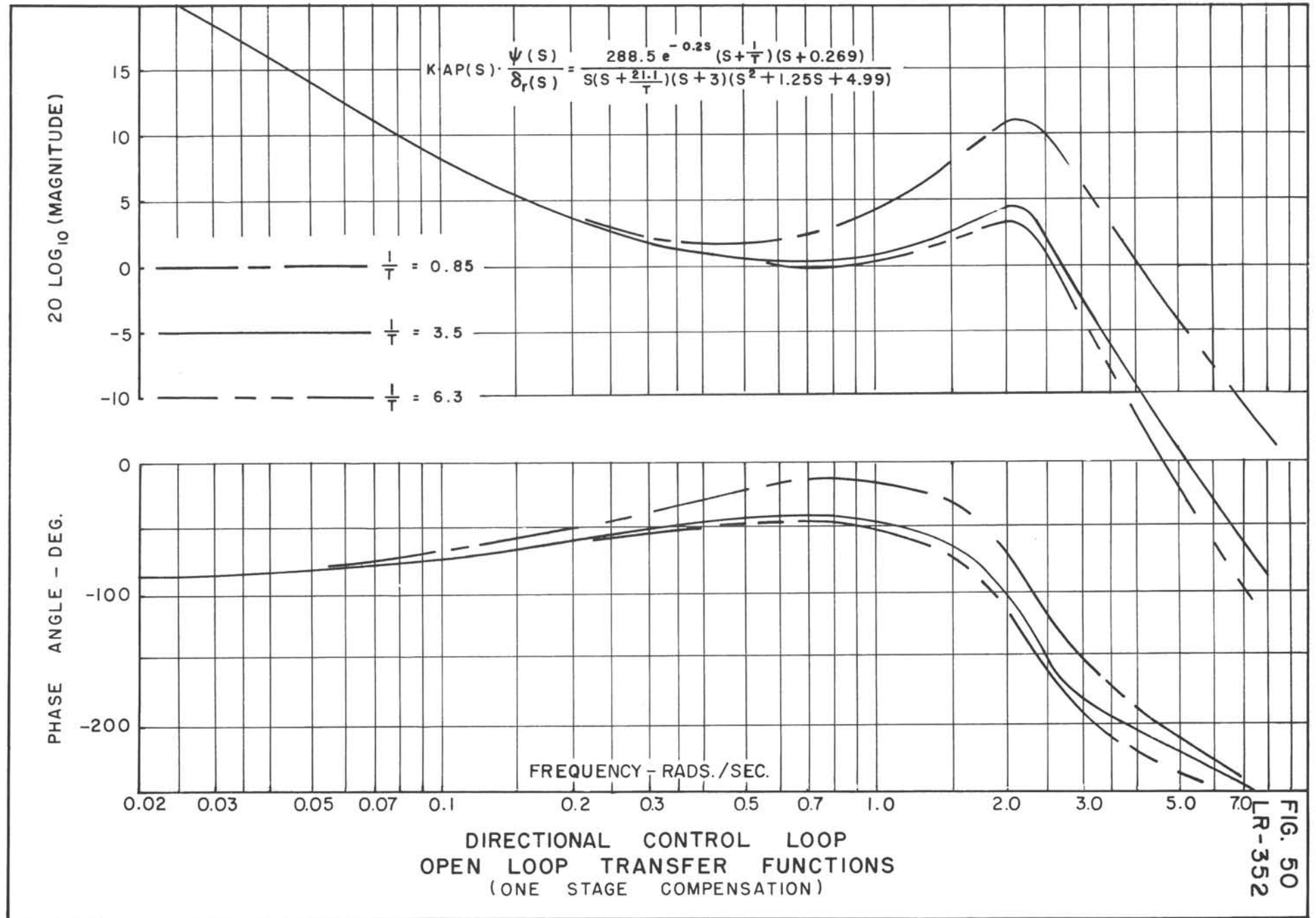


VARIATION OF $K_{MAX.}$, $K_{OPT.}$, AND ω_n WITH $\frac{1}{T}$
 (TWO STAGES OF COMPENSATION)

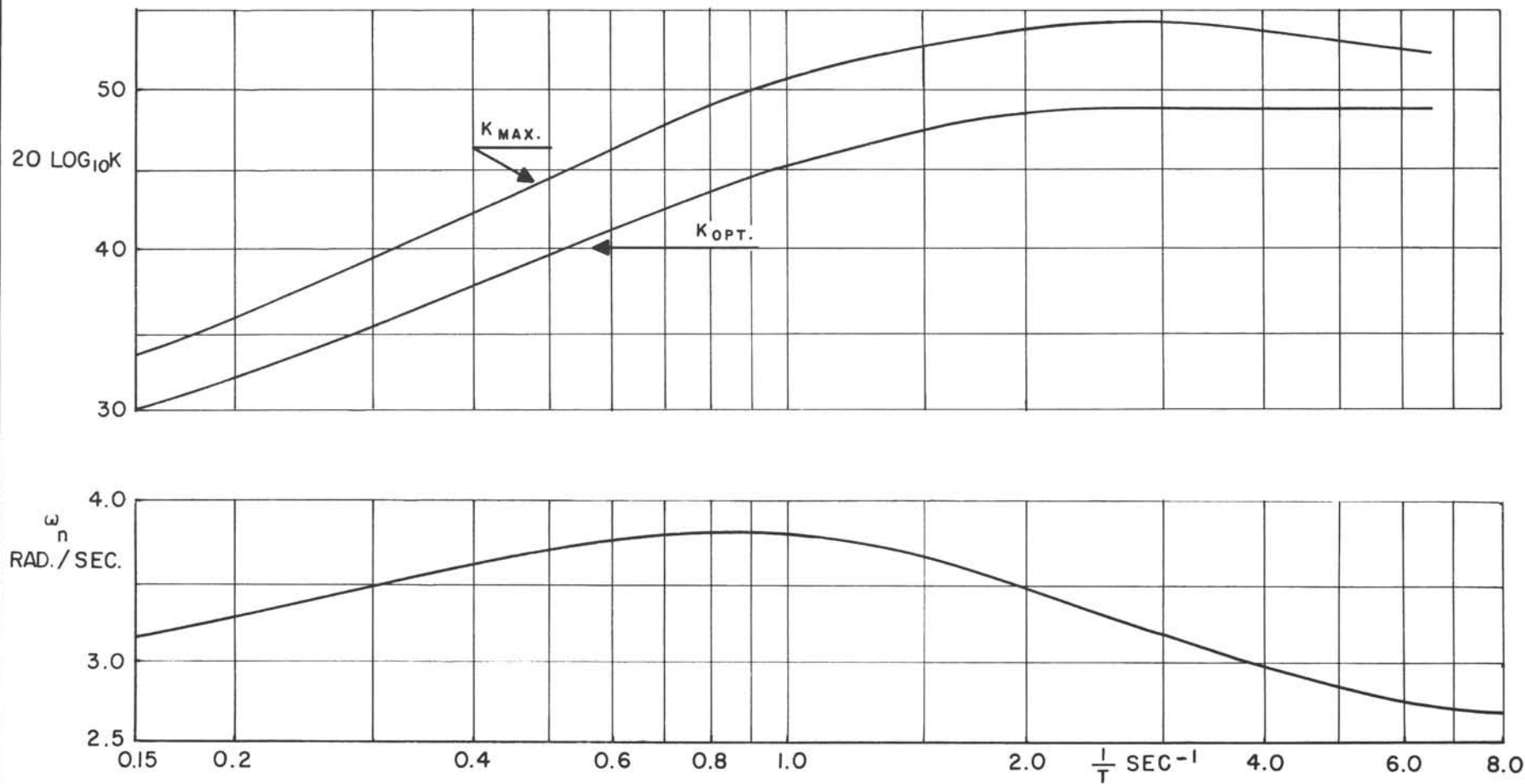




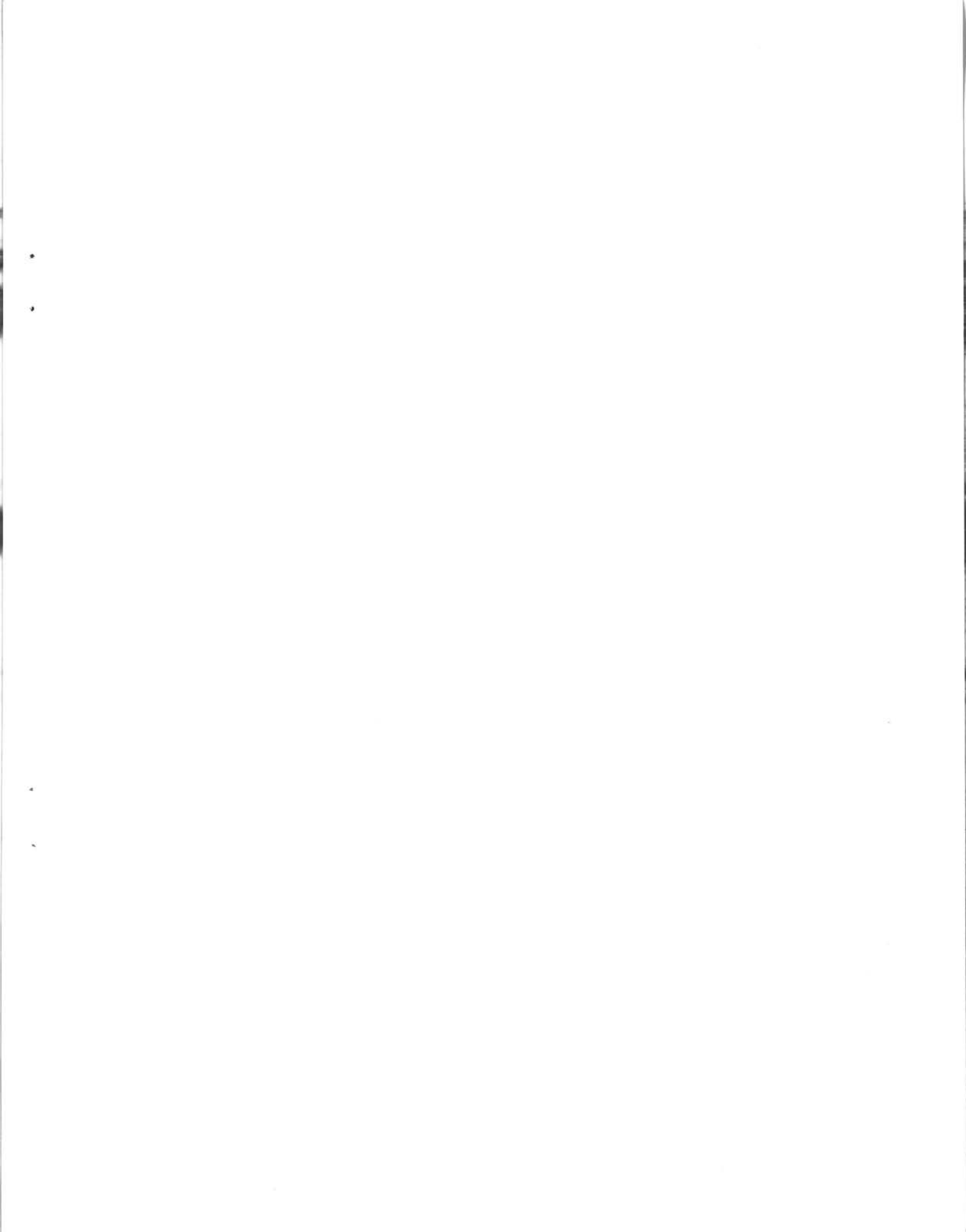








DIRECTIONAL CONTROL LOOP
 VARIATION OF $K_{\text{MAX.}}$, $K_{\text{OPT.}}$, AND ω_n WITH $\frac{1}{T}$
 (ONE STAGE COMPENSATION)



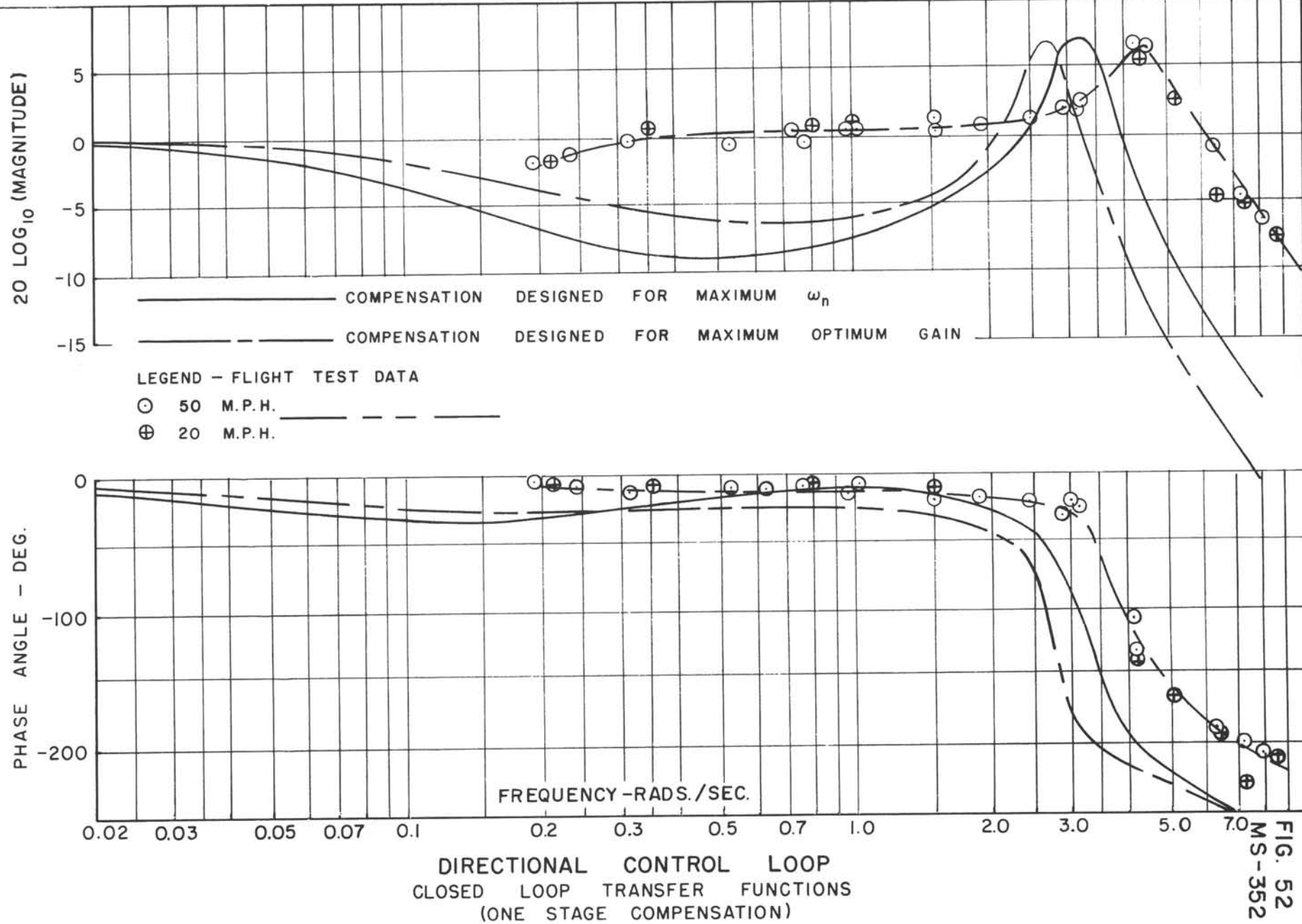
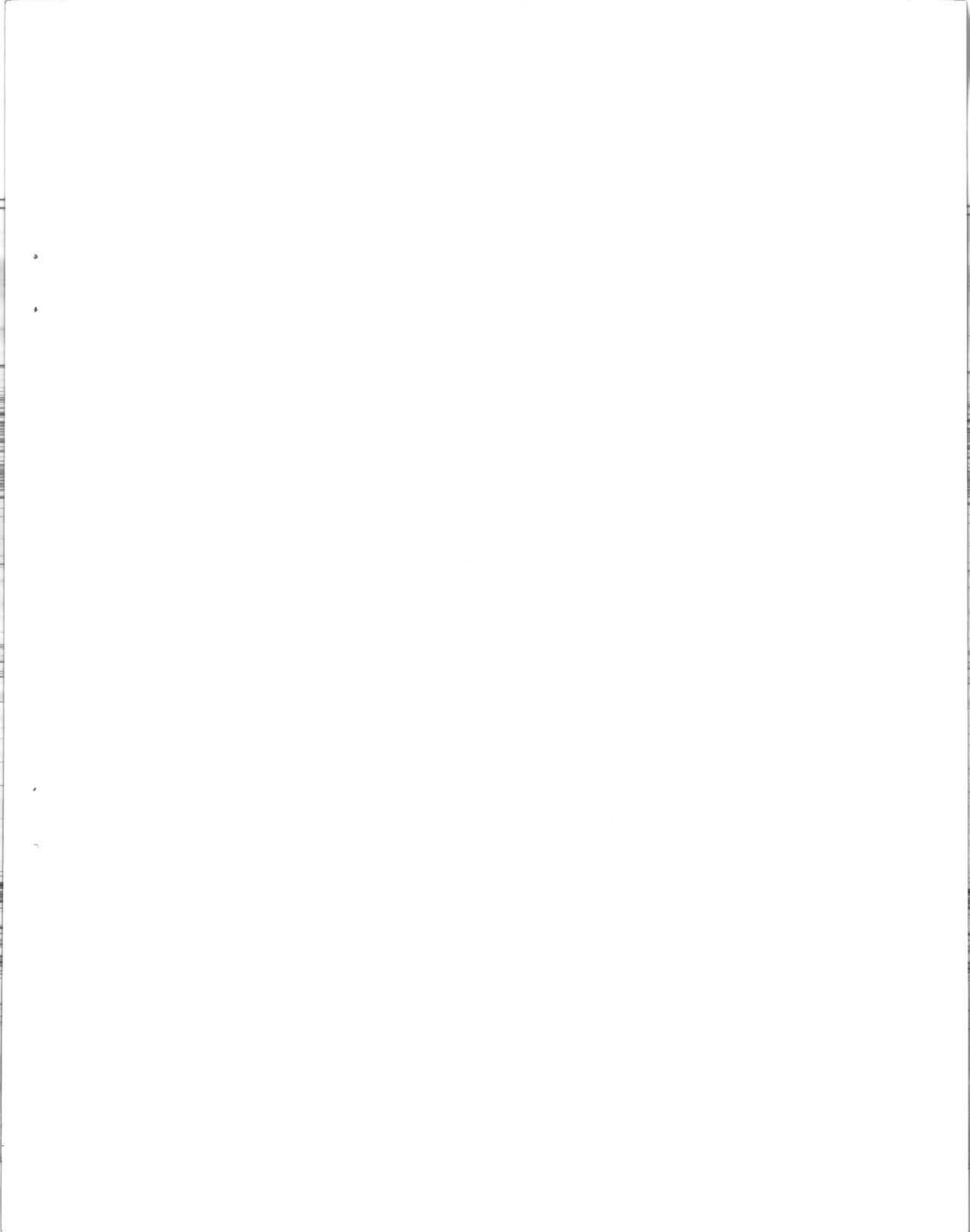


FIG. 52
 MS-352



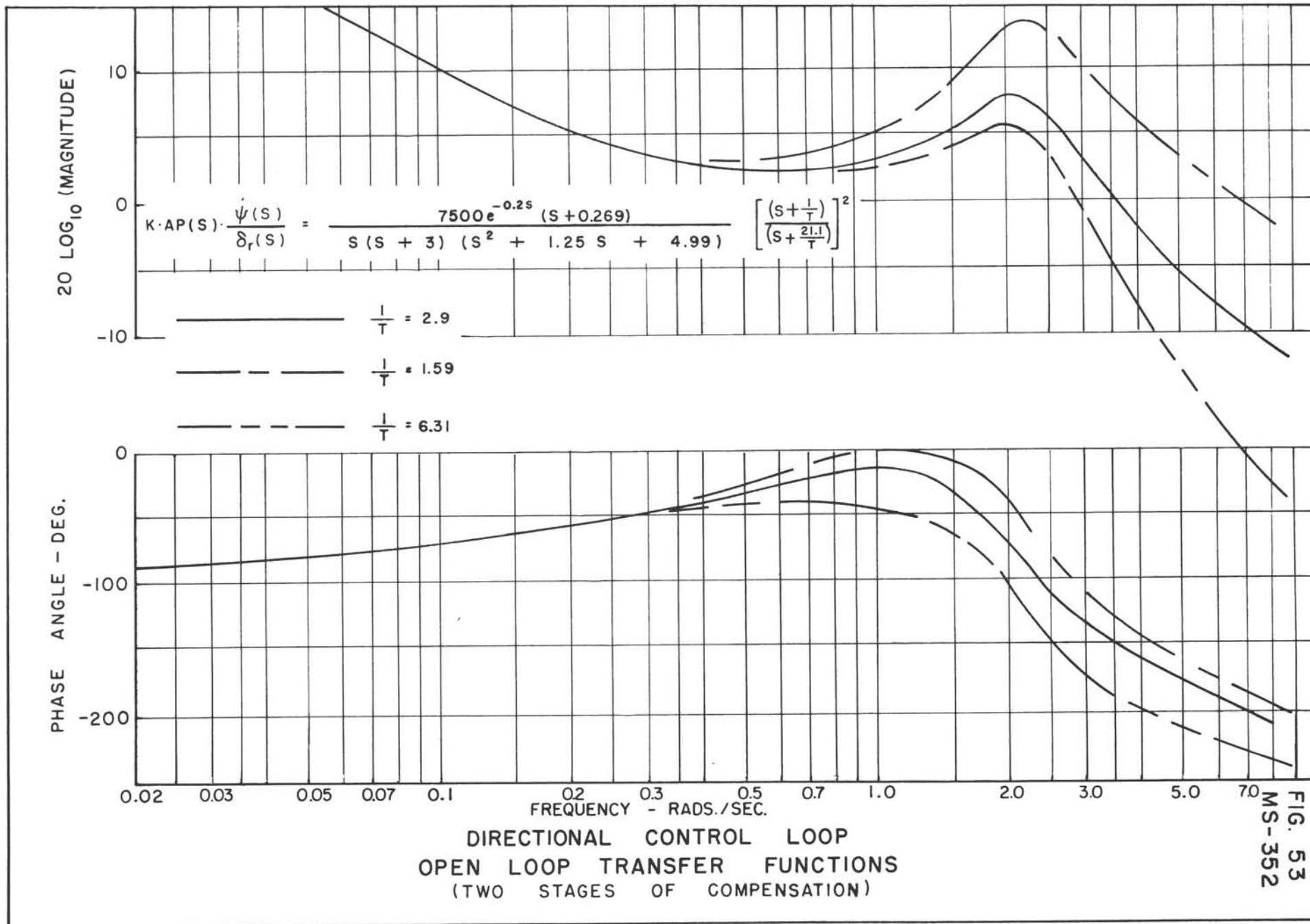
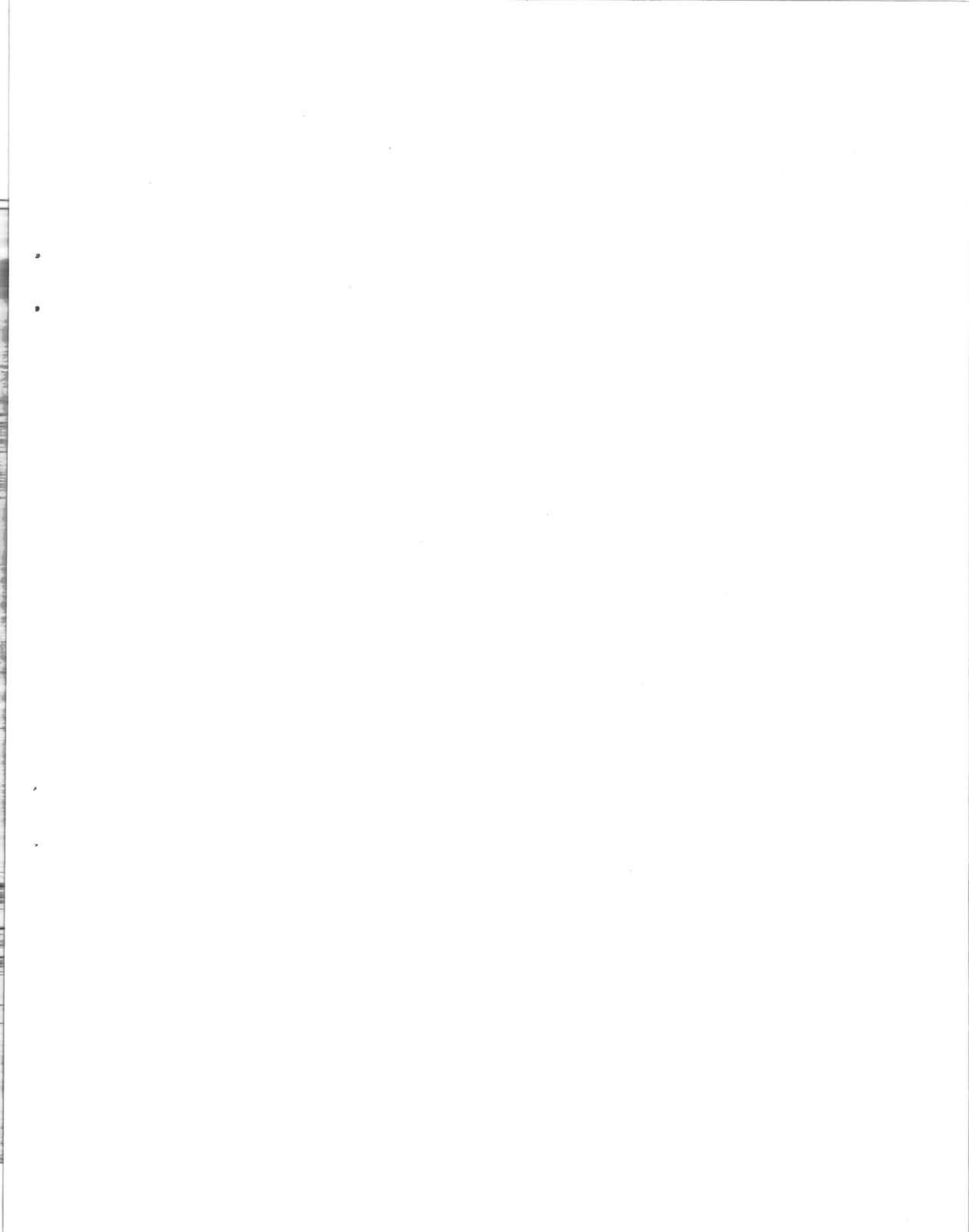
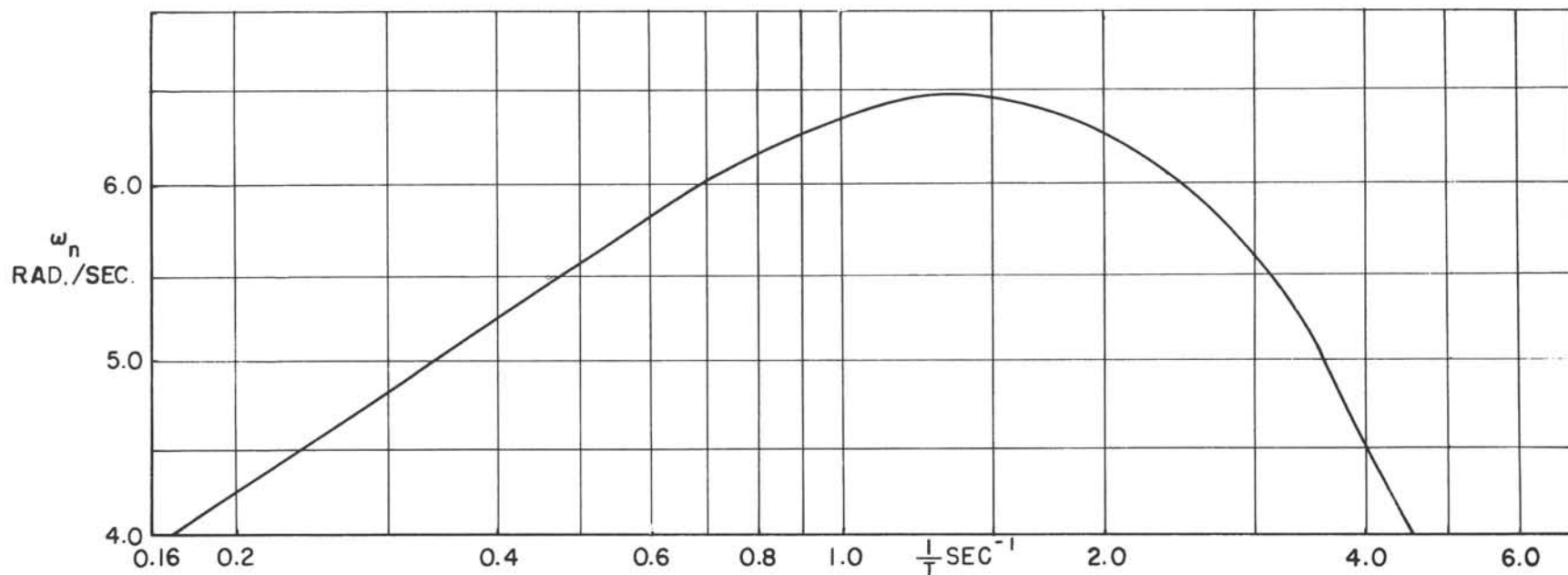
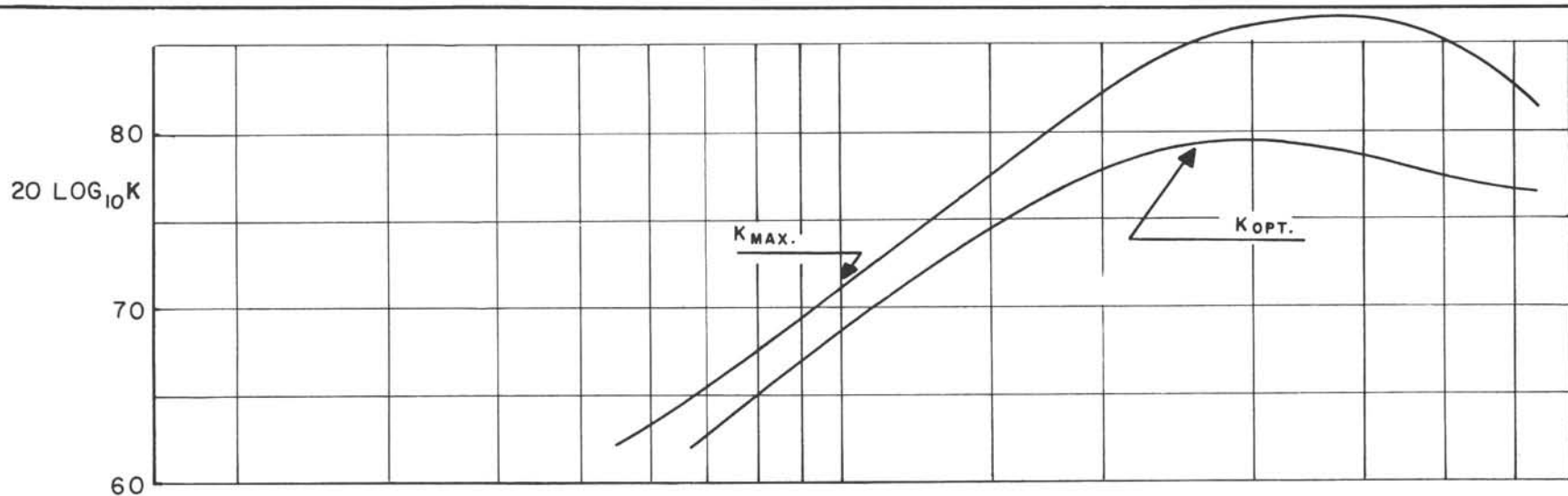
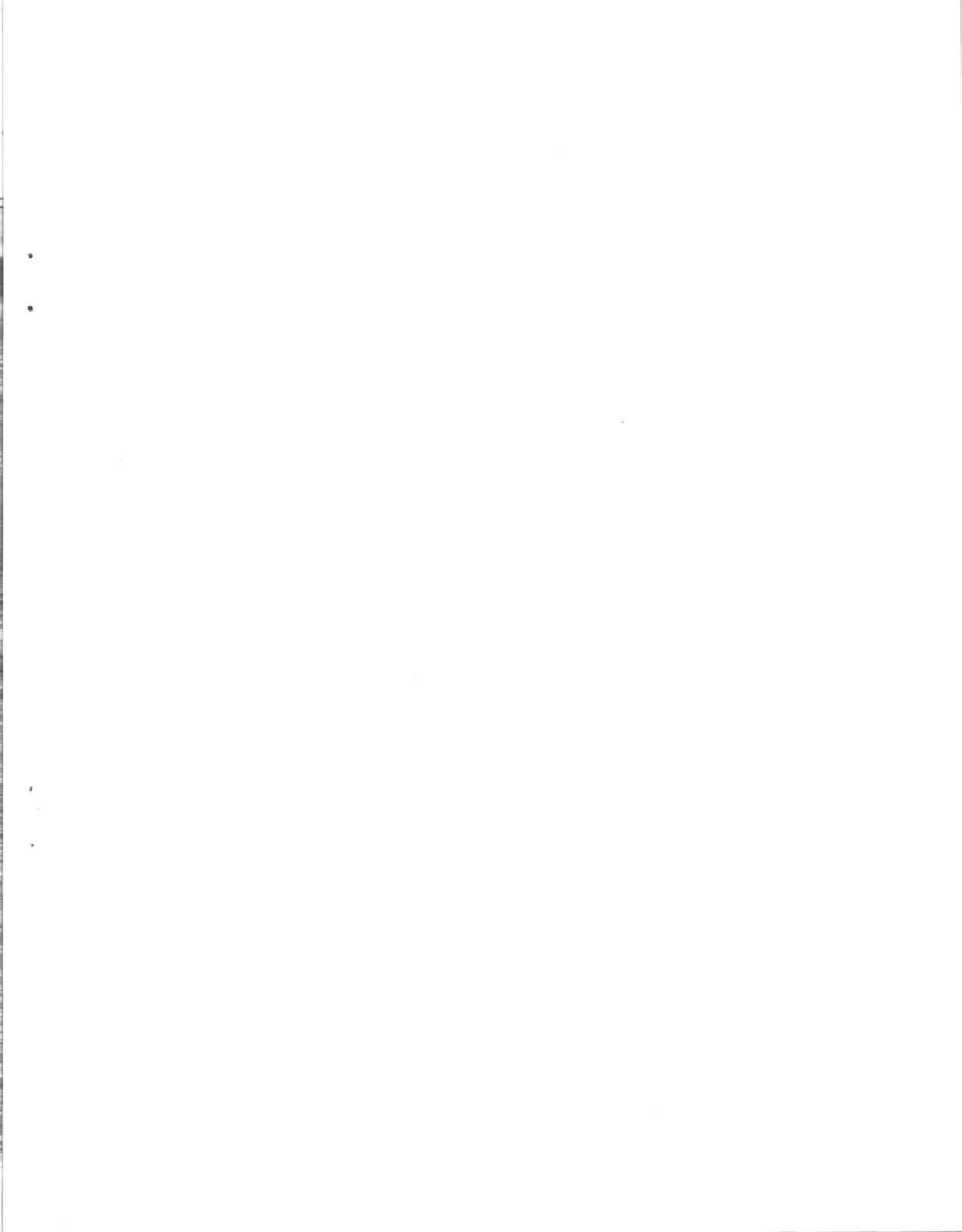


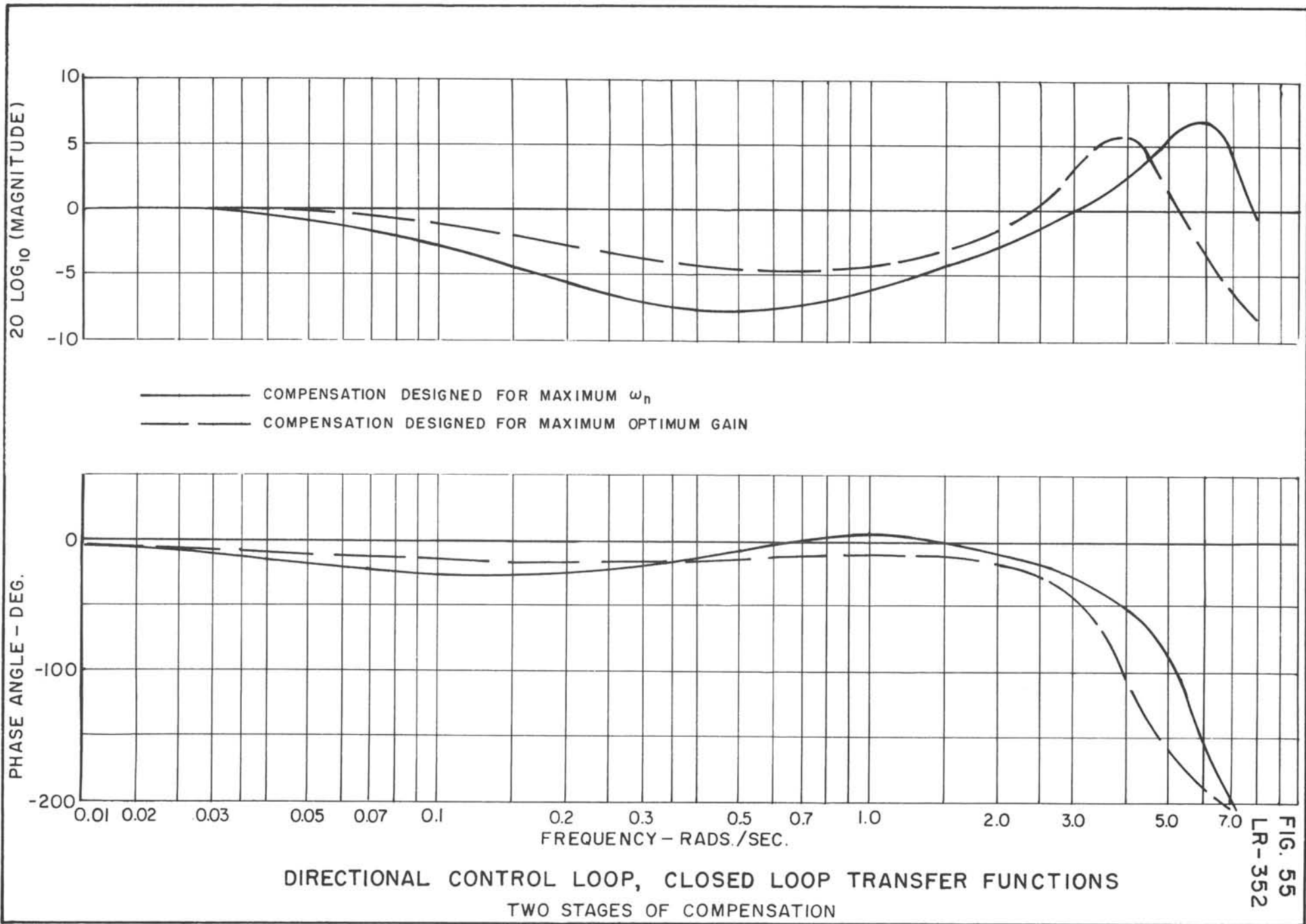
FIG. 53
MS-352

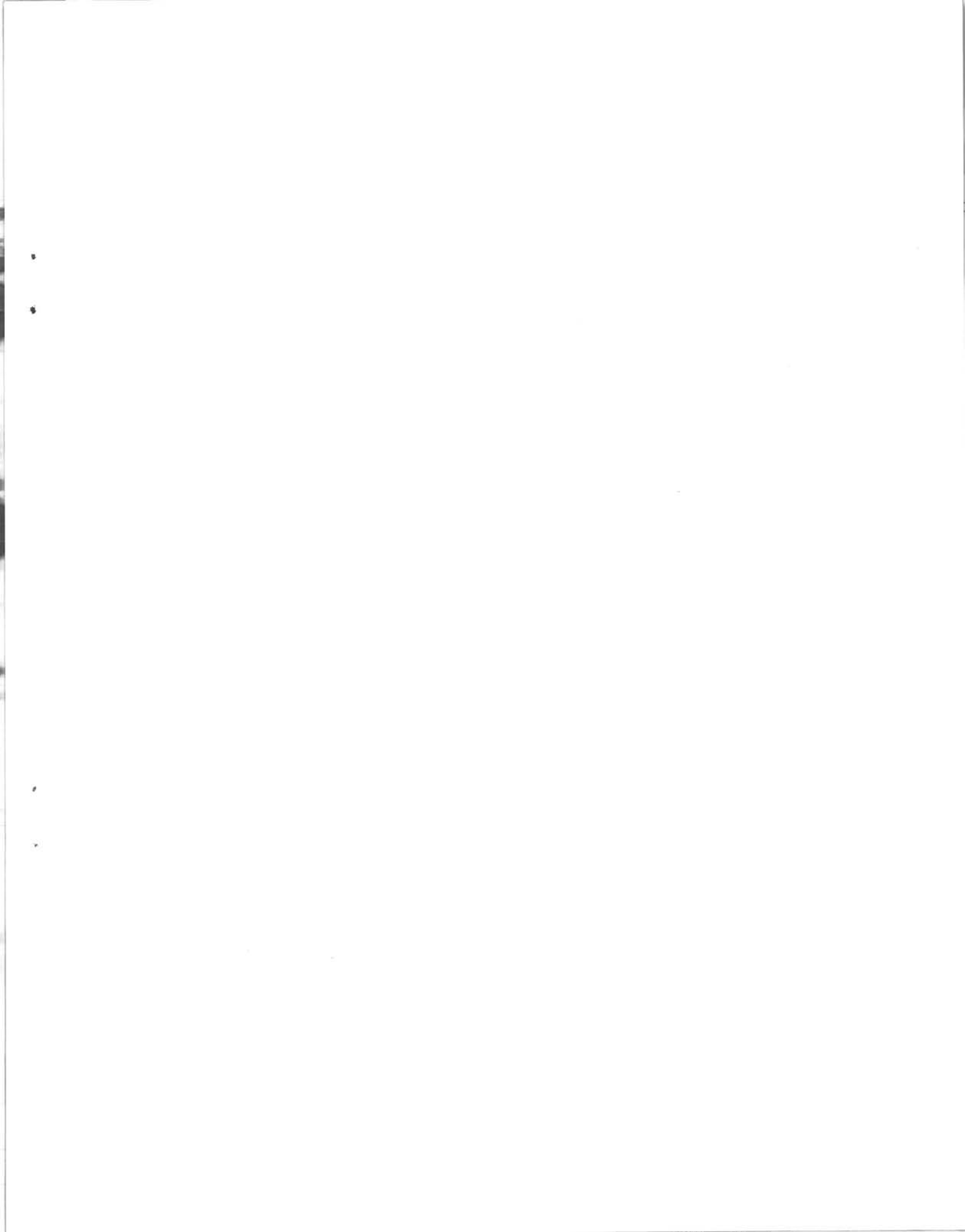


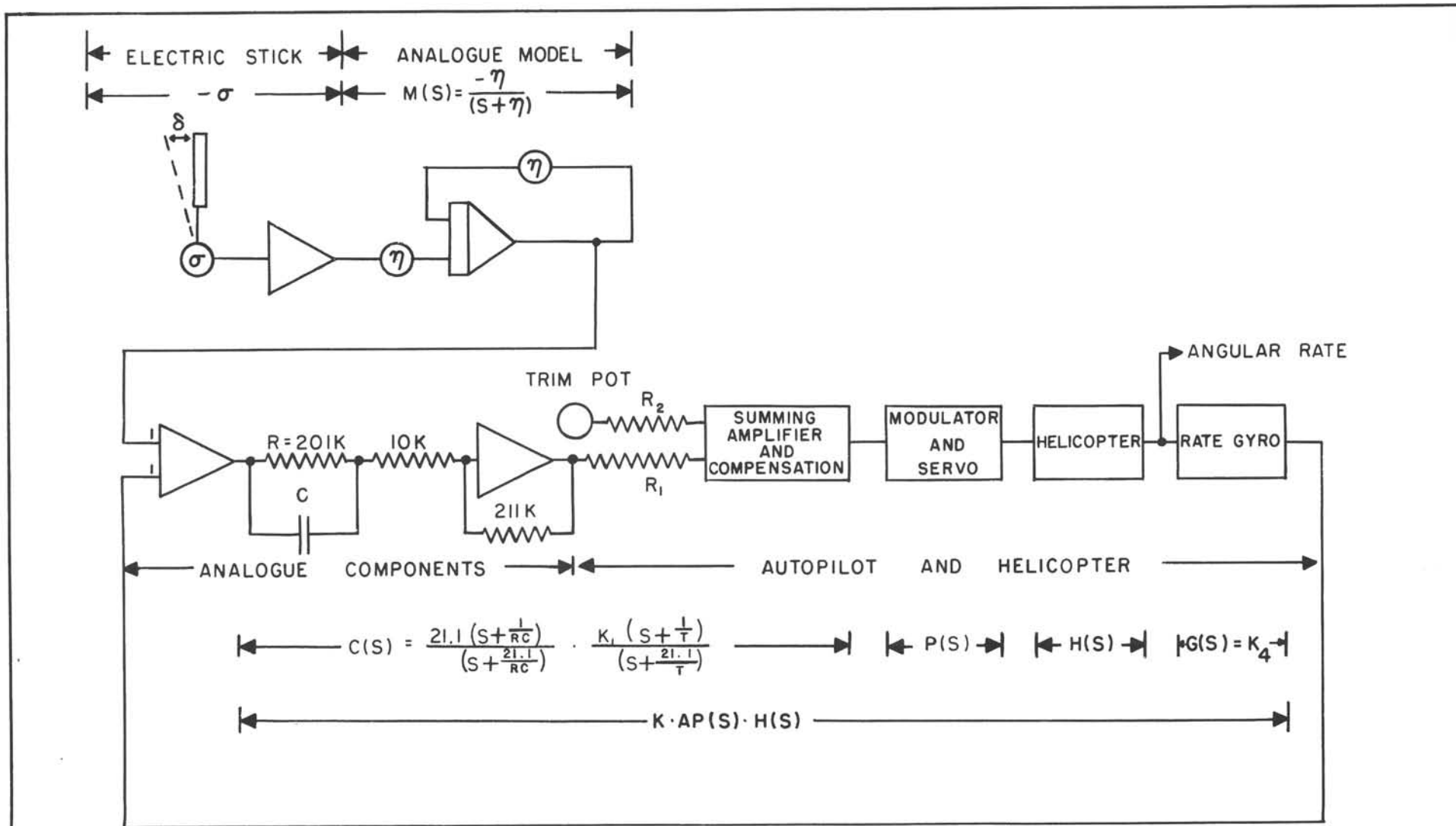


DIRECTIONAL CONTROL LOOP
 VARIATION OF $K_{MAX.}$, $K_{OPT.}$, AND ω_n WITH $\frac{1}{T}$
 (TWO STAGES OF COMPENSATION)



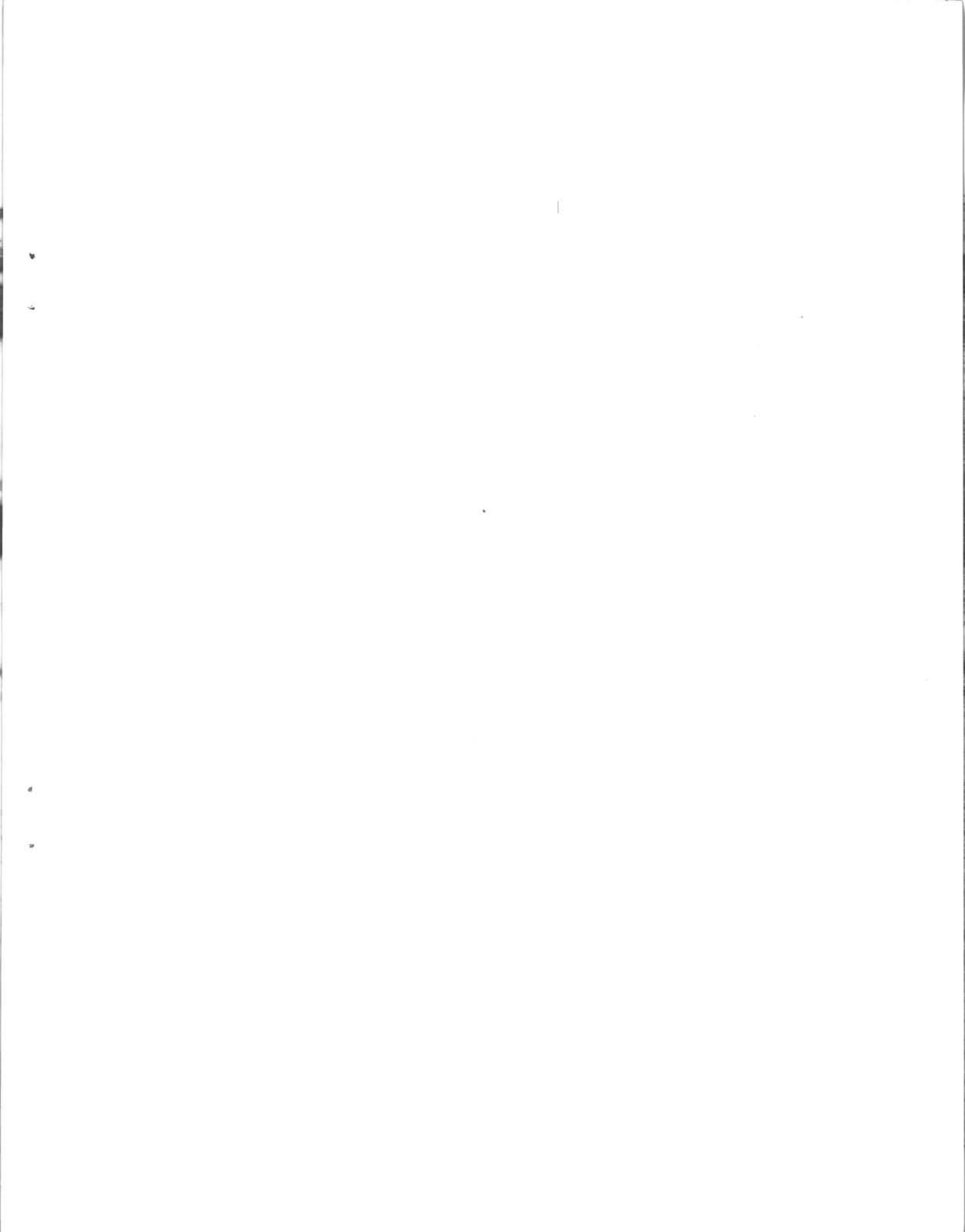






$$\frac{\text{ANGULAR RATE}}{\delta} = \frac{\sigma \eta}{(s + \eta)} \cdot \left[\frac{K \cdot AP(S) \cdot H(S)}{1 + K \cdot AP(S) \cdot H(S)} \right]$$

CIRCUIT DIAGRAM FOR CONTROL LOOP
WITH ADDITIONAL COMPENSATION AND AN ANALOGUE MODEL



INSTALLATION OF OSCILLATOR

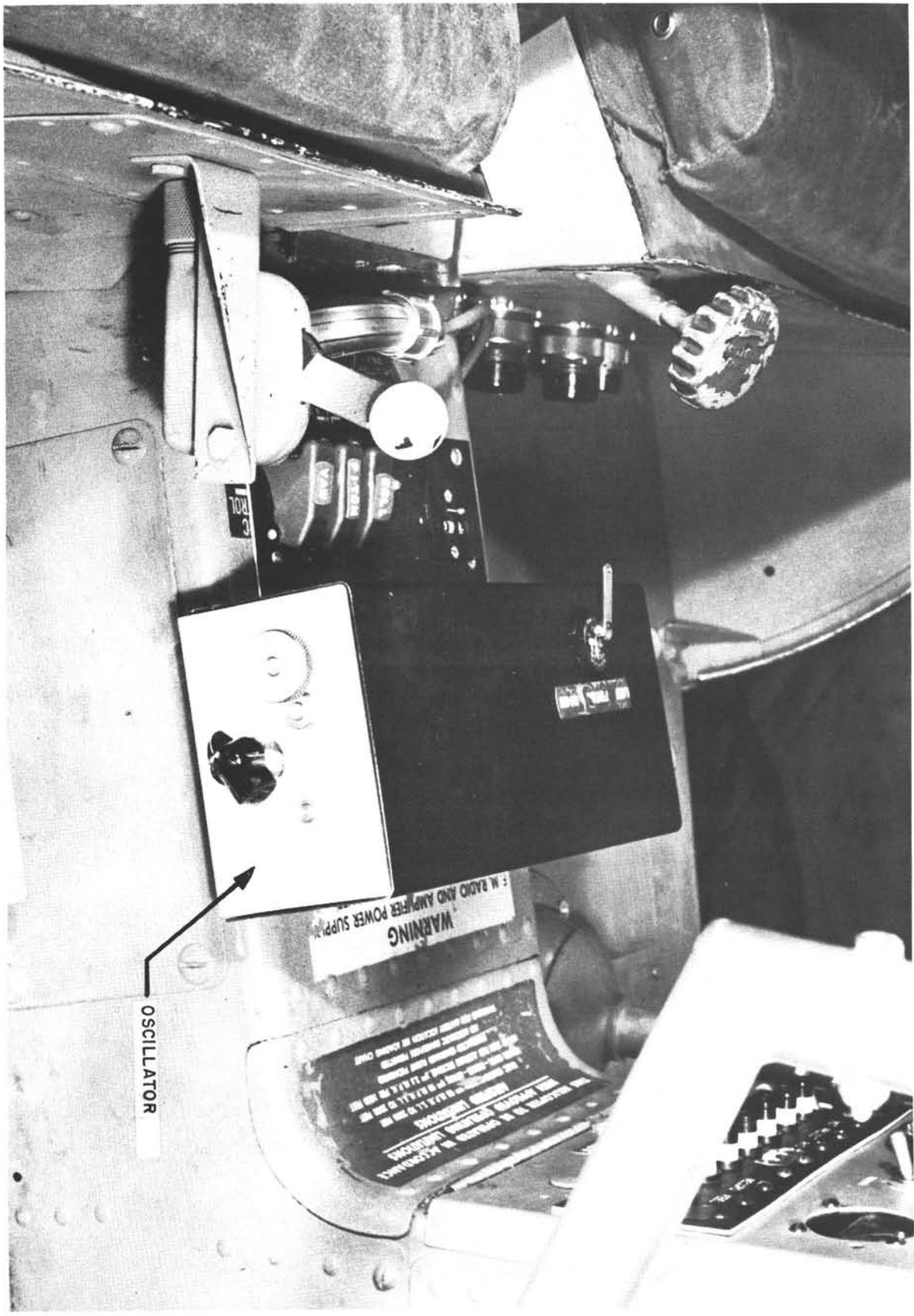


FIG. 57
LR-352

